2011

Phase coherent supercontinuum generation and atmospheric delivery of frequency references using a femtosecond frequency comb

Ravi Paul Gollapalli

PHASE COHERENT SUPERCONTINUUM GENERATION AND ATMOSPHERIC DELIVERY OF FREQUENCY REFERENCES USING A FEMTOSECOND FREQUENCY COMB

by

RAVI PAUL GOLLAPALLI

A DISSERTATION

Submitted in partial fulfillment of the requirements
for the degree of Doctor of Philosophy
in
The Department of Optical Science & Engineering
to
The School of Graduate Studies
of
The University of Alabama in Huntsville

HUNTSVILLE, ALABAMA

2011

In presenting this dissertation in partial fulfillment of the requirements for a doctoral degree from The University of Alabama in Huntsville, I agree that the Library of this University shall make it freely available for inspection. I further agree that permission for extensive copying for scholarly purposes may be granted by my advisor or, in his/her absence, by the Chair of the Department or the Dean of the School of Graduate Studies. It is also understood that due recognition shall be given to me and to The University of Alabama in Huntsville in any scholarly use which may be made of any material in this dissertation.

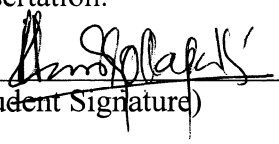

(Student Signature)

05/09/11

(Date)

DISSERTATION APPROVAL FORM

Submitted by Ravi Paul Gollapalli in partial fulfillment of the requirements for the degree of Doctor of Philosophy in Optical Science & Engineering and accepted on behalf of the Faculty of the School of Graduate Studies by the dissertation committee.

We, the undersigned members of the Graduate Faculty of The University of Alabama in Huntsville, certify that we have advised and/or supervised the candidate on the work described in this dissertation. We further certify that we have reviewed the dissertation manuscript and approve it in partial fulfillment of the requirements for the degree of Doctor of Philosophy in Optical Science & Engineering

11/24/2010 (Date) Committee Chair

11/24/10

12/1/2010

12/4/10

2/11/2011

2/5/11 Department Chair

2/15/11 College Dean

5/9/11 Graduate Dean

ABSTRACT
The School of Graduate Studies
The University of Alabama in Huntsville

Degree Doctor of Philosophy College/Dept. Engineering/Optical Science and Engineering

Name of Candidate Ravi Paul Gollapalli

Title Phase Coherent Supercontinuum Generation and Atmospheric Delivery of Frequency References using a Femtosecond Frequency Comb

In this dissertation, a phase coherent supercontinuum spanning from 1160 nm to 1780 nm was generated for potential development of a femtosecond frequency comb. Frequency references both in microwave and optical frequency regimes were remotely delivered over 60 m round-trip propagation distance via the atmosphere. For a microwave frequency reference transmission, the RMS timing jitter integrated over 1-10^5 Hz was 1.86 ps, and agrees with values indicated by atmospheric models for pulse propagation. The root Allan variance was 3 x 10^{-12} at 1 s averaging time with τ^{-1} dependence. With the transmission of optical frequency reference the root Allan variance value 3 x 10^{-13} at 1 s averaging time was achieved. The uncontrolled environment influences the long-term stability measurements of root Allan variance and the noise spectra indicate involvement of random processes. Better stability and longer transmission distances are possible with active-noise cancellation techniques and large-scale optics.

Abstract Approval:

Committee Chair 

Department Chair 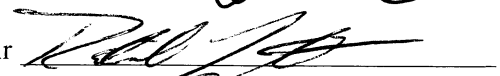

Graduate Dean 

ACKNOWLEDGMENTS

I take this opportunity to thank the one GOD ALMIGHTY, for giving me the strength to do this work and accomplish my dream to earn a doctorate.

I thank my advisor, Dr. Lingze Duan, who introduced me to the concept of frequency combs and their applications, inspired and encouraged me to pursue this research work and reach the goal. With his never diminishing smile, he was always there to teach me everything that I have learned in this field.

I thank the love of my life, my beautiful wife Jeevani, for her understanding and sacrifices while I spent long hours in the lab and was away at conferences and at times when she needed me by her side. I dedicate this work to my joy in this world, my beautiful daughters Amelia & Joanna. I thank my parents Paul & Aseervadamma Gollapalli and my sisters for their constant support and encouragement to accomplish this research work.

I thank Dr. Robert Lindquist, Director, Dr. Yongbin Lin and Mr. Ted Rogers of the Center for Applied Optics for letting me borrow and use the needed equipment and space on the Optics Building roof-top to perform the experiments.

I thank my committee including, Dr. Don A. Gregory, Dr. Robert Lindquist, Dr. Seyed Sadeghi & Dr. Mohan Sanghadasa for their constant encouragement and support in helping me accomplish this research work.

TABLE OF CONTENTS

LIST OF FIGURES

LIST OF TABLES

Chapter I

INTRODUCTION

It is common to get lost during travel in an unfamiliar place; however, it has become less common with the use of Global Positioning System (GPS) receiver units. A GPS receiver unit works using a network of navigation satellites in outer space. These satellites are located at known positions and constantly beam a radio-wave signal towards the earth. This radio-wave signal carries information of the name of the satellite, its position and the time-stamp indicating the time when the signal left the satellite. A GPS receiver unit receives and uses these radio-wave signals from three or more satellites to pinpoint the receiver unit's exact position geographically on earth. While in motion, it can also calculate how far it has moved relative to the satellites and based on the time-stamp information from them it can calculate the elapsed time to move from its earlier position and calculates it speed and other information. The key element in this whole process is the time-stamp information carried by the radio-wave signal. Each satellite generates the time-stamp using a high precision clock mounted on it, which is accurate to one second in 325,000 years. The time-stamp generated by this kind of highly accurately clock can provide us with location accuracy to within few feet or even better to few inches, which emphasizes the importance of a highly precise atomic clock generating the clock signal.

A clock signal can be generated by many sources such as the common wrist-watch and the quartz-crystal based oscillators used to generate the microwave frequency

(radio-wave) clock. Traditional atomic clocks are based on the microwave signal emitted by electrons when they change energy levels in atoms such as cesium, rubidium and hydrogen and they provide very high precision and accuracy. Optical atomic clocks, the next generation of atomic clocks rely on precision atomic transitions in the optical frequency range and promise better precision than the traditional atomic clocks due to the higher operating frequency. Many applications ranging from fundamental research for fundamental constants in physics, spectroscopic measurements in biology, chemistry, laser-based radar to optical communications can benefit from access to highly stable and precise, wide band of clock reference signals. However, these ultra-stable, high precision clock sources are very complex to build and expensive; when one needs access to frequency/timing references, the best viable option is to remotely deliver these references from a source to the distant user. The key feature of such a distribution system should be a faithful delivery of the original clock to the users, in other words, the ability to deliver the highly accurate clock signals to a necessary user with the same accuracy it has at the clock source.

Optically distributing clock signals offers much higher bandwidths and lower interference than microwave-based schemes (such as GPS). An optical clock signal can be delivered by three very distinct schemes. The first scheme involves transferring a microwave frequency clock using a continuous wave (CW) laser which is amplitude modulated at the frequency of the reference. Transfer of an optical reference can be achieved by transmitting a stabilized CW laser over and then disseminated to other optical and microwave regimes with the help of an optical frequency comb. Compared to these two conventional methods, using a femtosecond frequency comb as the carrier of

such high-fidelity frequency references holds many advantages. Prominently, the first advantage is the ability to transfer frequencies in both optical and microwave regimes and the second advantage is the ability to transfer multiples of clock signals in both regimes with a single system. These two advantages make an optical frequency comb an ideal and better candidate as the carrier of frequency references.

1.1 Motivation of the Research

Recently highly stable laser-based frequency references have been delivered successfully over kilometer range distances via fiber-optic networks with high accuracy and stability. However there are situations where delivery of clock signals over optical fibers is not possible or economical. A fiber-optic network inherently being a "wired" network system cannot be used to remotely deliver frequency references when there is a relative motion between the frequency reference transmitter and the receiver. Also in the case of ad-hoc network systems or when the frequency reference users are located at short distances it is not effective or economical to lay-down a fiber-optic network to deliver the frequency references. The obvious answer to this problem is to have a "non-wired" frequency reference distribution system. The primary motivation for this research work stems from the lack of an effective and economically feasible frequency reference distribution system for the earlier mentioned situations. The right choice to have a transmission medium with no need "wiring" would be the free-space or the atmosphere. With the atmosphere as transmission medium, there is no necessity to lay down an expensive fiber-optic network system and also the clock can be distributed to ad-hoc users.

Highly stable, high precision frequency references are also used in the field of free-space probing schemes such as long-distance ranging, coherent LIDAR, comb-based laser radar, etc. In all of these applications, there is an underlying issue that has not been sufficiently addressed, which is the impact of the transmission medium to the precision of the frequency comb. Using the atmosphere as a frequency reference distribution channel would facilitate the accurate assessment of the performance limitations of the above applications. This is the secondary motivation behind this research, and this comes as a by-product of a study on the feasibility of transferring laser-based high precision frequency references via the open atmosphere.

1.2 Research Goal

The aim of this research is to study and characterize the stability or faithful delivery of frequency references via an uncontrolled open atmosphere. It has been shown that it is feasible to transfer frequency references in a controlled laboratory environment; however, this has not been done via an open atmosphere. It is the goal of this research to study the feasibility and quantitatively measure the accuracy of the frequency reference received at a distant user via the atmosphere.

To achieve this goal the work in this research is divided into two major parts. The first goal is to generate the high precision frequency references. A frequency comb is an optical pulse-train, and is a common source of high precision frequency references, which can be obtained from a femtosecond mode-locked laser. The range of frequency references produced by a pulse-train from a mode-locked laser is not very wide which requires some kind of mechanism to increase the range of these frequency references.

This mechanism of generating a wide range of frequencies is called phase coherent supercontinuum generation. This forms the first goal of this research work.

The second goal is to transmit these frequency references from the phase coherent supercontinuum via the atmosphere. The first part in this remote delivery study is to transfer the microwave frequency signals first and study the type and the nature of noises affecting the frequency reference delivery. Also the accuracy of the transmitted microwave frequency should be measured to check the faithful delivery of the frequency reference. The second part is to transmit the optical frequencies via the atmosphere and study the stability with which the optical frequency can be delivered. Also in the optical frequency delivery study, measurements need to be done to study the nature and type of noise experienced by the remotely delivered optical frequency.

1.3 Outline of this Dissertation

The main goal of this research work is to study the uncontrolled atmosphere as a channel to transmit frequency references to a distant user. The primary source that is used is a femtosecond frequency comb. A femtosecond frequency comb carries a very broad spectrum of well defined and related femtosecond pulses. The concept of a femtosecond frequency comb and its characteristics are explained in the Chapter 2 and also the method of generation of such a comb. Chapter 3 presents the characteristics and applications of a phase coherent supercontinuum (PCSC), which is the building block to generate a frequency comb. The schematic and components needed to generate a PCSC are also presented. Chapter 4 introduces the reader to the concept of remote delivery of clock signals and the methods of clock delivery. In this chapter, reported work on the remote delivery of clock signals over fiber-optic networks are described, introducing the reader

to the reason and the need for the atmospheric delivery of frequency references. Chapter 5 describes the atmosphere as the transmission medium and its characteristics and its influence on femtosecond pulses propagating through it. Here the concept of pulse arrival-timing jitter is explained and how it is used to measure the phase noise. Chapter 6 provides the basics of how a clock delivery system is characterized, based on the phase noise and the Allan variance measurements. Basics concepts on the different types of noise are also addressed in this chapter.

Chapter 7 presents the initiative towards developing the Phase Coherent Supercontinuum (PCSC) and the results achieved. The femtosecond laser source in our lab provides femtosecond pulses with low average power prompting to build an Erbium Doped Fiber Amplifier (EDFA), the concept of which is explained in the Section 7.3. A detailed numerical study was done on the evolution of the femtosecond pulses in a gain medium such as the EDFA, which provided an in-depth knowledge of the phase evolution of the pulses. Knowledge from the simulations was used to perform an experimental study, to determine the type and length of chirping needed to compress the amplifier-broadened femtosecond pulses. These compressed pulses are passed through a photonic crystal fiber (PCF) that produces PCSC.

Chapters 8 presents the experimental setup used for launching the frequency comb into the atmosphere and how microwave clocks are delivered over a 60 m round-trip transmission distance. The issues with beam-wander and coupling of light into the detector system and how they were handled are presented in this chapter. The phase noise spectra and the root-mean-square (RMS) timing jitter calculations are presented. Allan deviation measurements and the nature of the underlying noise

influencing the microwave frequency reference transferred via the atmosphere are presented. Chapter 9 presents the concept of Optical heterodyning and how an optical frequency delivery is measured and analyzed for its fractional stability. Allan deviation measurements are presented along with the study of the heterodyne beat-note signal and the nature of its distribution. The experimental data is presented explaining how the large phase modulation by the atmosphere dominates the optical frequency regime for remote delivery and the spectral broadening of the signal.

The Appendices present the equations for the autocorrelation of a Gaussian pulse, RF circuits built and used to measure the phase noise and the Allan deviation of the frequency references transmitted via the atmosphere, and the MATLab code used to simulate a femtosecond pulse propagating in a gain medium. At the end, the References used in this dissertation are presented.

Chapter II

FEMTOSECOND FREQUENCY COMB

Theodore Hänsch and John Hall shared the prestigious 2005 Nobel Prize in Physics for their work involving the development of the Optical Frequency Comb, drawing much attention to the technology and the scope of its applications. An optical frequency comb can be viewed as a regularly spaced series of frequencies produced by a very short pulse laser. If the pulses are short enough (in the order of femtoseconds, 1 fs = 10^{-15} s), the spectrum of such short pulses can be wide to fit the entire visible spectrum, which produces a "comb" of colored lines as seen by a spectrometer. Femtosecond optical pulses are generated by establishing a fixed phase relationship between all of the lasing longitudinal modes, which is called "mode-locking." The resonator in a mode-locked laser contains an active element or a nonlinear passive element. Two methods exist to achieve mode locking, namely, active mode locking and passive mode locking. Active mode locking is the technique of modulating the resonator losses periodically or the modulation of the round-trip phase change achieved using an active element such as an acousto-optic modulator, electro-optic modulator, a Mach-Zehnder integrated-optic modulator or a semiconductor electro-absorption modulator. Synchronizing the modulation with the resonator round trips can lead to the generation of ultrashort pulses with pico-second pulse-width duration. Passive mode locking facilitates the generation of much shorter pulses with femtosecond pulse-width duration. A saturable-absorber is usually driven by shorter pulses, which can modulate the resonator

losses much faster than an electronic modulator. In some cases, such as mode-locked diode lasers, both active and passive mode locking are applied resulting in extremely controlled pulse repetition rates and much shorter pulses. The following sections describe the background towards the development of a frequency comb and its generation technique along with the possible applications.

2.1 Frequency Comb Development

Frequency is the physical quantity that can be measured with the highest possible precision. The highest precision in frequency measurement would enable us to study slow changes in the fundamental constants with highest sensitivity levels such as 10^{18}. This precision can be used in optical communications, navigation, spectroscopy and distance ranging and the highest accuracy achievable on the frequency measurement has been limited to the radio frequencies up to 100 GHz. To extend radio frequency precision to the optical frequency regimes, the traditional approach was to use harmonic frequency chains (Evenson, 1973). The method of this extension from the radio frequency regime to the optical regime involves the use of nonlinear diode mixers, crystals and other nonlinear devices. These harmonic extension chains proved to be more complex to build and required a lot of control to be exercised and very expensive. Even with all the complexity and the expense, only a single frequency can be measured with this technique. In 1990 a new and feasible idea was reported to solve the complexity of the traditional frequency chains. The basic idea is to generate the arithmetic average of two laser frequencies f_1 and f_2 by phase-locking the second harmonic of a third laser at frequency f_3 to the sum frequency of f_1 and f_2 given as $2f_3 = f_1 + f_2$. Cascading $'n'$ such stages would provide a difference frequency division by 2^n. This is an all-optical

method based on visible or near-IR laser diodes (Telle, 1990). Here again the drawback of this difference frequency division method is a less broad spectrum, about 1 THz.

The structure of stable combs of frequency components, produced by stable and evenly-space pulse trains was demonstrated in 1978. This comb structure was used to measure the frequency intervals of the sodium *3s - 4d* transition (Eckstein, 1978). This comb idea was jump-started again by the intra-cavity modulator based spectral comb generator (Kourogi, 1993). Using a high-frequency $LiNbO_3$ electro-optic phase modulator in a Fabry-Perot cavity, the pulses are modulated onto stable CW laser beams. These comb generators can provide spectrums about 4 THz wide; however, the pulses till then were not shorter than 30-ps and wider spectrums were not obtainable. Finite gain-bandwidth product and intra-cavity dispersion are the two limiting factors that dictated the pulse-width of the pulse at the lower end. The concept of Kerr-lens mode locking introduced the ability to produce sub-100 fs pulses from a Ti: Sapphire laser (Spence, 1991). The ability to link the radio-frequency to the optical-frequency regime still needed to be achieved, and the concept of spectral spreading was utilized to answer this dilemma. In 1999 it was shown that the modes of femtosecond mode-locked lasers form a frequency comb, which can be used as a ruler to measure the frequency of light (Reichert, 1999) (Udem, 1999). Based on these experiments, it was also shown that the phase of the nonlinearly generated light is stable to form an optical frequency comb (Bellini, 2000). This led to the search for methods to stretch the spectrum of the femtosecond pulsed laser. This marked the beginning of the era of femtosecond frequency comb. Around this time, a revolutionary idea that white light could be produced by passing a femtosecond pulse with large peak powers through an

internally structured fiber was presented (Ranka, 2000). This provided a way to generate an optical frequency comb and increase the band of these comb frequencies from radio-optical domains.

2.2 Femtosecond Frequency Comb: Definition and Characteristics

A femtosecond laser-based frequency comb is a pulse train with a controlled optical field. In the frequency domain, it is a sequence of equidistant spectral lines with a constant spacing of f_R and a fixed phase relation between them (Udem, 2002). Figure 2.1 (a) shows the time-domain picture of a frequency comb, which consists of a series of fs-pulses with the same envelope profile and pulse spacing, $T_R = 1/f_R$.

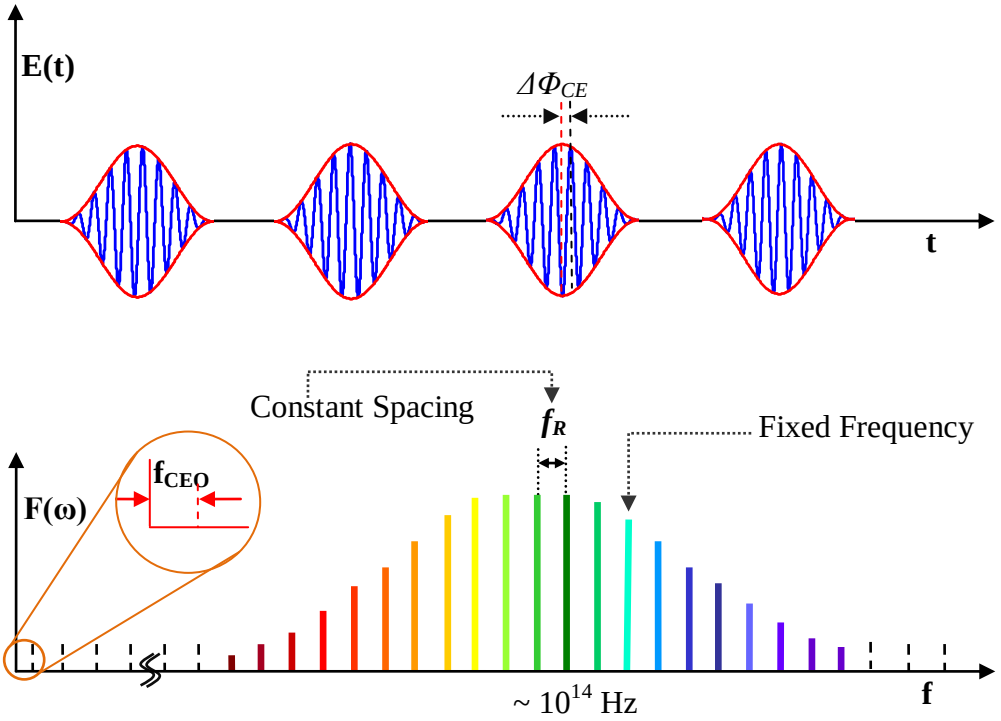

Figure 2.1 An optical frequency comb. (a) Time domain depiction of Frequency comb. The difference in the pulse peak and the oscillating electric field peak, known as the Carrier envelope phase offset is shown. (b) Frequency domain picture of comb where the offset from the origin is the Carrier envelope offset frequency.

Inside the pulse envelope, the phase of the oscillating optical field relative to the peak of the envelope drifts from pulse to pulse. Such a phase is called the Carrier-Envelope Phase (CEP), $\Delta\Phi_{CE}$. Usually, the CEP repeats itself after a certain number of pulses. Its repetition rate is called the Carrier-Envelope offset Frequency f_{CEO}. The significance of f_{CEO} becomes evident in the frequency domain, where a "comb-like" spectrum with equal line spacing f_R spans across a broad frequency range in an optical frequency regime (10^{14}-10^{15} Hz), as shown in Figure 2.1(b). f_{CEO} corresponds to the frequency of the lowest order spectral line when the "comb" is traced down to zero frequency. With f_{CEO} and f_R defined, the exact frequency of an arbitrary spectral line in a frequency comb is given by

$$f = n * f_R + f_{CEO}. \tag{2.1}$$

where m is the harmonic order of that particular spectral line with regard to the pulse repetition rate. Both f_{CEO} and f_R can be independently stabilized with atomic-clock accuracy. Such frequency accuracy is transferred to every spectral line within the comb according to Alfano (2006), leading to thousands of optical frequency standards. Moreover, these optical frequency references can be easily converted in to the radio-frequency (RF) regime by a photodetector, making frequency combs versatile carriers ideal for frequency reference distribution.

2.3 Applications of Femtosecond Frequency Comb

The femtosecond frequency comb is a versatile technology that has applications in various fields and is also opening up avenues for many more applications that have not been possible till today. Here is a brief description of the proven and potential applications of Femtosecond Frequency Comb.

a) One of the driving forces behind the development of femtosecond frequency combs is the desire to measure the absolute optical frequencies, which the femtosecond frequency comb technology can do.

b) Quantum Computing: Quantum Computing often needs frequencies that are widely separated and controlled with extreme precision. This wide range of multiple frequencies and the precision is provided by an optical frequency comb. A frequency comb can be used to drive transitions in a trapped ion, providing a way of performing operations required for quantum computing.

c) Using high-precision spectroscopy, the fundamental constants such as the Rydberg constant and the underlying theories, and this high precision is provided by an optical frequency comb. Prominently in Quantum electrodynamics (QED), the high precision characteristics of the frequency comb technology may allow calculating energy levels of simple atoms such as hydrogen, with 12 digits of accuracy. Using an optical frequency comb, a high precision spectrometer was developed at JILA, for the real time analysis of the quantity, structure and dynamics of atoms and molecules. This system can identify multiple elements in the test environment with a precision of 1 part in 100 million (Thorpe, 2006).

d) In the field of distance measurements, an optical frequency comb provides sub-attometer resolution. Using a femtosecond laser based wavelength synthesizer, high precise tuning was achieved, which provides sub-picometer length stability for an integration time of one minute and sub-10 picometer stability for half an hour integration time (Schibli, 2006).

e) Data transmission rates in an optical communication system is influenced by the noise of the lasers and the amplifiers, spectroscopic applications, metrology applications, which all require very low noise, and less phase fluctuations of the laser. The frequency comb provides a tool to characterize the fine features of the lasers.

f) Telecommunications: In present day telecommunications, WDM technology combines multiple optical wavelength signals onto a single optical fiber to carry different information. Multiple lasers need to be used to generate these multiple wavelength signals and a single femtosecond frequency comb system can replace these multiple lasers. Frequency combs because of their fine structure can also provide less cross-coupling compared to using multiple lasers, which increase the channel density.

g) Cavity Characterization: The research group with Theodor W. Hänsch has measured the chromatic dispersion of the elements of a high-finesse cavity with very high precision using a CEO-stabilized frequency comb. This was accomplished by monitoring the wavelength-dependent transmission of the frequency comb through the cavity, where the effect of cavity length drifts is eliminated by locking one particular cavity resonance to a comb line. This method allows the measurement of the group delay dispersion of optical components over significant wavelength ranges (above 100 nm) with RMS errors of only a few fs^2 (Schliesser, 2006).

2.4 Femtosecond Frequency Comb Generation

The basic components required to generate a femtosecond frequency comb are a femtosecond mode-locked laser, provision to generate a supercontinuum spanning an octave, and the means to detect and stabilize the parameters f_R, f_{CEO} and n. Pulse repetition rate, f_R can be determined by using a fast photodetector. The carrier-envelope

offset frequency is determined using a scheme called the "*f-2f*" self-referencing technique as shown in Figure 2.2.

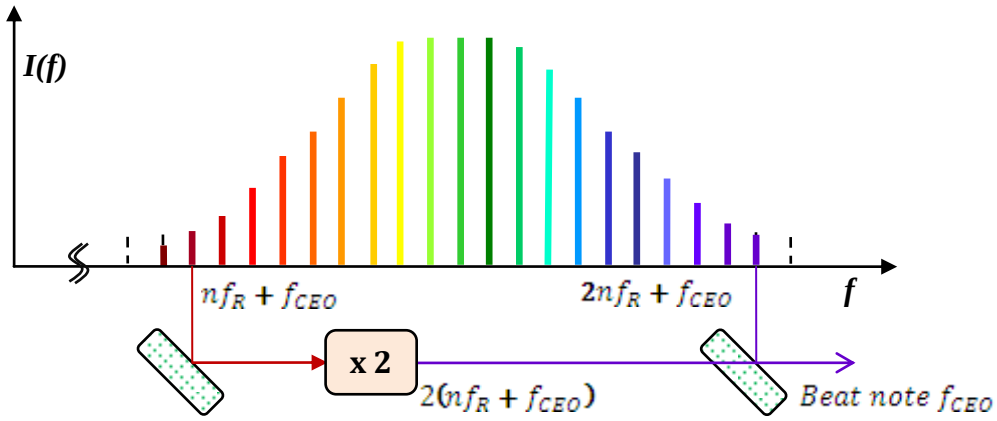

Figure 2.2 Schematic showing how to determine f_{CEO}. f_R, f_{CEO} are the pulse repetition rate and carrier-envelope offset frequency and 'n' is the order of the frequency comb mode (Udem, 2002)

Consider the lowest frequency mode at the beginning of the frequency comb, which is realized as $nf_R + f_{CEO}$ given by equation (2.1), is passed through a nonlinear crystal producing a second-harmonic frequency, $2(nf_R + f_{CEO})$. If the frequency comb is about an octave, then the highest frequency would be $2nf_R + f_{CEO}$, beating these two frequencies would result in $2(nf_R + f_{CEO}) - 2nf_R + f_{CEO} = f_{CEO}$. Phase-locking these quantities to an atomic clock such as a cesium clock can provide a stable femtosecond frequency comb. From this discussion we can see that we need an octave spanning frequency comb, where the phase relationship between each pulse in the pulse-train is preserved (Cundiff, 2002). Such a phase-coherent supercontinuum generation is the building block to generate a frequency comb.

Chapter III

PHASE COHERENT SUPERCONTINUUM (PCSC)

3.1 Properties and Applications of PCSC

Optical supercontinuum is light with a very broad spectrum. Supercontinuum finds its applications in spectroscopy, microscopy and other types of interferometer-based measurements (e.g., optical coherent tomography). White-light sources, such as tungsten-halogen lamps and super-luminescent diodes, are conventionally used to provide supercontinuum. They have low brightness and poor coupling efficiency to optical fibers, which limit their applications. Moreover, the broad spectra of white-light sources lead to poor temporal coherence. Different frequency components in the spectrum have random phase relation with each other, causing simple power addition (i.e., incoherent superposition) between these spectral components, as shown in Figure 3.1(a). In recent years, the femtosecond laser-based supercontinuum offers a new route toward generation of an ultra-broad spectrum. Combined with highly nonlinear fibers, such lasers are able to produce spectra as broad as or even wider than the conventional tungsten lamps with well-collimated beams and high power. In addition, these supercontinua also have high temporal coherence owing to the fact that they are composed of a series of discrete spectral lines. Spectral lines from different parts of the supercontinuum can be heterodyned to generate the sum and difference frequencies, as shown in Figure 3.1(b), making coherent measurement possible.

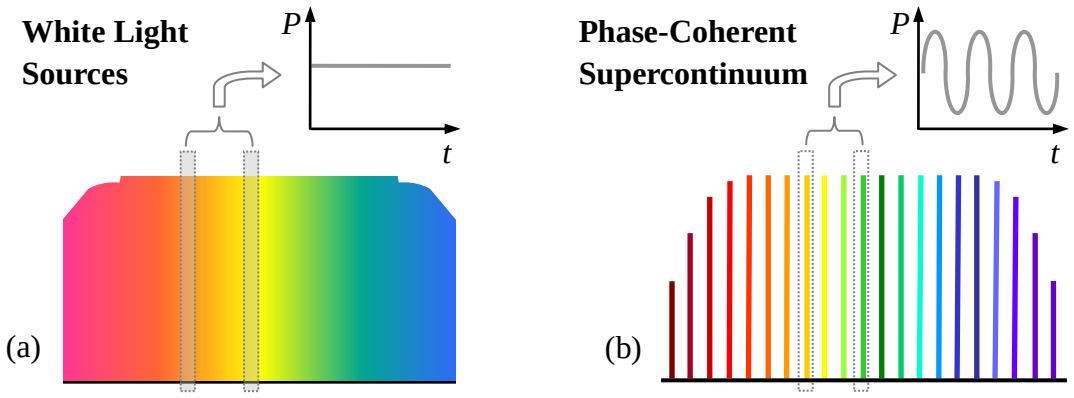

Figure 3.1 Comparison between conventional supercontinuum and Phase Coherent Supercontinuum

Promising applications of phase coherent supercontinuum (PCSC) include large-capacity, high speed fiber-optic communication systems, where a large number of wavelengths and high coherence between different wavelength channels are desired. In optical coherence tomography (OCT), resolutions better than 2 µm can be made possible using PCSC (Ye, 2005). Other prominent applications of PCSC include precision frequency metrology, optical waveform synthesis, and Coherent Anti-Stokes Raman Scattering (CARS).

3.2 Phase Coherent Supercontinuum (PCSC) Generation

A phase-coherent supercontinuum is usually generated by injecting a highly-stable femtosecond pulse train into a nonlinear medium such as a photonic crystal fiber. The generated spectrum depends on the nonlinear properties of the medium, the propagation distance of the pulse, the pulse energy and pulse-width, as well as the dispersion of the medium. When optical fibers are used as the nonlinear medium, the dominant spectral-broadening process is self-phase modulation (SPM). Other coherent effects such as wave-mixing and the Raman Effect may also contribute to the generation

of new wavelength components. With careful control of the spectral broadening process, for example, limiting the length of the nonlinear fiber, the phase stability in the initial femtosecond pulse train can be largely preserved, leading to a supercontinuum that consists of a series of discrete narrow spectral lines as shown in Figure 3.1(b).

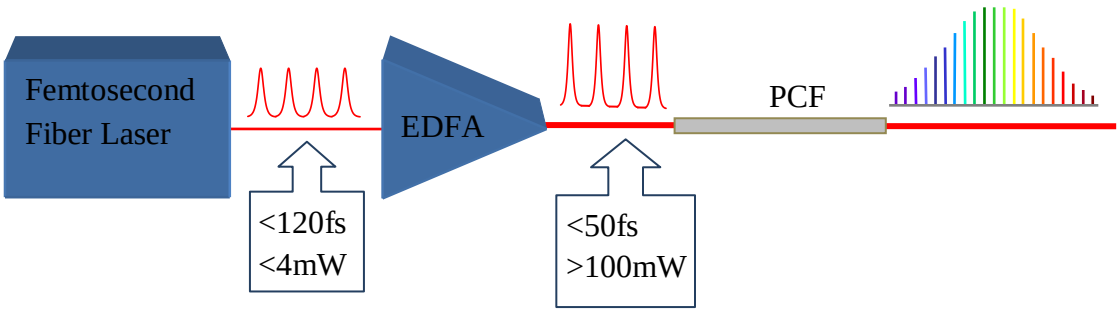

Figure 3.2 Conceptual layout of a Phase Coherent Supercontinuum Generation system. EDFA: Erbium Doped Fiber Amplifier, PCF: Photonic Crystal Fiber

A layout is shown in Figure 3.2 for a typical PCSC generation system in the 1.5 μm wavelength range. Pulses coming from a femtosecond fiber laser are first amplified by an erbium-doped fiber amplifier (EDFA). Typical pulse energy at the output of the amplifier is in the order of nJ and the peak power of the pulses reaches 10 kW. These pulses are then injected into a section of highly nonlinear photonic crystal fiber (PCF), usually less than 1 m long. Supercontinuum as broad as an octave can be obtained at the output of the PCF. Their phase coherence has been experimentally confirmed.

3.2.1 Femtosecond Fiber Laser

Femtosecond lasers are normally used to provide highly stable pulse trains for PCSC generation. In the 1.5-μm wavelength range, mode-locked fiber lasers have

emerged as a cost-effective solution. Compared to conventional femtosecond sources such as Ti:Sapphire lasers, which operate in the 800 nm range, fiber lasers not only offer much better compactness and robustness but also cover the important wavelength range of 1-2 μm, which is of great importance to telecom and gas molecule spectroscopy. Femtosecond fiber lasers are now commercially available.

3.2.2. Erbium-Doped Fiber Amplifier (EDFA)

A key step in the aforementioned PCSC-generation scheme is pulse amplification. Femtosecond pulses directly from fiber lasers normally have pulse energy in the order of 10 pJ and peak power about 100 W. Such a power level is not sufficient to produce the strong nonlinear effect needed for a significant spectral broadening, even in highly-nonlinear fibers. A 15-20dB increase in both pulse energy and peak power is usually required. EDFAs have proved to be very effective in achieving such specifications. EDFA belongs to the class of doped fiber amplifiers where the gain medium is a regular single mode fiber doped with Er^{3+} with typical concentrations in the range of 1.22×10^{25} to 6.6×10^{25} ions per cubic meter. The common pump wavelength is around 980nm (sometimes also at 1450nm), which excites Er^{3+} ions from the ground-state manifold $^4I_{15/2}$ to $^4I_{11/2}$, from where there is a quick non-radiative transfer to the upper laser level $^4I_{13/2}$. The stimulated emission back to the ground-state $^4I_{15/2}$ from $^4I_{13/2}$ amplifies the light in the 1.5- μm wavelength region. EDFA can provide gain efficiencies in the order of 20dB and the lowest noise figure. Compared to other amplifiers, EDFAs have an edge with their large gain bandwidth typically in the range of tens of nanometers and high saturation power levels.

Due to the unique properties of femtosecond pulses, EDFAs used for fs-pulse amplification are different from the conventional EDFAs used in the telecom industry. They usually use highly-doped erbium fibers with short lengths to limit the total dispersion. They also require precise control of the gain fiber length and often come with pre- and post-amplifier dispersion control systems. Because of the complex dynamics involved in fs-pulse propagation inside erbium-doped fibers, each amplifier must be specifically tailored according to the properties of the input pulses. Thus we have decided to build our own EDFA in the lab and develop a numerical model to facilitate the design.

3.2.3 Photonic Crystal Fiber (PCF)

A PCF is a class of optical fiber that gains its characteristics by a special arrangement of very tiny and closely spaced holes that go through the whole length of the fiber. The most common arrangement is the triangular arrangement of holes in the fiber. One such arrangement is shown in Figure 3.3, where three holes are missing at the center of the solid core. The arrangement of tiny holes in a PCF can be tailored to obtain different values of refractive index and various other properties. PCFs are advantageous over conventional optical fiber because of the unique dispersion control capability. Compared to conventional optical fibers, a higher effective-refractive index contrast between core and cladding can be obtained. Due to this high refractive index contrast, the photonic band-gap structure confines light modes into a very small core (~1 μm diameter), leading to very high optical power concentration inside the core material and, hence, large nonlinearity.

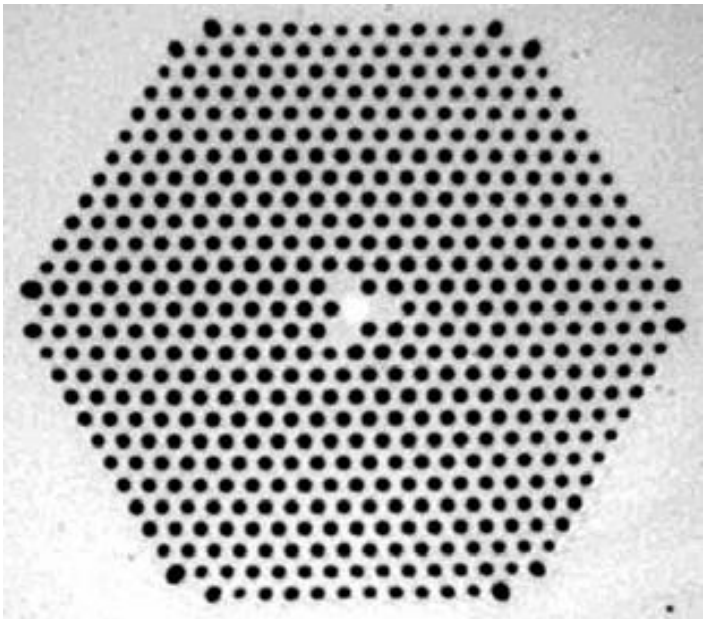

Figure 3.3 Core of Photonic Crystal Fiber. The black color represents holes and grey represents glass material. [Crystal Fibre: NL-1550-POS]

The key mechanism leading to spectral broadening of the pulse propagating through a highly nonlinear medium is Self-Phase Modulation (SPM). SPM is a nonlinear effect, where a short and intense pulse propagating in a medium induces an intensity-dependent refractive index variation in the medium due to the optical Kerr effect:

$$n(I) = n_0 + n_2 \cdot I, \tag{3.1}$$

where n_0 and n_2 are the linear and second-order nonlinear refractive indices respectively and I is the irradiance of the propagating pulse. The time varying pulse intensity can be written as

$$\frac{dn(I)}{dt} = n_2 \cdot \frac{dn}{dt} + I \cdot \frac{dn_2}{dt}, \tag{3.2}$$

This variation in refractive index results in a shift in the instantaneous phase of the pulse, which in turn results in a frequency shift of the pulse as shown in the following equations.

$$\varphi(t) = \omega_0 t - \frac{2\pi}{\lambda_0} \cdot n(I)L, \tag{3.3}$$

where $\varphi(t)$ is the instantaneous phase, ω_0 and λ_0 are the carrier frequency and wavelength of the pulse, and L is the distance the pulse has propagated. The instantaneous frequency $\omega(t)$ is given as

$$\omega(t) = \frac{d\varphi(t)}{dt} = \omega_0 - \frac{2\pi L}{\lambda_0}\frac{dn(I)}{dt}. \tag{3.4}$$

From the above equation we see that SPM causes the generation of extra frequencies resulting in a symmetrical broadening of the pulse frequency spectrum. The leading edge of the spectrum shifts to lower frequencies while the trailing edge shifts to the higher frequencies. The group-velocity dispersion (GVD) of the fiber and the Kerr effect counteract with one another and lead to pulse propagation over longer distances in the fiber without dispersing. This long distance of propagation leads to wider spectral broadening. In the present work, pulses amplified by the EDFA and subsequently compressed have very high peak power and sub-100 fs pulse-width (FWHM) which when propagated through a PCF will produce a supercontinuum.

Chapter IV

REMOTE DELIVERY OF TIME AND FREQUENCY REFERENCES

4.1 Introduction

"Time" is one of the seven base units defined under the SI system of base units, which is used to derive or define the unit "Frequency." A regular wrist-watch is one example of a time source. Table 4.1 provides a list of different oscillators and the requirements on their fractional frequency stability of these oscillators along with different fields of applications of these oscillators. Many commercially available instruments can provide high precision in the form of microwave frequency synthesizers based on quartz oscillators. Higher quality oscillators based on microwave atomic clocks and hydrogen masers are available. A cesium-fountain clock provides a microwave frequency reference by a value better than six parts in 10^{16}. Frequency references based on optical transitions in laser-cooled and trapped atoms and ions will eventually provide accuracies about one part in 10^{18} and also short-term instabilities of a few parts in 10^{17} for a 1s averaging time. This value is three orders of magnitude better than the best microwave atomic clocks.

Different types of high precision microwave and optical frequency reference sources along with the fractional stability provided by them in terms of Allan deviation (at 1 s averaging time) are listed in Table 4.2. Many applications can make use of this high precision in frequency references, e.g., the current microwave frequency standards demand highly stable transfer protocols for signal comparison and clock synchronization.

These high precision frequency reference sources are usually highly complex, expensive and more often not portable. Such scenarios call for the remote distribution of frequency references to the necessary applications. The following section outlines some of the applications that can benefit from such remote transfer of frequency references.

Table 4.1 Various oscillators and requirements on their fractional stabilities(Cruz, 2003)

Fractional Frequency Stability (Time stability)	**Examples of Oscillator Uses**
10^{-5} (1 s/day)	Wrist and wall watches; computer systems; police radars; radio amateur
10^{-8} (1 ms/day)	Radio and TV transmitters; precise voltage measurements; telecommunication systems; power networks
10^{-11} (1 μs/day)	Navigation; secure communications systems; space tracking; precise distance measurements; mobile phones
10^{-14} (1 ns/day)	Radio astronomy; geophysics studies; gravitational wave research; international centers for time dissemination
10^{-17} (1 ps/day)	Test of gravitational theories; tests of atomic theories; frequency standards based on cold atoms; optical frequency standards

Table 4.2 Fractional instabilities of various high-stability frequency references (Foreman, 2007)

Type of frequency reference source	**Allan deviation at 1 s averaging time**
Hydrogen Maser (1 – Hz BW)	$\sim 10^{-13}$
Cryogenic sapphire oscillator	$\sim 5 \times 10^{-15}$
0.3 – Hz-line-width laser	$\sim 10^{-15}$
Residual comb (RF, 10 GHz)	$\sim 10^{-15}$
Projected Sr Optical clock	$\sim 10^{-16}$
Residual comb (Optical)	$\sim 2 \times 10^{-17}$

4.2 Need for Remote Delivery of Frequency References

A number of exciting applications exist that can benefit from access to highly stable frequency reference transfer (Foreman, 2007), some of which are outlined here.

a) Optical clocks are based on the optical transitions of the laser-cooled and trapped atoms and ions. If the fundamental constant, the fine structure constant α changes over time, the frequencies of the optical transitions based on different atomic systems would change with respect to each other. Due to the cost and complexity of these optical clocks, clocks based on different optical systems cannot be built at the same place. The ability to transfer frequency references would enable comparison of frequency references from these different optic-based clocks. Such comparison would enable evaluating the relative instability and systematic shifts in these different clocks. This would facilitate the measurements of changes in the fundamental constants over extended periods of time (Karshenboim, 2000).

b) Applications such as long-baseline interferometry for radio astronomy require all the components to be synchronized with high stability and low phase noise in short time-scale regimes. A highly stable low-jitter frequency reference may be transferred from a central source to each telescope in an array of radio telescopes over distances in the km range. By phase-coherently collecting data, a single telescope can be simulated with a very large aperture (Shillue, 2004).

c) In a linear accelerator facility, using a low-jitter frequency reference transfer, various components of the accelerator can be synchronized with bunches of accelerated electrons; ultrashort x-ray pulses can be produced. In an accelerator facility the various components are distributed over km-wide distances, which would require a low noise and

ultralow-jitter frequency reference transfer. This feature and capability has spurred an interest in the utilization of the ultrashort x-ray pulses to study the ultrashort phenomena in several fields including physics, biology, chemistry and materials science (Stanford) (Schoenlein, 1996) (Leemans, 1996).

4.3 Methods of Clock Delivery

Time and frequency are two related quantities; however, the very definitions of these quantities affect how they are delivered and the uncertainties with these processes. Time transfer is affected directly by the delay induced by the transmission path between the transmitter and the receiver. Frequency, defined as a time interval, is affected by the temporal fluctuations in the transmission delay than by the absolute magnitude.

Primarily the time and frequency standards are distributed in two frequency regimes; first the radio frequency and the optical frequency regimes. The earliest time and frequency delivery systems were based on transferring the frequency references using simple radio broadcasts. Short wave signals from radio stations are still in wide use to transmit time and frequency information. The common-view Global Positioning System (GPS) is the most common method to transfer the frequency and time standards over long distances (Levine, 1999). Interestingly, GPS is the method used to compare the frequency and time standards of the national laboratories around the world. On averaging over a day, the instability obtainable with GPS is about 10^{15}. One of the major drawback in using radio signal sources for frequency distribution is the long times of averaging required to reach low-jitter in the orders of 10^{15} as in the case of the GPS distribution system. Another drawback is that the microwave clocks are not suitable in all applications. These drawbacks are answered by the optical clock-based frequency

reference distribution systems. Optical clock-based frequencies distributions have proven to provide short-term instabilities in the orders of 10^{-17} at 1 s averaging time.

Recently the laser-based frequency distribution systems have gained a tremendous amount of momentum with the advent of frequency comb technology. The highest precision and the wide band of spectrum that may be transmitted with a frequency comb have ushered in a new era into the laser-based frequency distribution systems. Different techniques exist to transmit frequency references using laser-based frequency reference sources. Using an amplitude-modulated continuous wave laser, a microwave frequency reference can be transmitted (Sprenger, 2009) and an optical frequency reference can be transmitted by directly transmitting a stabilized continuous wave laser (Foreman, 2007). However, it is interesting to note that both microwave and optical frequency references can be transmitted simultaneously using an optical frequency comb. This ability to transmit frequency references in both the regimes is one of the key advantages of an optical frequency comb. Primarily the frequency references maybe transmitted via a physical medium such as fiber-optics networks and/or the atmosphere. The following two sections outline the research and the results achieved using laser-based frequency distribution systems.

4.4 Laser-based Clock Delivery via Fiber Optic Networks

a) In a ~30 m fiber link, an ultralow-jitter microwave frequency reference signal was demonstrated (Chen, 2006). The timing jitter integrated from 1 Hz to 10 MHz, was reduced to ~30 as (1 as = 10^{-18} s) over this transmission link. In this case the reference signal was generated by a mode-locked fiber laser and also using an all-optical generation

of synchronization error signal and out-of-loop optical detection technique for the verification of the jitter performance.

b) Using an amplitude-modulated continuous wave (CW) laser, a microwave frequency reference was transferred over kilometer-scale lengths with an instability of 3×10^{-14} at 1 s without stabilization of the fiber-induced noise and 1×10^{-14} at 1 s with active noise cancellation. By direct transfer of a stabilized CW laser over an optical fiber, an optical frequency reference was transmitted with an instability of 2×10^{-14} at 1 s without active noise cancellation and 6×10^{-18} at 1 s with active noise cancellation. Using an optical frequency comb, for the transfer of a microwave frequency reference, an instability of 3×10^{-14} at 1 s without active noise cancellation and 7×10^{-15} at 1 s with active noise cancellation were obtained.

4.5 Laser-based Clock Delivery via the Atmosphere

A compelling situation arises when one realizes that there are many cases where fiber-optic links may not be the most effective route for information transmission or may even be unavailable. These cases include frequency reference distribution to many receivers in small geographical areas, such as a university campus, and reference transfer between mobile transmitters and receivers. Clearly, these situations call for free-space transmission of frequency combs. Free-space transmission of optical pulses has been extensively studied in the context of optical communications and LIDAR since the 1970s. Major research topics include wave scattering in random media, optical beam transportation in the atmosphere, etc. More contemporary research involves studying the nonlinear and dispersive effects experienced by femtosecond pulses during free-space transmission. These studies, however, focus on single pulses and very little work has

been devoted so far to the transmission of highly stable pulse trains and the extra timing jitter induced by fluctuations in the atmosphere. *Young et al.* have developed a statistical model to calculate the fluctuations in the time-of-arrival of pulses in a weak turbulence media. It provides an analytic solution to the amount of pulse broadening experienced by pulses of different pulse-width. However there is no discussion on the impact of this pulse broadening on the spectral characteristics of the pulse train and also no experimental effort was made to back the theoretical predictions. This research work aims to explore the relation between the atmospheric fluctuations, mainly turbulence, and the spectral properties of frequency combs and the scale of the resulted degradation of frequency references.

Chapter V

OPTICAL PULSE PROPAGATION THROUGH THE ATMOSPHERE

The atmosphere is random in nature and is influenced by the humidity, wind speed, temperature, aerosols and all the other particles that make up the atmosphere. The atmosphere is a medium that is a freely and readily available medium which can be used for information transfer, high rate communications systems, LIDAR, etc. The random nature of the atmosphere limits the precision and the efficiency with which these applications can be utilized. Three primary phenomena affect optical wave propagation in the atmosphere, which are absorption, scattering and refractive-index fluctuations. Absorption and scattering by atmospheric elements such as gases and particulates are wavelength dependent and primarily result in the attenuation of the optical signal. The random fluctuations in the index of refraction of the atmosphere, also called optical turbulence, affects an optical signal causing irradiance fluctuations, beam spreading and a loss or decrease in the spatial and temporal coherence. These affects can limit the performance of communications systems.

5.1 Optical Turbulence in the Atmosphere

The turbulent motion of the atmosphere in the presence of moisture and temperature gradients gives rise to disturbances in the atmosphere's refractive index. The statistical description of the random field of turbulence-induced fluctuations in the

atmospheric refractive index is similar to the random turbulent velocities in a viscous field. This study can be related to the turbulent fluctuations in the atmosphere and a statistical approach is a proven method to describe atmospheric turbulence and its effects on both optical and IR systems. The distances in the transmission path in the atmosphere over which fluctuations in the index of refraction are correlated are known as "turbulent eddies." The inner scale is represented as l_0 and the outer scale as L_0. For a statistically homogeneous and isotropic turbulence, the related *structure function* has a behavior accepted to be

$$D_n(\boldsymbol{R}) = f(x) = \begin{cases} C_n^2 l_0^{-\frac{4}{3}} \boldsymbol{R}^2, & 0 \leq \boldsymbol{R} \ll l_0 \\ C_n^2 \boldsymbol{R}^2, & l_0 \ll \boldsymbol{R} \ll L_0, \end{cases} \tag{5.1}$$

where C_n^2 is the index-of-refraction *structure constant* (units $m^{-\frac{2}{3}}$) sometimes called the *structure parameter*, and $\boldsymbol{R}$ is the point in the space (Tatarskii, 1971), (Hill, 1978).

Physically, the refractive-index structure constant C_n^2 is a measure of the strength of the fluctuations in the refractive index. The behavior of C_n^2 at a point along the propagation path can be deduced from the temperature structure function. In a turbulent atmosphere, the range of inner scale and outer scale eddies is between 1 micron to 100 m. Path-average values of C_n^2 and inner scale l_0 can be obtained simultaneously by optical measurements over a short path length (typically 150 m) using an instrument called a scintillometer (Hill, 1992). The refractive-index structure constant, C_n^2, typically ranges from 10^{-17} [$m^{-\frac{2}{3}}$] or less for conditions of "weak turbulence" and up to 10^{-13} [$m^{-\frac{2}{3}}$] or more when the turbulence is "strong." Over short intervals at a fixed propagation distance and constant height above the ground, it may be reasonable to

assume that C_n^2 is essentially constant. However, for vertical and slant propagation paths, C_n^2 varies as a function of height above ground.

The index of refraction n, the most significant parameter of the atmosphere for optical wave propagation, is very sensitive to small-scale temperature fluctuations. In particular, temperature fluctuations combined with turbulent mixing induce a random behavior in the field of atmospheric index of refraction. At a point R in space and time t, the index of refraction can be mathematically expressed as

$$n(R) = n_0 + n_1(R,t), \tag{5.2}$$

where $n_0 = \langle n(R,t) \rangle = 1$ is the mean value of the index of refraction and $n_1(R,t)$ represents the random deviation of $n(R,t)$ from its mean value; thus, $\langle n_1(R,t) \rangle = 0$. Time variations in the refractive index are often expressed in the treatment of optical wave propagation. This means that the wave maintains a single frequency as it propagates. It is customary, therefore to express equation (5.2) as

$$n(R) = 1 + n_1(R), \tag{5.3}$$

where $n(R)$ has been normalized by its mean value n_0.

Fluctuations in the index of refraction are related to corresponding temperature and pressure fluctuations. In particular, the index of refraction for the atmosphere can be written for optical and IR wavelengths as (Owens, 1967)

$$\begin{aligned} n(R) &= 1 + 77.6 \cdot 10^{-6}(1 + 7.52 \cdot 10^{-3}\lambda^{-2}) \frac{P(R)}{T(R)} \\ &= 1 + 79 \cdot 10^{-6} \frac{P(R)}{T(R)}, \end{aligned} \tag{5.4}$$

where λ is the optical wavelength in $\mu m, P$ is the pressure in millibars, and T is the temperature in Kelvin.

5.2 Model of the Atmosphere as a Transmission Medium

The atmosphere is made up of gases and particles spreading to several hundred kilometers above the surface of the Earth. The major constituents of the atmosphere are water vapor, carbon dioxide, ozone, etc. The Earth's atmosphere is an absorbing medium. *Absorption* occurs when a photon of radiation is absorbed by a gaseous molecule of the atmosphere that converts the photon into the molecule's kinetic energy, resulting in heating the atmosphere. *Scattering* of electromagnetic waves in the visible and IR wavelengths occurs when the radiation propagated through certain air molecules and particles. The physical size of the scatterers determines the type of scattering. When the size of the scatterers or air molecules is small in comparison with the wavelength of the radiation, the scattering is called Rayleigh scattering, and applies only to a very clear atmosphere. Another type of scattering, called Mie scattering is caused by the air particles that are comparable in size to the radiation wavelength.

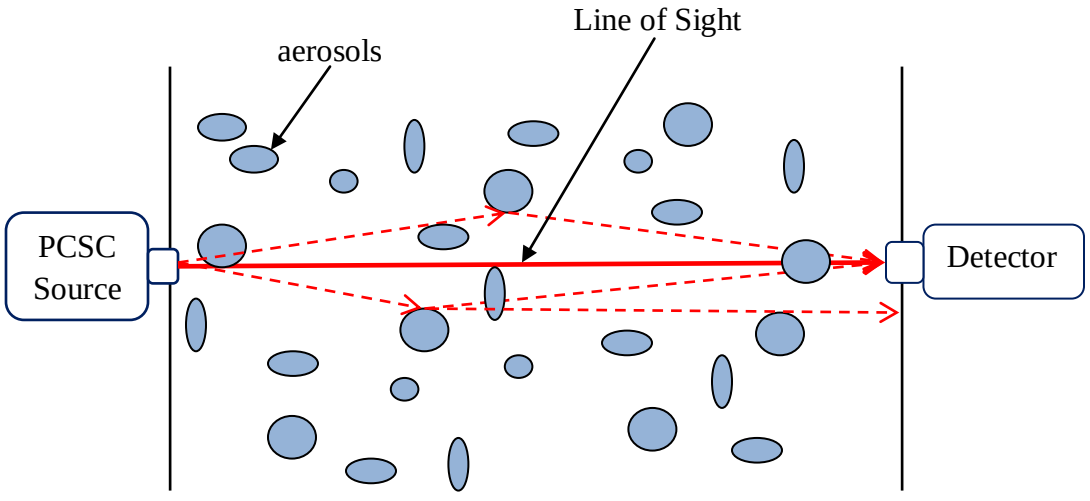

Figure 5.1 Laser beam propagation in the atmosphere.

Figure 5.1 shows the propagation of a laser beam in the atmosphere, consisting of the air molecules or the particles, called the scatterers. As the optical beam propagates in the atmosphere, it is absorbed and also scattered by these molecules and the scatterers. For a ground-level short distance line of sight transmission, clear air and very weak turbulence can be assumed and scattering effects can be neglected and line-of-sight propagation only needs to be considered.

5.3 Ultrashort Pulse Propagation via the Atmosphere

An optical signal propagating through the atmosphere is not affected by the dispersion of the atmosphere if it is either a continuous-wave signal or pulsed-signal with pulse-width longer than ~100 ps (Fante, 1975). However if the propagating optical pulses are shorter than 100 ps, the effects of dispersion due to turbulent atmosphere also should be considered. This becomes prominent because the random delays incurred by the radiation in propagating from the turbulent eddies to the receiver can cause pulse distortion and broadening. The frequency reference sources used in this work are generated from a mode-locked fiber laser that produces optical pulses with pulse-widths in the femtosecond range. Due to the broad spectrum associated with ultrashort pulses, the analysis of propagation of these femtosecond pulses should be performed in the frequency domain using the two-dimensional and four-dimensional coherence functions. The broadening of the pulses due to propagation in the atmosphere can be calculated using an analytical model based on the two-frequency mutual coherence function (MCF) (Sreenivasiah, 1976), (Fante, 1981), (Young, 1996).

When a pulse train propagates across in air path, it is altered due to various optical characteristics of the air path, including the average refractive index, the total dispersion,

the distribution of the scattering particles, etc. If these characteristics are stationary, i.e., their change is negligible within the time span of the measurement, they will not cause extra timing jitter (or pulse arrival-time fluctuation) even though they modify the properties of individual pulses. On the other hand, if some of these factors, for example, the average refractive index, have temporal fluctuations, they will add time-dependent modulations to the pulse train, which leads to timing jitter of the pulse train. The timing jitter of the pulses results in broadening the spectral lines carried by the frequency comb and the quality of the frequency references carried by the frequency comb will degrade as a result of such line broadening. The method of temporal moments is used to study and calculate the mean pulse-width and arrival time fluctuations of an optical pulse under weak optical turbulence conditions.

The variance of the pulse arrival time is given by

$$4\sigma_{ta}^2 = T_2^2 = T_0^2 + 8\alpha, \qquad \text{(Young, 1998) (5.5)}$$

where σ_{ta}^2 is the variance in the pulse arrival time, T_0 and T_2 are the transmitted and the received pulse half-widths respectively, and parameter α is defined as

$$\alpha = \frac{0.3908\, C_n^2\, z\, L_0^{\frac{5}{3}}}{c^2}, \qquad \text{(Young, 1998) (5.6)}$$

where C_n^2 is the refractive-index structure constant, z is the propagation distance, L_0 is the outer-scale size of turbulence and c is the speed of light.

5.4 Measurement of Pulse-Arrival Jitter

An optical pulse train propagating through the atmosphere is affected by the random time-dependent fluctuations of the refractive index in the transmission path, which results in pulse-arrival jitter at the receiver. When the pulses are unaffected by the

transmission medium, here the atmosphere, they maintain the same spacing between each other. Figure 5.2(a) illustrates the RF spectrum resulted from direct photo-detection of an ideal frequency comb, with no pulse-arrival jitter at the receiver. It is clear that the spectral lines are sharp with no broadening. Figure 5.2(b) shows the broadened spectrum due to the excessive timing jitter in the pulse train after it propagates through a turbulent medium. The broadened spectral lines in the optical-frequency regime are converted into a RF (radio-frequency) regime by the photodetector. Using the heterodyning technique, this spectral broadening can be quantified in terms of extra phase noise in the baseband. Figure 5.2(c) conceptually illustrates a typical phase noise spectrum against an instrument noise floor, usually white-noise in nature, in log-log scale. This phase noise can be analyzed using a Fast-Fourier Transform (FFT) Analyzer. The measured excess phase noise can be used to calculate the pulse-arrival jitter. This method would provide the means to measure the stability of the microwave frequency references transmitted through the atmosphere.

The integrated RMS timing jitter calculated from the phase noise can be compared to values suggested by the theoretical models as given by equation (5.5). The amount of spectral broadening of the frequency references after propagating in a turbulent media can be quantified and related to the strength of the turbulence and other characteristics of the free-space transmission media, the atmosphere. This forms the basis and the essence of the present research work.

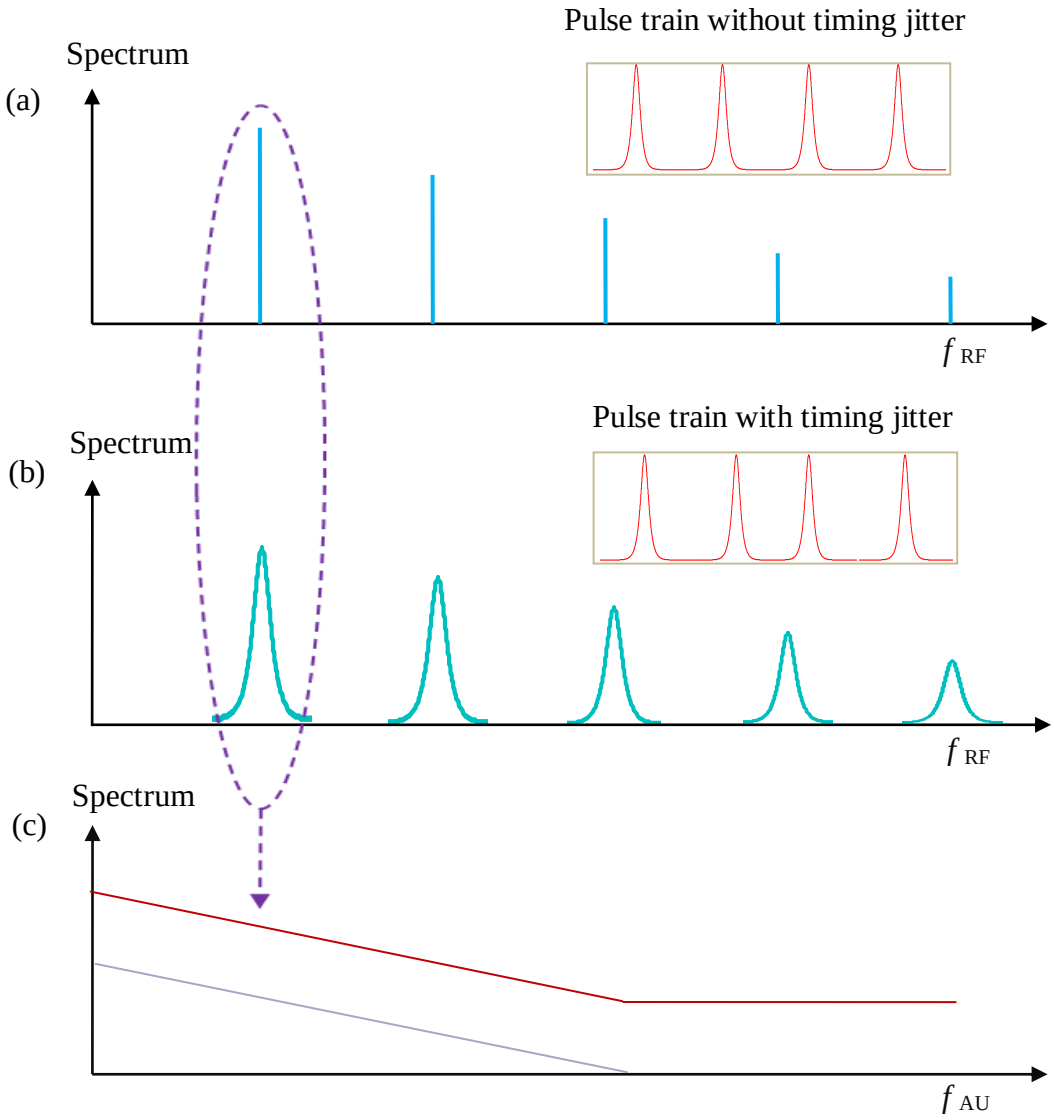

Figure 5.2 (a) Frequency comb with sharp frequency references from a pulse train without timing jitter as shown in the inset. (b) Frequency comb with spectal broadening due to timing jitter in the pulse train as shown in the inset. (c) Heterodyning of the above two cases of ideal frequency comb and frequency comb due to pulse wandering. The top curve is the phase noise and the bottom curve is the instrument noise.

5.5 Impact of Air Dispersion on the Heterodyne Measurement System

An optical signal from a CW laser carries only one spectral feature with it, but an optical pulse from a pulsed-laser carries multiple spectral features/lines along with it. When such an optical pulse with multiple spectral lines is used for frequency reference transfer along with heterodyning to analyze the transmitted frequency references, the measured beat note is a result of the heterodyning all of the multiple spectral lines. To achieve an effective heterodyning, the phase difference between these spectral lines should be much less than π . If the phase difference is larger than π , the phases cancel out each other and cause in loss of the beat-note signal. The dispersion of the transmission medium, in this case air, impacts this phase difference, placing an upper limit on the spectral bandwidth of the heterodyne measurement system.

The refractive index of air at a wavelength can be calculated using the following equation (Ciddor, 1996).

$$10^8(n_{as} - 1) = \frac{k_1}{(k_0 - \sigma^2)} + \frac{k_3}{(k_2 - \sigma^2)} \tag{5.7}$$

$$k_0 = 238.0185\ \mu m^{-2} \qquad k_1 = 5792105\ \mu m^{-2}$$

$$k_2 = 57.362\ \ \mu m^{-2} \qquad k_3 = 167917\ \mu m^{-2},$$

where n_{as} is the refractive index of air defined at temperature 0^0 C, 0% relative humidity, pressure of 101325 Pa and CO_2 content of 450 ppm in air, and σ is the wavenumber at a particular wavelength in vacuum. For atmospheric weather conditions different from the above mentioned conditions, for example, different temperature or different relative humidity, the same reference (Ciddor, 1996) provides a procedure to modify the above equation and calculate the refractive index of air under various weather conditions.

For effective heterodyning the following inequality should be satisfied

$$[[n]_{air}([\lambda_2) - n_{air}(\lambda]_1)] * L < \pi \quad , \tag{5.8}$$

where L is the propagation distance of the optical pulse in air.

When the phase difference between the spectral extremes due to transmission is less than π , it ensures that the heterodyne measurement system would provide an effective beat-note signal. The spectral bandwidth of the AOM used in the optical frequency reference transfer study performed in this work is measured to make sure that the dispersion of the air does not impact the beat-note signal. These calculations are provided in the Section 9.3.

Chapter VI

NOISE CHARACTERIZATION FOR CLOCK SIGNAL DELIVERY

A clock signal delivery scheme can be characterized by the amount of noise experienced by the clock signal at the receiving end of the clock signal. The noise experienced by a clock signal is usually expressed in terms of the phase and/or frequency noise in frequency domain and Allan deviation in time domain. A propagating signal is usually influenced by many types of noise as described following.

6.1 Sources and Types of Noise

There are many types of noises and most important among them are the following three: the thermal noise, the flicker noise and the shot noise.

6.1.1 Thermal Noise

Thermal noise is a type of electronic noise caused by the thermal agitation of the charge carriers inside an electrical conductor. This noise is present regardless of any applied voltage across a conductor at equilibrium. The noise power P in watts is given by

$$P = k * T * f \quad , \tag{6.1}$$

where k is Boltzmann's constant in J/K, T is the temperature in K and f is the bandwidth in Hertz. Thermal noise has a nearly equal power spectral density throughout the frequency spectrum and the probability density function of the signal amplitude has a nearly Gaussian probability distribution. Thermal noise is also frequently referred to as Johnson-Nyquist noise and White noise.

6.1.2 Flicker Noise

Flicker noise is a type of electronic noise that is related to a direct current, with a $\frac{1}{f}$ spectrum, which gives it the name $\frac{1}{f}$ noise. The origin of this noise type is not well known, but it occurs in all electronic devices and is a result of many effects such as impurities in a conductive channel, generation and recombination noise in a transistor due to base current, and so on. Flicker noise is dominant at lower frequencies and is overshadowed by white noise from other sources at higher frequencies. However, in oscillators, the low-frequency noise is mixed up to frequencies close to the carrier which results in oscillator phase noise. Flicker noise is often characterized by the corner frequency f_c between the regions dominated by each type. Since flicker noise is related to the level of DC, if the current is kept low, thermal noise will be the predominant effect in the resistor, and the type of resistor used will not affect noise levels.

6.1.3 Shot Noise

Shot Noise is a type of electronic noise caused by the random fluctuations in the arrival time of the signal carriers in a circuit and is small enough to show up as detectable fluctuations in a measurement. An electrical current is a motion of charged particles (electrons and/or holes) which are discrete and independent, and this motion is not uniform. At small levels of current, the currents vary in a random fashion, and this random variation is called Shot Noise. Shot noise prominently shows up at lower levels of current and increases with the average magnitude current or light intensity. However as the current level increases rapidly, shot noise cannot follow the current and generally dies out, and is often only a problem with small levels of current. Shot noise unlike Johnson-Nyquist noise is present only when there is a flow of current in a circuit, while

Johnson-Nyquist noise is due to current fluctuations in equilibrium that can happen with or without any applied voltage and without any average current flowing in a circuit. Shot noise is a Poisson process and the charger carriers follow a Poisson distribution.

6.2 Noise Characterization in Frequency Domain

The frequency stability of a frequency reference is defined as the degree to which a signal maintains the same value of frequency over a given period of time. The variations from the nominal frequency of a signal are in turn due to the variations or fluctuations of the phase component of the signal. Phase noise is the term used to describe phase fluctuations of a signal. There are a number of definitions used to describe the phase noise of a signal and many methods to characterize the phase noise. All the methods measure the frequency of phase fluctuations in either the frequency or time domain. The most common method of phase noise description is the one-sided "spectral density" of phase fluctuations per unit bandwidth. The spectral density, PSD, describes how the power (or variance) of a time series is distributed with frequency. Mathematically it is defined as the Fourier Transform of the autocorrelation sequence of the time series; in other terms, it is the squared modulus of the Fourier Transform of the time series, scaled by a proper constant term. The spectral density is characterized by measuring the noise "sidebands" on either side of the signal nominal/center frequency. Single side-band (SSB) phase noise is specified in dBc/Hz at a given frequency offset from the carrier. The frequency domain information about phase or frequency is contained in the power spectral density $S_{\Delta\Phi}(f)$ of the phase or in the power spectral density $S_{\Delta f}(f)$ of the frequency. Here f refers to the modulation frequency or offset frequency associated with the noise-like variations in $\Phi(t)$.

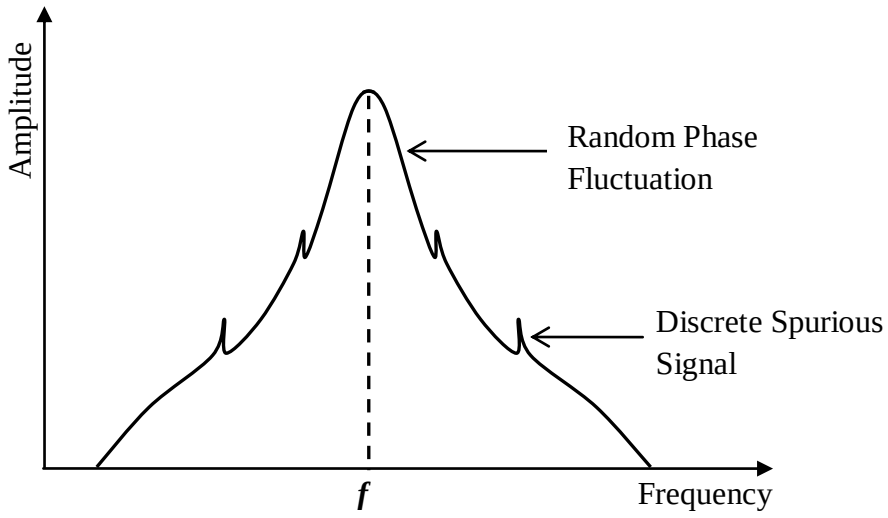

Figure 6.1 Concept of phase noise displayed on a spectrum analyzer, showing double sided phase noise.

In the frequency domain, the noise is expressed in terms of the amount of phase fluctuations as experienced by the frequency source/reference that is being delivered. This method of characterization is useful for determining the short-term stability of a frequency reference that may be used for synchronization of various system components. As defined, the phase noise is the rapid random fluctuations in the phase component of the reference signal.

Consider a transmitted signal represented as

$$V(t) = A_0 \sin\left(2\pi f_0 t + \Delta\Phi(t)\right), \tag{6.2}$$

where A_0 is the nominal peak voltage, f_0 is the carrier frequency and $\Phi(t)$ is the instantaneous phase of the signal.

The peak phase modulation $\Delta\Phi(t)$ and peak frequency modulation $\Delta f(t)$ are related as $\Delta\Phi_{peak} = \frac{\Delta f_{peak}}{f}$, in terms of RMS values, the relation is $\Delta\Phi_{rms} = \frac{\Delta f_{rms}}{f}$. The

one sided spectral distribution of the phase fluctuations per Hz bandwidth is $S_{\Delta\Phi}(f)$ given by

$$S_{\Delta\Phi}(f) = \frac{[(\Delta\Phi]_{rms})^2}{BW} \quad \left[\frac{rad^2}{Hz}\right] \tag{6.3}$$

where BW is the bandwidth of $\Delta\Phi_{rms}$ measurement. Similarly one-sided spectral distribution of the frequency fluctuations per Hz bandwidth is

$$S_{\Delta\Phi}(f) = \frac{[(\Delta f]_{rms})^2}{BW} \quad \left[\frac{rad^2}{Hz}\right] \tag{6.4}$$

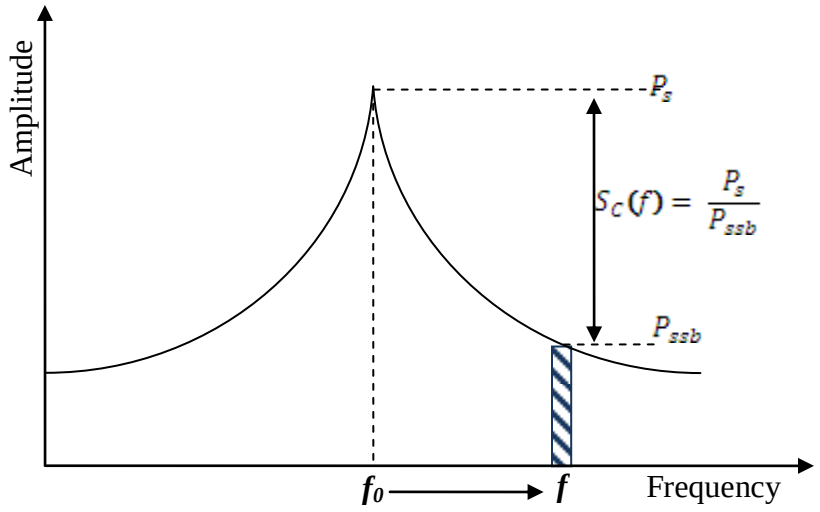

Figure 6.2 Single-sideband phase noise to carrier ratio.

The National Institute of Standards and Technology (NIST) defines the single-side band phase noise as the ratio of power in one phase modulation side-band per Hertz bandwidth, at an offset f Hertz away from the carrier, to the total signal power. Here f is the offset frequency from the carrier. $S_C(f) = \frac{P_s}{P_{ssb}}$, where P_s is the carrier power and P_{ssb} is the sideband power in one Hz bandwidth at an offset frequency f from the center. Logarithmically it is given as

$$S_C(f)\ in\ dB = 10\log[S_C(f)]. \quad (6.5)$$

6.3 Noise Characterization in Frequency Domain

The noise performance characterized in the time domain is known as *jitter*. *Jitter is defined as the variation in the zero-crossing times of a signal, or a variation in the period of the signal*. Similar to the phase noise, the jitter is composed of two major components, one of which is predictable and the other is random in nature. The predictable component of the jitter is called *deterministic jitter*, which is a result of the deterministic noise, and the random component of the jitter is called *random jitter*, which is a result of the random phase noise (Box, 1970)(Rutman, 1978)(Stein, 1985).

In applications such as remote synchronization, phase noise of a transmitted signal is expressed in terms of its timing jitter. The timing jitter spectral density, $\Delta\tilde{T}(f)$, which represents the RMS timing jitter at each Fourier frequency in a 1 Hz measurement bandwidth, is proportional to $\Delta\tilde{\Phi}(f)$ and related as

$$\Delta\tilde{T}(f) = \frac{\Delta\tilde{\Phi}(f)}{2\pi\nu_0} \quad \left[\frac{s}{\sqrt{Hz}}\right]. \quad (6.6)$$

The total RMS timing jitter, T_{rms}, expressed over a bandwidth from f_l to f_h, is then given as

$$T_{rms} = \sqrt{\int_{f_l}^{f_h} [\Delta\tilde{\Phi}(f)]^2\, df} \quad [s]. \quad (6.7)$$

The key objective of the time domain characterization is to answer the ubiquitous question regarding the stability of the transferred frequency reference over a time

interval τ , where the time interval can range from sub-seconds to months and years. To assess frequency stability over a time interval τ with the sampling time, a series of measurements each of duration τ is made with an average, $\overline{y_i}$ with, $i = 1 \ldots\ldots N$. Due to the random nature of $y(t)$, the frequency stability is expressed in terms of the variance σ^2 or the standard deviation the sigma σ . Various kinds of variances have been defined among them a few are explained in the following sections.

6.3.1 True Variance

True Variance is a theoretical parameter defined as

$$I^2(t) = < \overline{y}_k{}^2 >. \tag{6.8}$$

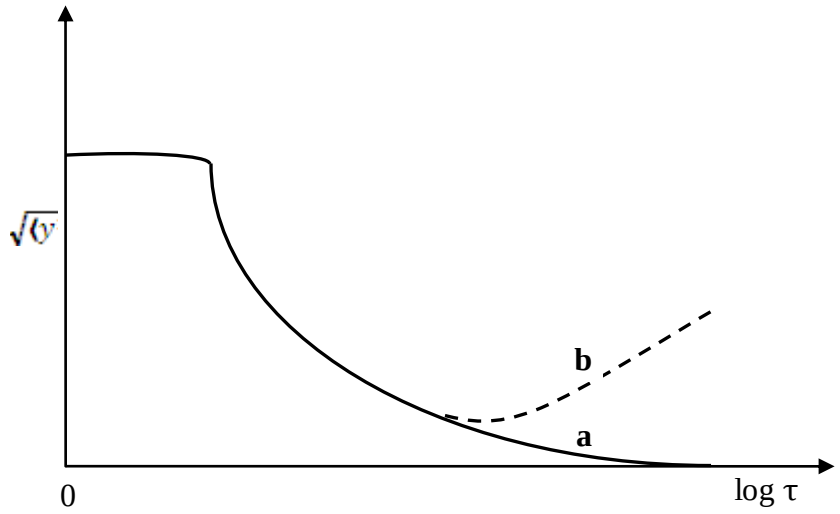

Figure 6.3 Frequency instability in the time domain. (a) Square root of the true variance for stationary frequency noise. (b) Performance of practical frequency sources.

When the frequency fluctuates around υ_0, $I^2(t)$ decreases from $< y^2(t) > for\ \tau = 0$ and $I^2(t) = 0\ as\ \tau \rightarrow \infty$, where fluctuations are completely averaged away as shown as curve *'a'* in Figure 6.3; however, the real time oscillations

follow the curve *'b'*. So the estimate of variance based on 'true variance' is not useful in the practical world.

6.3.2 Sample Variance

Sample variance is based on a finite number of N samples, where each sample has a duration τ and the k^{th} sample begins at t_k; the k^{th} sample begins at $t_{k+1} = t_k + T$; the dead time between two successive samples is then $T - \tau$. Now the sample variance is defined as

$$\sigma_y^2(N, T, \tau) = \frac{1}{N-1}\sum_{i=1}^{N}\left(\overline{y_i} - \frac{1}{N}\sum_{j=1}^{N}[\overline{y_j})^2\right] . \qquad (6.9)$$

With sample variance defined as above, now frequency stability over a time interval can be estimated using $< \sigma_y^2(N, T, \tau) >$, which also gives us these possible values for the parameters N, T and τ. Based on the work of David Allan in 1966, another variance is recommended for estimation of frequency stability, which is explained in the following section.

6.3.3 Allan Variance

Allan variance, also known as the two-sample variance, is the average of variance with *N = 2* and adjacent samples (that is, *T = τ*, or zero dead time). The resulting measure is defined as

$$\sigma_y^2(\tau) = \frac{1}{2} < (\overline{y_2} - \overline{y_1})^2 > . \qquad (6.10)$$

The same as the *true variance*, the Allan Variance is a theoretical measure too; however, it has a much greater practical utility than $I^2(\tau)$ since it exists for all the spectral density power laws encountered in real oscillators including flicker frequency

noise. Also, simple experimental estimates may be derived for $\sigma_y^2(\tau)$ since groups of only two measurements are involved, which is the key feature in the definition of $\sigma_y^2(\tau)$. The Allan variance has a main drawback where it cannot differentiate and separate the white phase modulation from the flicker phase modulation; this is rectified by another type of variance known as modified Allan variance.

6.3.4 Modified Allan Variance

Modified Allan Variance is variable bandwidth modified variant of Allan variance, represented as $mod\ \sigma_y^2(\tau)$. Both white phase modulation and flicker phase modulation have almost the same response to averaging time τ ; however, white phase modulation is linearly sensitive to the system bandwidth while flicker phase modulation is less dependent on the system bandwidth. Thus the white phase noise and the flicker phase noise can be separated by changing the system bandwidth. This is usually accomplished by post-processing the samples using a software-based bandwidth modification. It is defined as

$$mod\ \sigma_y^2(n\tau) = \frac{1}{2}\left\langle\left[\frac{1}{n}\sum_{i=0}^{n-1}\bar{y}_{i+n} - \bar{y}_i\right]^2\right\rangle . \tag{6.11}$$

6.4 Summary

Phase noise and jitter are two linked quantities associated with noisy frequency signal sources, and usually, as the phase noise increases, the jitter increases too. The frequency domain model for the spectrum $S(f)$ of a low-frequency time series is the power-law given as

$$S(f) = f^{\alpha}. \tag{6.12}$$

There is a one-to-one correspondence between the slopes of the log-log spectrum (the α) and the log-log Allan variance (AV) plot. This relation is given in Table 6.1 for five common types of noises.

Table 6.1 Relation of slope of log-log spectrum to slope of log-log Allan Variance plot for five common types of noise (Riley, 2008).

Name of Noise (Time series model)	**α (Slope of log-log spectrum)**	$\frac{-\alpha - 1}{2}$ **, Slope of log-log AV plot)**
White Phase	2	-1.5
Flicker Phase	1	-1
White frequency	0	-0.5
Flicker frequency	-1	0
Random-walk frequency	-2	0.5

From the knowledge of a time series with a dominant low-frequency component, the nature of the low-frequency component can be estimated using the Allan variance plot. It can also be used to estimate the power, α, of the spectral power-law model. This knowledge would help us study the nature of the underlying noise affecting the stability of the frequency references transmitted via the atmosphere.

Chapter VII

PHASE COHERENT SUPERCONTINUUM GENERATION

A femtosecond laser can generate highly coherent pulse trains and this coherence can be extended to a broad spectrum such as a supercontinuum using a highly nonlinear medium. This chapter presents the numerical studies performed to understand the phase and intensity evolution of a femtosecond pulse in a gain medium. This chapter also highlights the building of the EDFA and the results of the supercontinuum generated.

7.1 Characteristics of the Femtosecond Fiber Laser

The laser used in this research work is a femtosecond fiber laser source (Precision Photonics, FPL-1560). The laser produces femtosecond pulses of 120 fs (FWHM) with an average power of 4 mW and at 90 MHz repetition rate and a 40 nm bandwidth.

Table 7.1 Femtosecond Fiber Laser Source Parameters

Repetition Rate	90 MHz
Pulse-width	120 fs
Bandwidth	40 nm
Center wavelength	1558 nm
Output Power	4 mW
Peak Power	280 W
Make	Precision Photonics

7.2 Numerical Studies of Femtosecond Pulse Propagation in an Er-doped Gain Fiber

The pulse propagation in a dispersive medium, such as an optical fiber, is governed by the nonlinear Schrödinger equation (NLSE). When the transmission medium is a gain medium such as an Er^{3+}-doped fiber as in an EDFA, the interaction of the light with the Er^{3+} ions is modeled as a two-level system. These mechanisms are described by the Maxwell-Bloch equations (Agrawal, 2001). Using the rate-equation approximation (Milonni, 1988), the Maxwell-Bloch equations can be reduced to a generalized NLSE (Agrawal, 2001). As we are simulating femtosecond pulses, including the higher order nonlinear effects due to high peak power and higher order dispersive terms due to broad spectrum of femtosecond pulses, the normalized NLSE is given as

$$i\frac{\partial u}{\partial \xi} - \frac{1}{2}(sgn(\beta_2) + id)\frac{\partial^2 u}{\partial \tau^2} - i\delta\frac{\partial^3 u}{\partial \tau^3} + |u^2|u = \frac{i}{2}(\mu u) - is\frac{\partial |u^2| u}{\partial \tau} - \tau_R\frac{\partial |u^2|}{\partial \tau}, \tag{7.1}$$

where

$$u = NU, \qquad U = \frac{A}{\sqrt{P_0}}, \qquad \xi = \frac{z}{L_d}, \qquad L_d = \frac{T_0^2}{|\beta_2|}, \qquad d = g_0 L_d \frac{T_2^2}{T_0^2},$$

$$\tau = \frac{t - \beta_1 z}{T_0}, \qquad \delta = \frac{\beta_3}{6|\beta_2|T_0}, \qquad N^2 = \gamma L_d P_0, \qquad \tau_R = \frac{T_R}{T_0},$$

while *A(z,t)* is the slowly varying pulse envelope as a function of distance and time respectively, β_1 is the propagation constant, β_2 is group-velocity dispersion and β_3 third order dispersion of the fiber, α is the absorption coefficient and γ is the nonlinear parameter, *s* is the self-steepening effect factor, T_R is the intra-pulse Raman scattering and

L_d is the dispersion length. The impact of Er^{3+} ions is given by the terms g_0, the gain, and d, the gain dispersion due to the frequency dependence of gain, and T_2 is the dipole relaxation time of Er^{3+} ions. P_0, T_0 and N are the peak power, pulse-width and soliton order of the initial pulse.

The NLSE is solved numerically using the Split-Step Fourier Method (SSFM) which is based on the assumption that over an infinitesimally small propagation distance the dispersive and nonlinear terms act independently. The impact of dispersion, gain and gain dispersion alone on a pulse from a previous step is calculated in the frequency domain over a small distance and the pulse is transformed into the time domain; the pulse is then acted upon by self-steepening Raman and nonlinear parameters over the same short distance in the time domain. This process is sequentially repeated over the length of the fiber. The fiber parameters are based on regular single-mode fibers with $T_R = 3$ *fs* $\beta_2 = -20$ *ps*^{2}*/ km,* $\beta_3 = 0.1$ *ps*^{3}*/km, and* $\gamma = 0.002$ *1/W-m,* $T_2 = 80$*fs;* and the parameters that are dependent on the initial fiber laser pulse are $P_0 = 238$ *W,* $L_d = 0.23244$*,* $T_0 = 68.18$ *fs;* $N = 0.332$ and the gain of the Er^{3+}-doped gain fiber, $g_0 = 10$ *dB.*

Figure 7.1(a) shows the pulse evolution along the length of a gain fiber affected by all the terms mentioned in equation (7.1). It can be seen that as the pulse propagates, it gains intensity and decreases in pulse-width simultaneously. This is a desirable characteristic for supercontinuum generation. The pulse gains a maximum intensity at ~2.5L_d and then it starts to split up; also beyond this point, the pulse shifts towards it trailing edge. Figure 7.1(b) shows the peak intensity attained by the pulse along the length of the gain fiber. We can clearly see that the pulse peaks at ~*2.5*L_d and then starts to lose peak power due to pulse breaking. Also the FWHM of this peak intensity profile

is about 8.1cm, which suggests that in the design of the EDFA, the length of the gain fiber is an important factor and it should be controlled with relatively high precision.

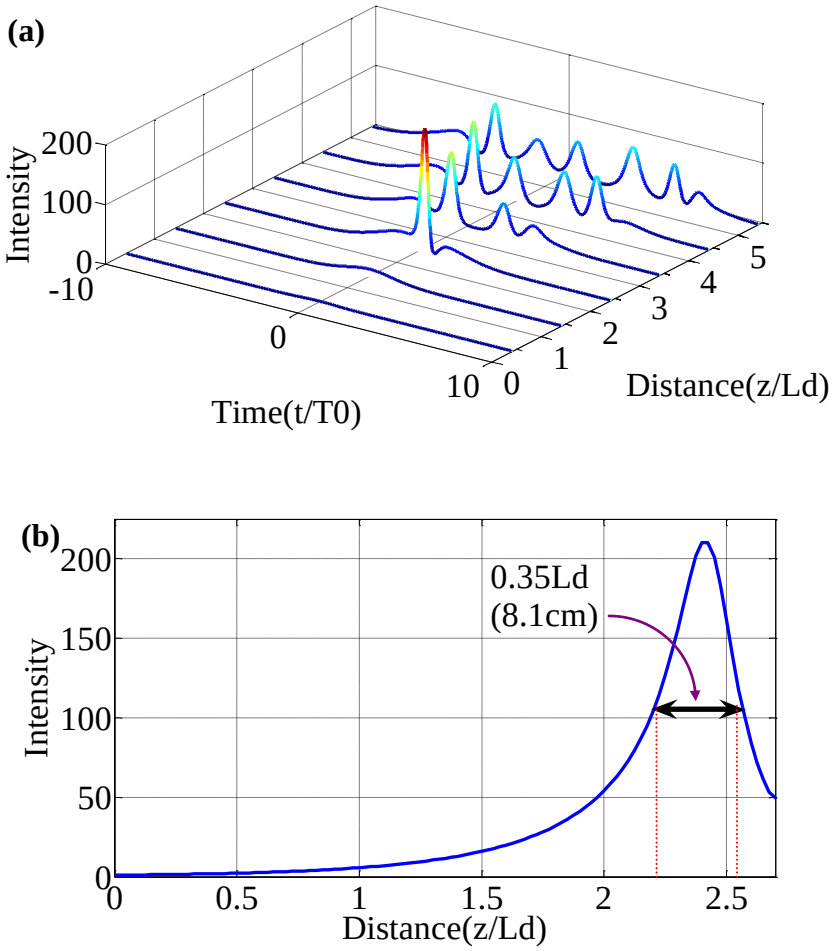

Figure 7.1 (a) Evolution of a femtosecond pulse in an optically pumped Er^{3+}-doped fiber. (b) Evolution of pulse peak intensity in a gain fiber. T_0 = 68.18 fs is the characteristic width of the initial sech pulse. L_d is the dispersion length (23.2 cm).

Pulses propagating in a medium are usually chirped. To use this to our advantage to achieve very intense and short pulses, a study was done to determine the type and amount of de-chirping to be applied to the amplified pulses. Also a study was done on the type and amount of pre-chirping to be given to the fiber laser pulses needed that would

give pulses with shorter pulse-width after amplification and de-chirping. Figure 7.2 summarizes the study results.

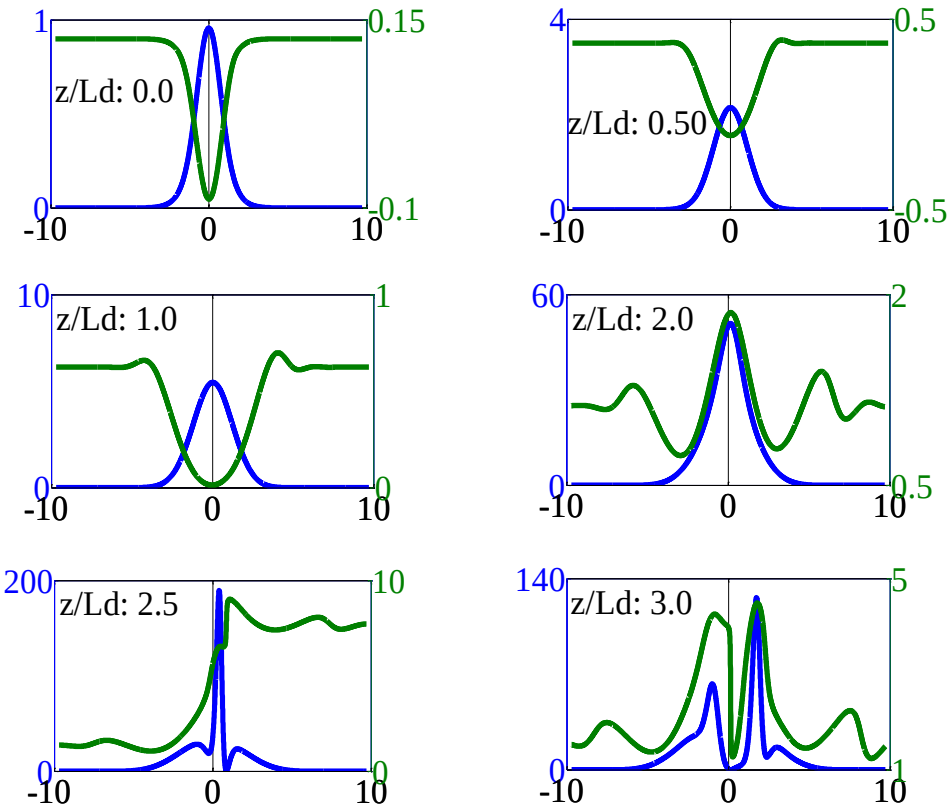

Figure 7.2 Pulse intensity and temporal phase at various propagation distances in the gain fiber. The initial pulse has negative pre-chirp generated through propagation in a single mode fiber. The change in the temporal phase indicates added positive chirp by the gain fiber.

The green curves in the pictures in Figure 7.2 are the instantaneous phase experienced by the pulse along the length of the gain fiber at intervals shown on the pictures. As shown, the gain fiber adds positive chirp to the pulse along the path of pulse propagation. The initial pulse considered here has a negative chirp after a propagation of in a regular single mode fiber.

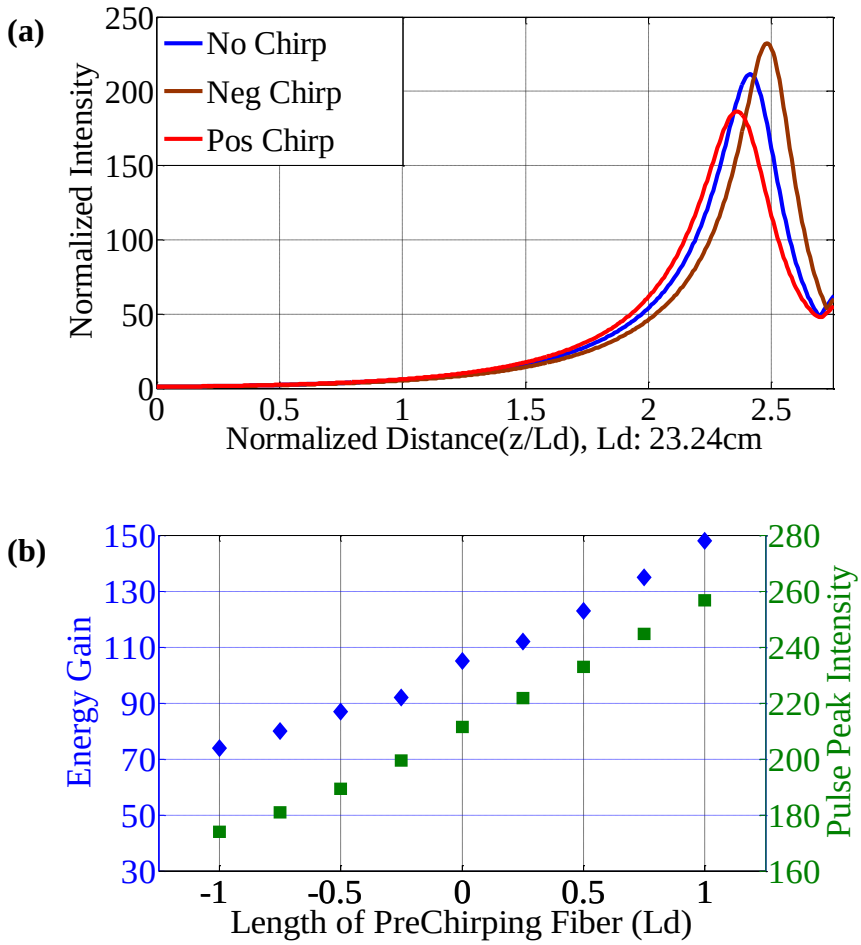

Figure 7.3 (a) Peak intensity evolution of the pulse in the gain fiber under different pre-chirping conditions. (b) Maximum peak intensity and energy gain *vs* pre-chirping values (represented here by the pre-chirping fiber length. Negative length corresponds to normally dispersive fiber.)

The negative linear chirp can be seen as the up-curving parabolic shape at the center of the pulse in the first figure in the first row. As we go along, the figures in the first row show the amount of distance the pulse has propagated in the gain fiber; the chirp gained seems to be more positive than the previous case. This increase in the chirp continues till the pulse starts to break up which happens at $2.5L_d$. This suggests that a negatively dispersive fiber should be used to compensate the positive chirp added by the

gain fiber during the amplification process. Then a study was done on how and what type of dispersion should be used to pre-chirp the input pulse to the gain fiber and how it would affect the pulse peak and the pulse-width of the pulse. Figure 7.3(a) shows that when the pulse is negative pre-chirped, it achieves higher peak values of amplification in the gain fiber and also at longer lengths of the gain fiber. Conversely if the pulse is pre-chirped positively, then the pulse amplification peak values are relatively smaller and also happen at shorter fiber lengths before the pulse splitting occurs. The case of not adding any type of pre-chirp to the pulse falls between these cases of positive and negative pre-chirp cases. Analyzing the data on these combinations relative to the energy gain and the pulse peak intensity against the length of the pre-chirping fiber is shown in Figure 7.3(b). It is interesting to know that as the length of fiber inducing positive pre-chirp increases, the amount of energy gain achieved and the peak intensity attained is less. Conversely when the length of the fiber inducing negative pre-chirp increases, the amount of energy gain achieved increases along with the pulse peak intensity.

7.3 Erbium Doped Fiber Amplifier

An Erbium Doped Fiber Amplifier (EDFA) was developed to amplify the femtosecond pulses from the fiber laser. The fiber laser (Precision Photonics FPL-1560) used as a source for femtosecond pulses emits pulses centered at 1558 nm with 24 pJ energy that are 120 fs (FWHM) wide at 90 MHz repetition rate. The aim is to amplify these pulses to an energy level about a few nJ. Figure 7.4 shows the schematic used for the EDFA built in the lab. Two possible configurations exist to pump the gain fiber. The first is with one pump either at the input or the output end of the gain fiber, termed co-directional and counter-directional pumping respectively; the other configuration is

pumping the gain fiber at both its ends, which is termed bi-directional method of pumping. Bi-directional pumping was used to pump the gain fiber and build the EDFA in this work.

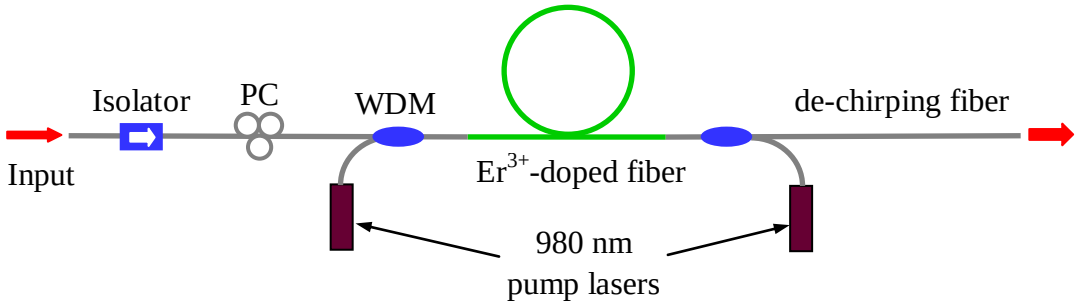

Figure 7.4 Schematic of an EDFA in a bi-directional pumping configuration. PC: Polarization Controller. WDM: Wavelength-Division Multiplexing

Erbium-doped fiber [ER80-4/125 from Thorlabs], doped with 4.8×10^{25} Er^{3+} ions per cubic meter, is used as the gain fiber and a 980 nm wavelength laser diode as the pump which gives 300 mW at 565 mA drive current. The fiber laser pulses were amplified to pulses with 6.2 kW peak power and 1.11 nJ energy.

An experimental study was performed to determine the amount of pre-chirping and de-chirping of the input and amplified pulses to obtain pulses shorter than 120 fs (FWHM). From the simulations, it has been learned that negative pre-chirping a pulse would add to more amplification. Based on this knowledge, three different amounts of pre-chirping were applied to the pre-amplified pulse using 1 m, 2 m and 3 m of single mode fiber (SMF-28). The amount of de-chirping from a single mode fiber (SMF-28) was changed in steps of 1 m to a total length of 13 m. A polarization loop controller (PLC) was used to tune the polarization mode of the pre-amplified pulse which would result in a better autocorrelation, at the output of the de-chirping fiber. For a fixed length

of de-chirping fiber, the loops in the PLC are rotated slowly to achieve a better autocorrelation, which is shown on a scope. There are three loops on the PLC and the first loop-slot on the PLC has one loop, the second loop-slot has two loops and the third loop-slot has three loops of single mode fiber (SMF-28) in them. This PLC was placed at the input end of the gain fiber, which controls the minimum length of the single mode fiber for pre-chirping, which is 1 m for this setup. This limits not having any pre-chirping less than 1 m of a single mode fiber. Using an in-line polarization tuner, a trial was done to check the influence of a polarization mode controller/tuner at the output end of the gain fiber. The study results have shown that tuning the polarization mode of the pulse at the output end of the gain fiber has no effect on the pulse shape as seen on the scope showing its autocorrelation. This clearly shows the polarization mode of the input pulse does affect the pulse shape and is primarily influenced by the gain fiber only. Among all the three cases of pre-chirping, the combination of a 2 m single mode fiber (SMF-28) for pre-chirping and a 9 m single mode fiber (SMF-28) seems to give a compressed pulse with 85 fs (FWHM).

Figure 7.5 shows the variation of the amplified pulse after compressed by the single mode fiber (SMF-28), for the same amount of pre-chirping mentioned above. As the length of the de-chirping fiber increases, the pulse-width of the amplified pulse oscillates, but with a steady decrease in its pulse-width. This decrease continues along to the de-chirping fiber length a little longer than 8.75 m and starts to increase. This increase continues, however, with the characteristic oscillations. So the combination mentioned above was selected to be used for all frequency reference transfer purposes.

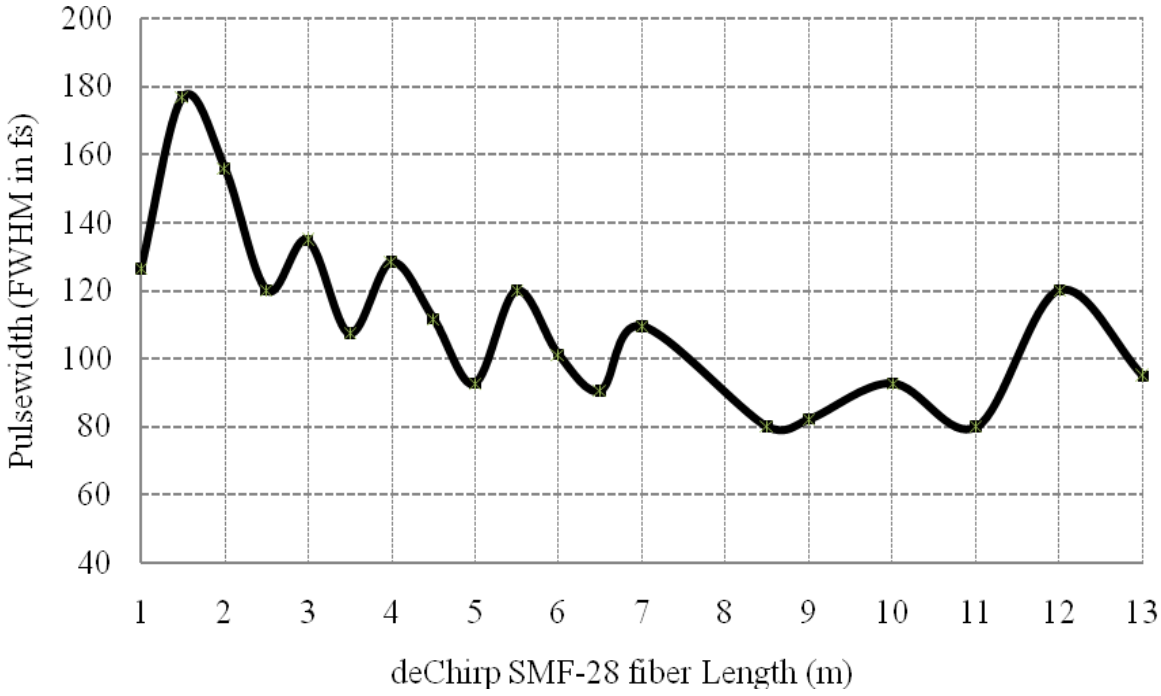

Figure 7.5 Variation of the pulse-width of the pre-chirped amplified pulse with change in the amount of de-chirping fiber after amplification. 2-m long single mode fiber (SMF-28) was used to pre-chirp the input pulse.

Figure 7.6 shows the spectrum of the amplified pulse for the pre-chirping and de-chirping mentioned above. Compared to the spectrum of the femtosecond pulse from the fiber laser source, it is clear that the spectrum has broadened by about 40 nm from 1558 nm, the central wavelength of the input pulse at the amplifier. Figure 7.9 shows the calibrated autocorrelation trace of the amplified pulse after de-chirping, with a femtosecond as the timescale. The autocorrelation results are processed by the PICASO software which gives the pulse shape and phase information.

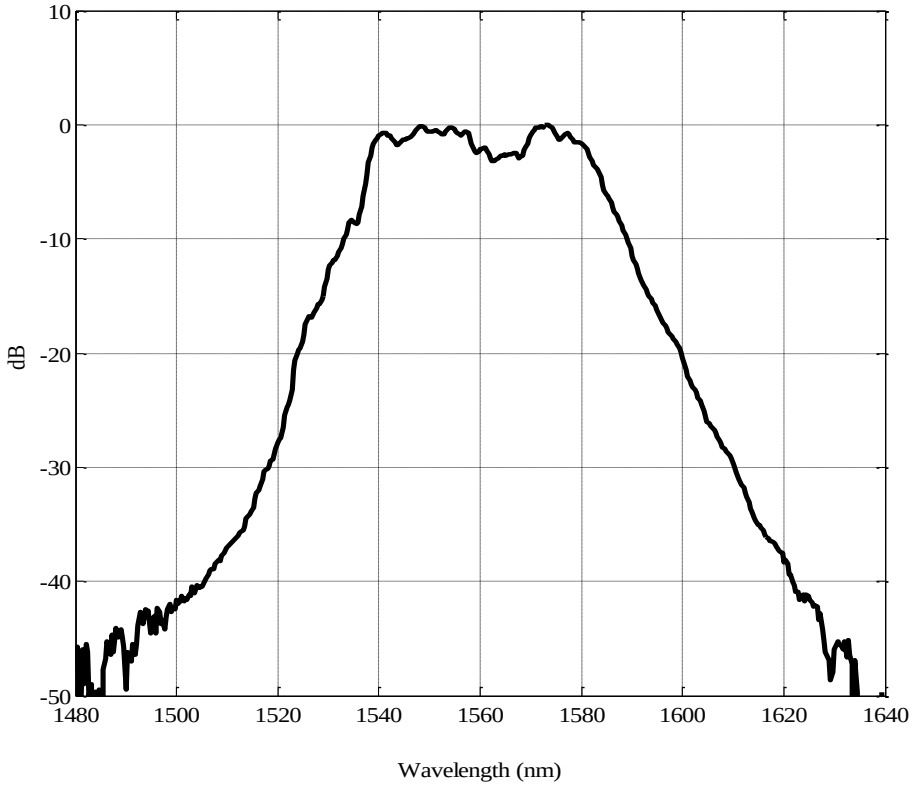

Figure 7.6 Spectrum of the femtosecond pulse amplified by the EDFA. The pulse was pre-chirped with 2 m and de-chirped using a 9 m single mode fiber (SMF-28)

This research work involves and requires the pulse-shape and phase information of the femtosecond pulses at the various stages that they are utilized. A number of measurement techniques such as FROG (Frequency Resolved Optical Gating) exist to measure and retrieve the characteristics of shorter pulses (Diels, 2006). An interferometric autocorrelator is a cost-effective instrument that can characterize femtosecond pulses; one was built to characterize the pulses involved in this work based on the Michelson interferometer configuration. The moving arm of the interferometer is computer controlled which gives it a very steady and repeatable velocity profile, and a

940 nm LED is used as a two-photon-absorption detector. Using pulse-shape and phase retrieval software PICASO, the autocorrelation data along with the spectrum obtained were analyzed for the characterizing the pulse-width and the phase of the pulses. Figure 7.7 shows the interferometric autocorrelator.

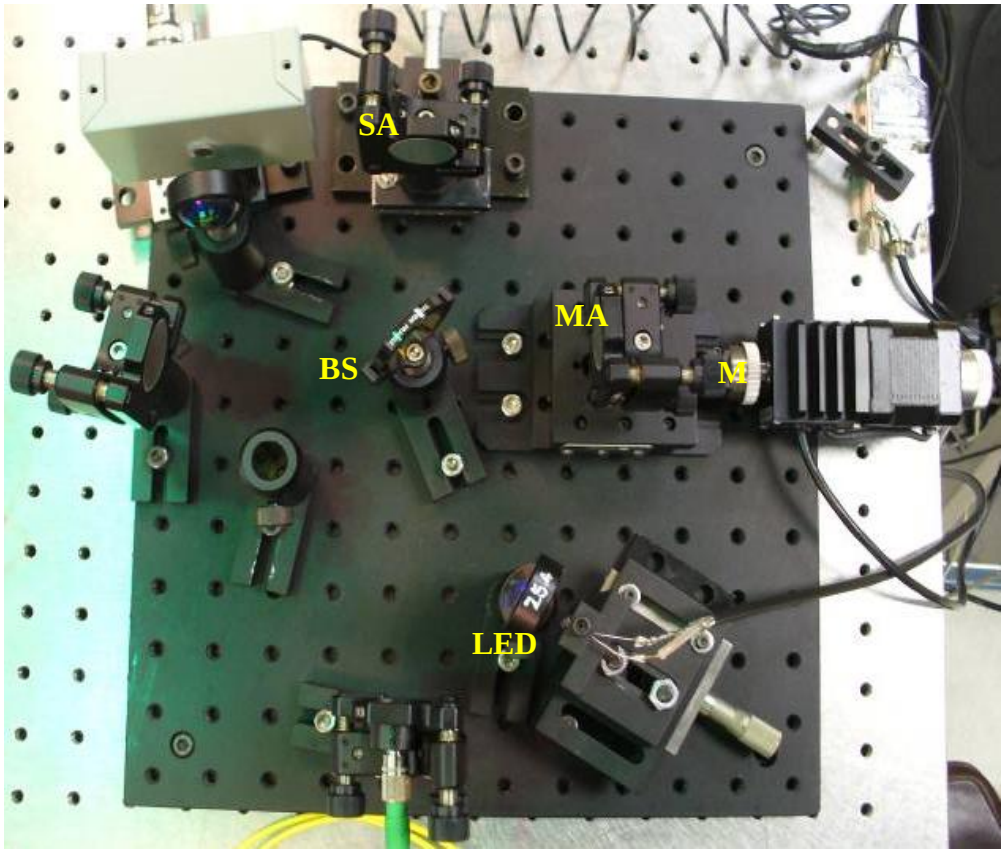

Figure 7.5 Interferometric Autocorrelator. SA: Stationary Arm, BS: Beam Splitter, MA: Moving Arm, M: Motor driving the Moving Arm.

Figure 7.7 (a) shows the autocorrelation of the femtosecond pulse from the fiber laser source, the autocorrelation sample and (b) the PICASO retrieved pulse-shape and phase information of the fiber laser pulse.

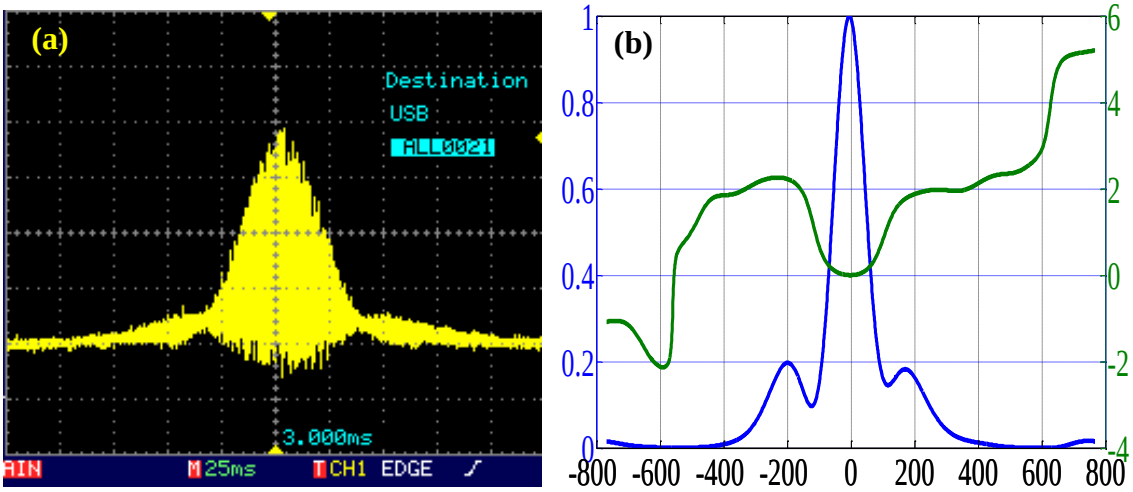

Figure 7.8 (a) Fiber laser pulse autocorrelation sample. (b) Intensity and phase information vs time in fs, retrieved using the PICASO program

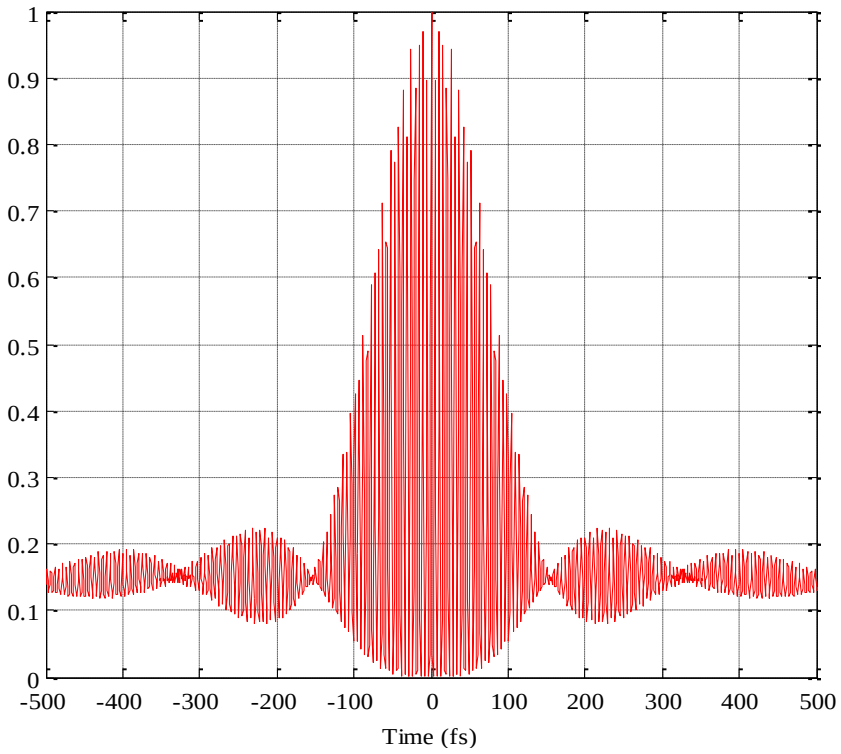

Figure 7.9 Autocorrelation trace of the amplified pulse

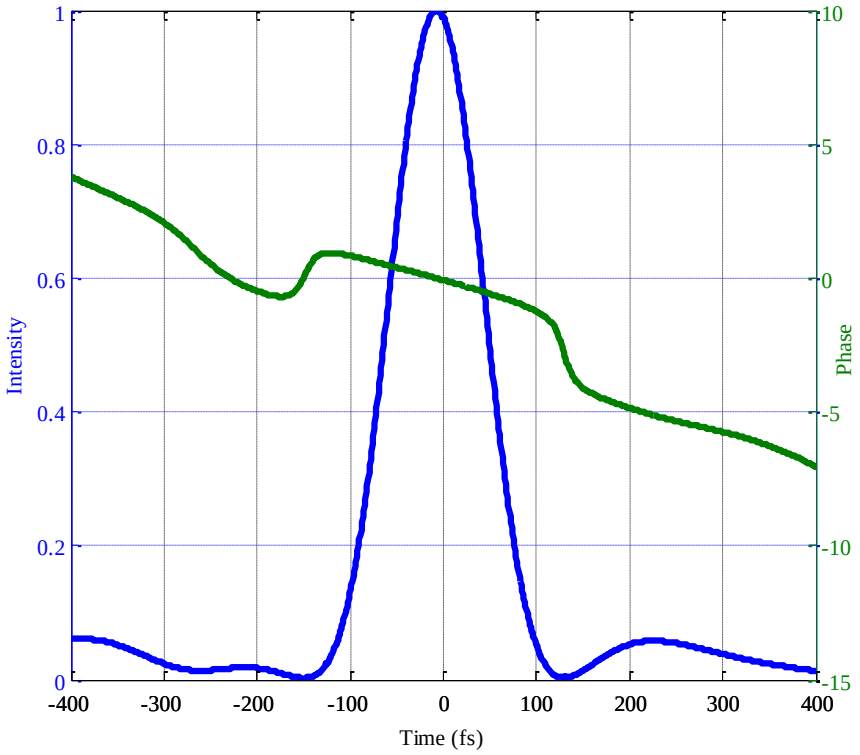

Figure 7.10 Characteristics of the amplified and subsequently compressed pulse obtained with 2 m pre-chirping and 9 m de-chirping.

Passing these short pulses through 2m long PCF, a “supercontinuum” spanning from 1160 nm to 1780 nm was generated, which is shown in Figure 7.11. It is encouraging to see that the spectrum appears to extend beyond 1800 nm; however, limited by the spectral range of the optical spectrum analyzer, this part of the spectral data was not collected.

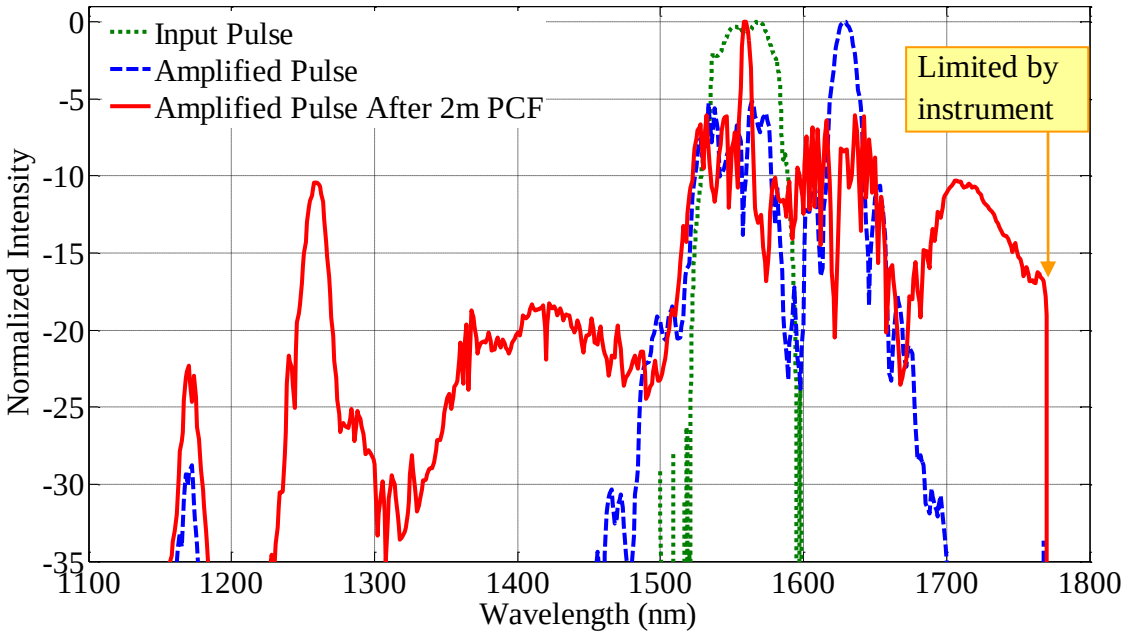

Figure 7.11 Spectrum comparison. Green dot: Input fiber laser; Blue dot: EDFA amplified pulse; Red solid: Amplified pulse after propagating 2m in the PCF

7.4 Results and Summary

A phase coherent supercontinuum was generated spanning from 1160 nm to 1780 nm. Numerical studies were performed to study the femtosecond pulse evolution in a gain medium, such as the EDFA, solving the Nonlinear Schrodinger Equation (NLSE) using the Split-Step Fourier Method (SSFM) implemented using MATLab software. The study of the instantaneous phase evolution gave insight to the way the phase evolves in the gain medium and how the type of pre-chirping affects the pulse evolution. The simulations revealed that negatively pre-chirping the pulses causes them to travel longer in the gain medium, thereby causing them to attain higher gain level before the pulse splitting occurs. However, positively pre-chirping causes the pulses to travel a lesser distance in the gain medium and attain lesser gain before pulse splitting occurs. The simulations show that right before the pulse split occurs, the phase of the pulse attains a

characteristic sharp edge. This information can be used to realize the position along the length of the gain medium when the pulse split occurs and achieve the maximum attainable gain. An EDFA was built in the lab to amplify the lower power femtosecond pulses from a commercial fiber laser (Precision Photonics FPL-1560). The 120 fs (FWHM) pulses with 4 mW average power at a 90 MHz repetition rate were amplified to ~ 110 mW average power and also compressed to 110 fs (FWHM) pulses using a combination of pre-chirping and post-chirping the amplified pulses from the EDFA, using a single mode fiber (SMF-28).

Chapter VIII

ATMOSPHERIC DELIVERY OF MICROWAVE CLOCK

8.1 Introduction

In optical communications, bits are encoded on an optical signal at microwave frequencies and an error-free recovery of the information bits at the receiver requires a precise microwave clock. In a scenario of multiple receivers in a short-distance optical communications system, the availability of a high precise microwave clock would enable recovery of the transmitted information bits with less error. This situation may be addressed with microwave clock distribution to multiple receivers via the atmosphere. A microwave clock signal is used as the reference frequency in the field of navigation; for synchronization purposes, a highly precise clock enables high precision in navigating objects. The ability to transmit the microwave clock with the highest precision to many such objects would be an asset. Using an FFC, a microwave clock can be transmitted via the atmosphere which can be recovered at the receiver using a fast-photodiode. This chapter addresses this question, "What are the precision and the fractional stability with which a microwave frequency reference can be transmitted via the atmosphere?"

8.2 Experimental Setup for Microwave Clock Transmission

The experimental setup is located on the rooftop of the Optics Building, on the campus of the University of Alabama in Huntsville. This building has four floors and an observatory room on the fifth floor with an open rooftop, and this rooftop space has no

other equipment to cause any hindrance, an ideal space to perform an atmosphere related experiment, as shown in Figure 8.1.

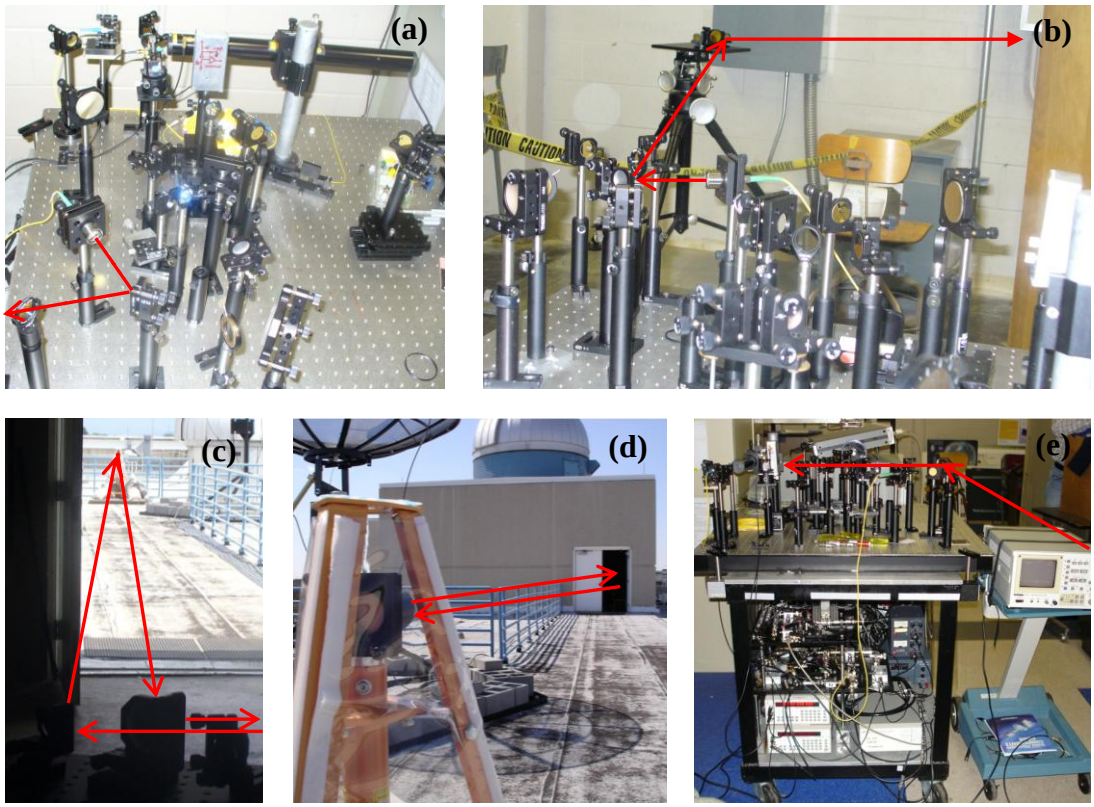

Figure 8.1 Pictures showing the experimental setup on the rooftop of the Optics Building in the University of Alabama in Huntsville campus. The red line indicates the path taken by the optical pulse as it propagates through the atmosphere and reaches the photodetector. (a) This picture shows the optics comprising of the beam launcher to the atmosphere, which also includes the receiving optics and the detector for the optical beam coming back after propagation through atmosphere. (b) This picture shows the intermediate tripod that diverts the beam onto the mirror out in the atmosphere. (c) This picture shows the mirrors on the intermediate tripod and also the reflecting mirror out in the atmosphere. (d) Here we can see the mirror out in the atmosphere that receives the launched optical beam and reflects it back to the receiving optics. This provides an overall two-path transmission. The distance of the reflecting mirror to the edge of the room shown here is approximately 60 m. (e) Here is the setup for the receiving optics, the photodetector and the electronics used for the frequency characterization of the received optical beam that has propagated through the atmosphere.

The laser source, the optics and the electronics are housed in the observatory room. A 2 inch diameter mirror located at the one end of the open space at about 30 m from the edge of the observatory room provides a total round trip distance of 60 m for our experiment purposes. A commercial fiber laser is the source of the frequency comb used in all the experiments. The pulses are 120 fs wide at FWHM, at a 90 MHz repetition rate with an average power of 4 mW. These pulses are amplified by the EDFA to 110 mW and passed through a 70:30 fiber coupler. The smaller portion (30%) of the laser pulse is collected by a fast photodetector, PD1, and used as the reference signal. The large portion (70%) of optical power from the fiber coupler is collimated to an optical beam that is 7 mm diameter wide and launched into the atmosphere. The 2 inch mirror at the other end of the open space reflects this launched beam back to the optics located in the housing room. The incoming beam is collected by the receiving optics and focused on a fast photodetector, PD2.

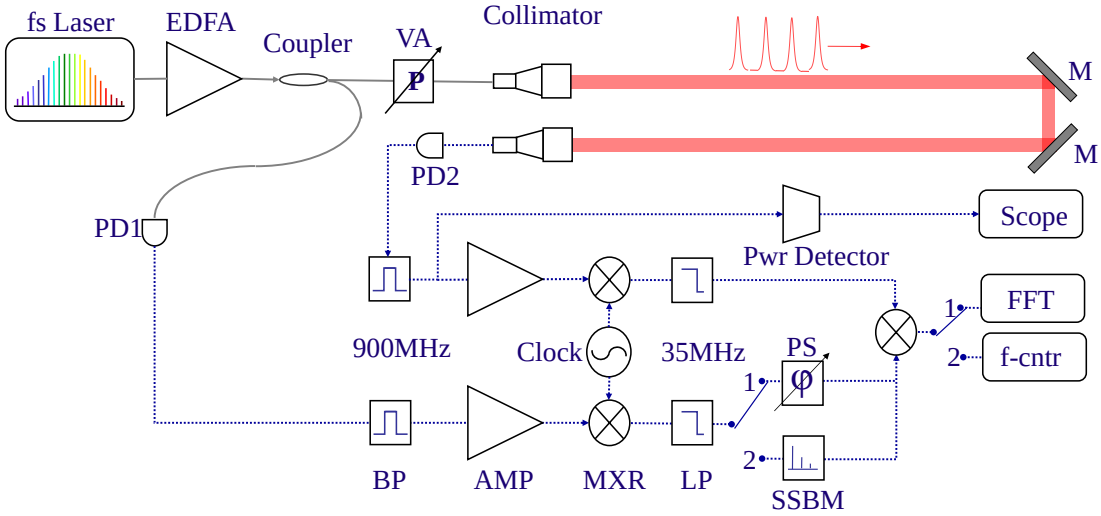

Figure 8.2 Preliminary experimental schematic for outdoor microwave clock transmission system. AMP: microwave amplifiers, BP: band-pass filters, EDFA: erbium-doped fiber amplifier, LP: low-pass filters, M: silver mirrors, MXR: mixers, PD: photodetector, PS: phase shifter, and VA: variable attenuator.

Both the reference and the transmitted signals are filtered to select the 10^{th} harmonic of the fundamental repetition rate of the source laser, i.e., 900 MHz, which forms the central frequency for noise characterization. As the RF electronic filters we used were not efficient to filter the adjacent harmonics, with a clock generator (SRS CG635) used as a local oscillator, both the reference and the transmitted signals are mixed down to 35 MHz, and, at this frequency the other frequencies were filtered out. In the phase noise characterization, both the reference signals and transmitted signals are mixed in-quadrature using a double-balanced mixer, producing a dc signal proportional to the phase difference between the two signals. This signal is frequency analyzed using a Fast Fourier Transform (FFT) analyzer (SRS SR785). For the Allan deviation measurement experiment, the reference signal is frequency-shifted to 500 kHz by a single side-band modulator (SSBM) and mixed with the transmitted signal. The resulting beat-note is analyzed by a frequency counter (SRS SR620) to measure the root Allan variance. All the clocks used in the experiment are locked to an Rb-disciplined crystal oscillator (SRS FS725).

8.3 Phase Noise Measurements and Results

The phase noise measurements were done between mid-October 2009 and the first week of January 2010 under various weather conditions such as hot and cold, calm and a little windy climates and also both during the night and day times, except for foggy and rainy conditions. The preliminary phase noise measurements in terms of the timing jitter are shown in Figure 8.3; the primary axis shows the excess phase noise and the secondary axis shows the total RMS timing jitter integrated from 1 Hz to 100 kHz. It is seen that the excess phase noise is above the system noise level below the 1 kHz

frequency, and is nearer to the system noise above 1 kHz. The excess phase noise below 100 mHz is between 10,000 $\frac{fs}{\sqrt{Hz}}$ and 100,000 $\frac{fs}{\sqrt{Hz}}$. The corresponding integrated RMS timing jitter is as large as 14 ps and is near the 10 ps value. Based on the knowledge from the indoor clock transmission studies (Alatawi, 2009), the integrated RMS timing jitter in the order of tens of picoseconds is a larger value that can be expected for a 60 m propagation distance in the open atmosphere. This large excess phase noise indicates the presence of other mechanisms that might be causing this excessive phase noise.

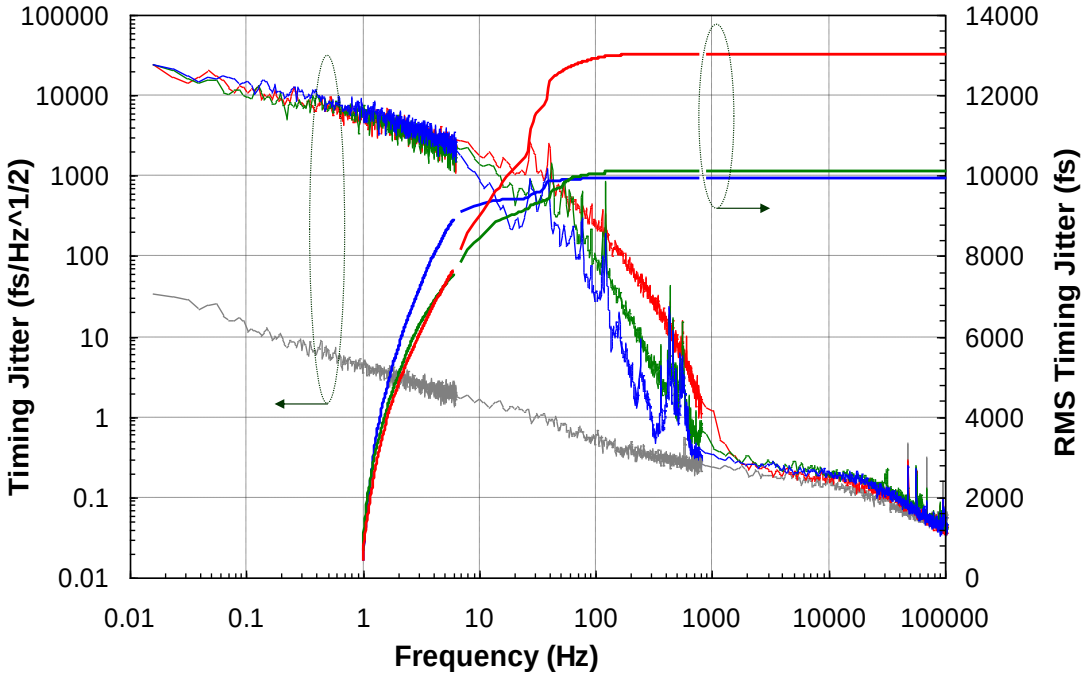

Figure 8.3 Preliminary excess phase noise measurements of microwave clock transfer via atmosphere in terms of timing jitter shown on the primary axis, with a scale larger than 10,000 $\frac{\mathbf{fs}}{\sqrt{\mathbf{Hz}}}$ and the corresponding integrated RMS timing jitter shown on the secondary axis with scale larger than 10,000 fs.

Usually in the experiments of coupling light into a fast photodetector, it is common to see the space and time-dependent fluctuations in the optical power received

by the detector, couples as phase variations as perceived by the detector, known as amplitude-phase modulation. As our final analysis is based on the amount of phase variations seen by the mixer, this optical power fluctuation induced phase noise contaminates the actual phase noise that we need to measure. The large phase noise measured in the preliminary results raises the issue of this kind of phase-coupling at the detector. This stems from the reason that in the initial setup, where the transmitted signal was fiber-coupled to the detector using a fiber-collimator. To ensure that this kind of phase coupling does not happen in our system, a study was performed to measure the correlation between the phase and the power of the transmitted clock, the coherence between the phase and the power versus frequency of the transmitted signal was measured.

The coherence function is defined as

$$C_{yx}(f) = \frac{\Phi_{yx}(f)}{\sqrt{\Phi_{yy}(f).\Phi_{xx}(f)}}, \tag{8.1}$$

where $\Phi_{xx}(f)$ and $\Phi_{yy}(f)$ are the power spectral densities of time series x and y as functions of fourier frequency f, and $\Phi_{yx}(f)$ is the cross-power spectral density between the two series.

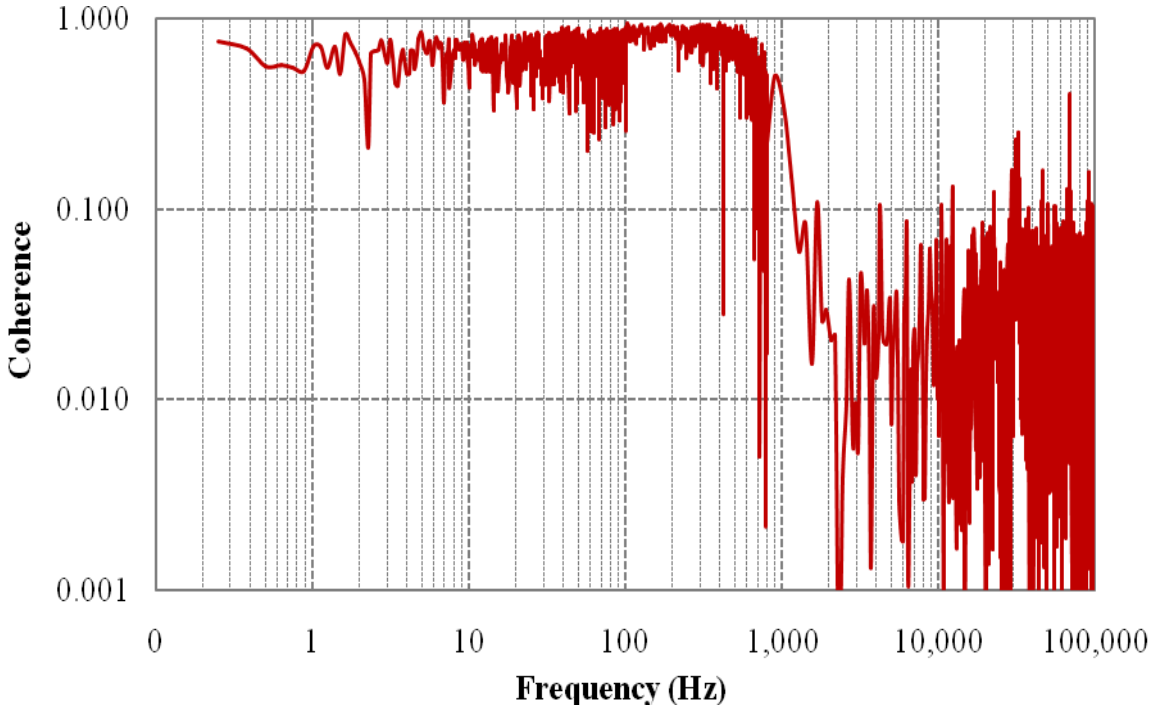

Figure 8.4 Coherence function, showing the high degree of correlation between the power and the phase of the transmitted signal (Gollapalli, 2010).

The measured coherence function is shown in Figure 8.4. In this graph we can see that the coherence function is close to unity below 1 kHz which indicates a high degree of correlation between the phase and the power. Above 1 kHz to 100 kHz, we see the coherence function is close to zero due to the reason that the phase noise is below the system noise. The strong correlation is confirmed by the time domain plots of the power and the phase of the clock signal recorded simultaneously, as shown in Figure 8.5. It may be said that this large correlation is caused by large fluctuation of the optical power and the power-to-phase coupling of the photodiode. This large power fluctuation is possibly caused by the beam wandering and the speckle, and in-effect, to minimize the power fluctuations, the receiving system should be modified.

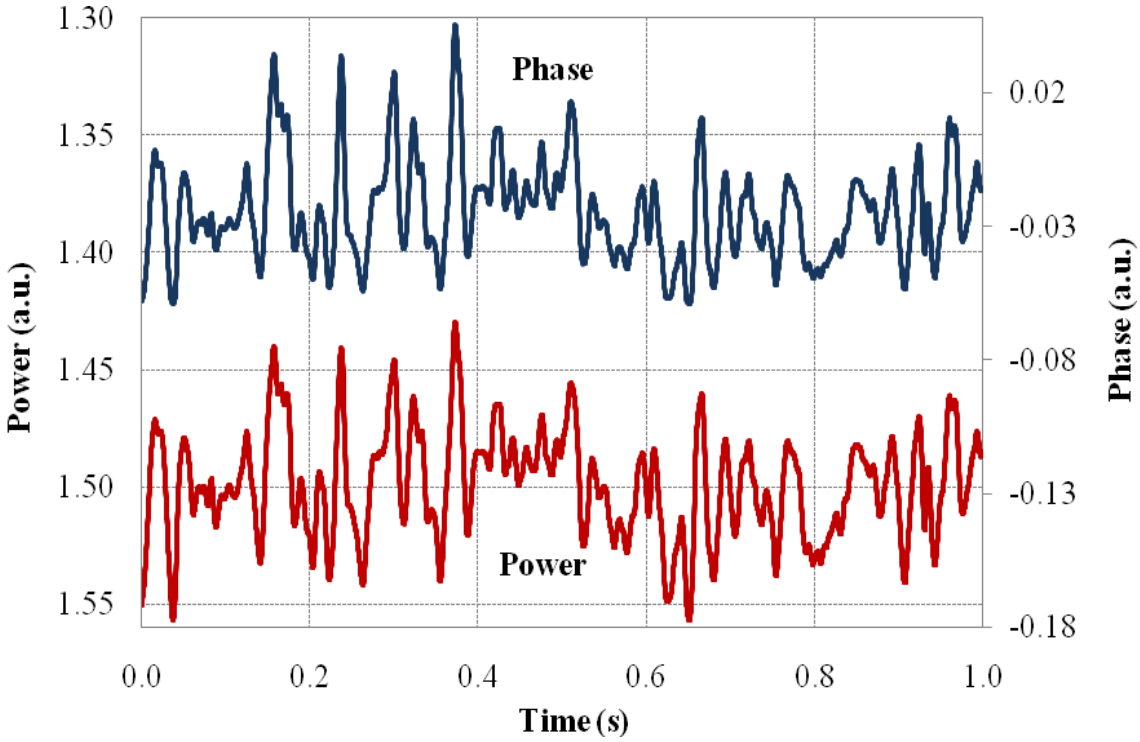

Figure 8.5 Time-domain measurement of instantaneous phase and power of the received signal. Clear correlation between phase and the power can be seen, implying a strong power-to-phase conversion.

As mentioned earlier, the previous receiving system uses a collimator to collect the transmitted signal. The fiber collimator requires precise beam alignment and mode-matching in order to achieve optimum coupling. When beam wander & speckle are present, such conditions cannot be always met. So the optical power coupled into the fiber suffers large fluctuations, and so the fiber coupler was replaced. Using large diameter optics and also focusing the beam tightly onto the photodiode, the size of the focus was made smaller than the active area of the photodiode. This effectively increases the receiving aperture making the receiving system more tolerant to the beam fluctuations. The modified setup is shown in Figure 8.6 and the highlighted looking part

of the setup is where it shows the use of a focusing lens to focus the beam tightly onto a detector. Also as the commercial photodetector can only be used in combination with a fiber collimator to collect light, it was replaced with a lab-made detector, which is shown in Figure 8.7.

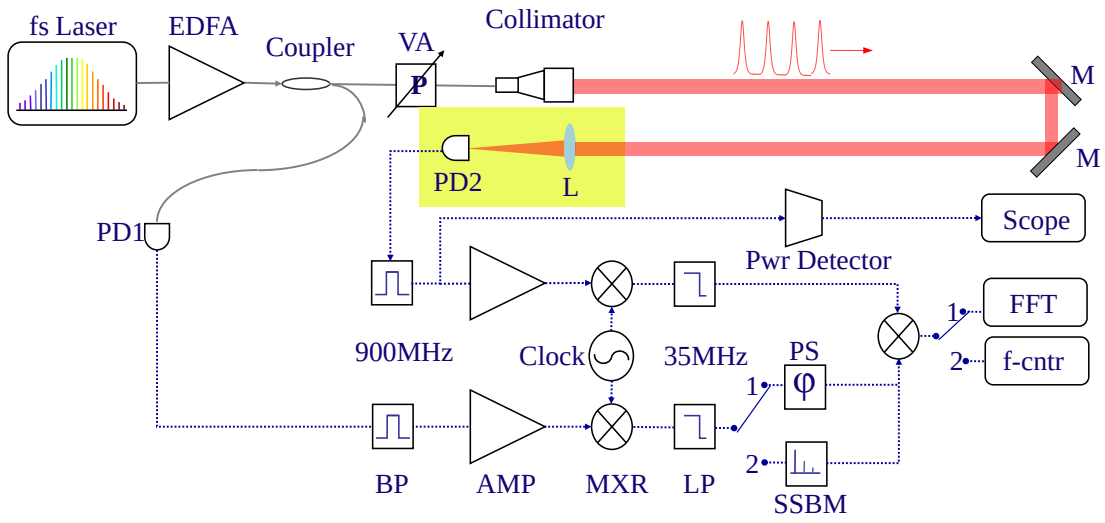

Figure 8.6 Modified schematic of the outdoor transmission test system, where the fiber collimator and commercial PD2 combination is replaced with the focusing lens and home-made photodetector. AMP: microwave amplifiers, BP: band-pass filters, EDFA: erbium-doped fiber amplifier, LP: low-pass filters, M: silver mirrors, MXR: mixers, PD: photodiode, PS: phase shifter, and VA: variable attenuator

With this modified setup, the coherence between the power fluctuations and the excess phase noise was measured, which is shown in Figure 8.8. The top plot shows the phase noise and the bottom plot shows the coherence both measured simultaneously. It should be noted that the coherence is nearer to zero just below 100 Hz, with some residue from 300 – 500 Hz, and again nearer to zero above 1 kHz where the phase noise is below the system noise.

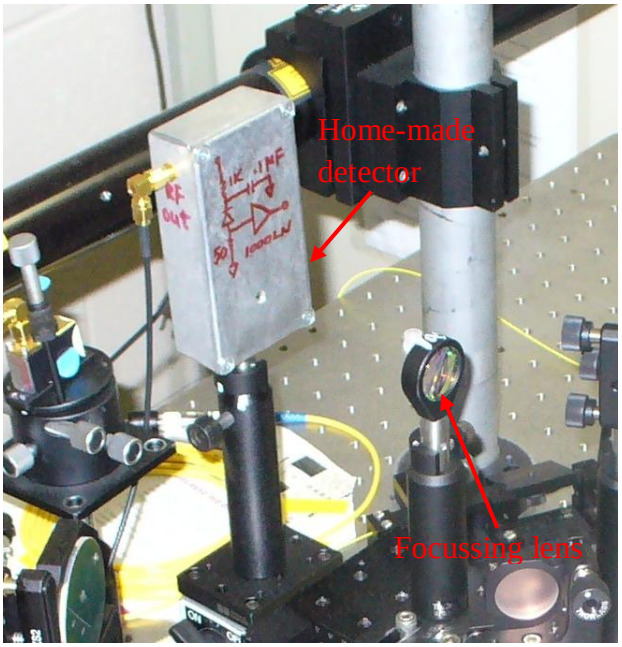

Figure 8.7 Home-made photodetector shown along with the focusing lens.

The nearer to zero coherence implies reduced power-to-phase coupling, and the new value is less compared to the previous case with this modified receiver system. Even though we have some residue at around 400 Hz, fortunately starting at this frequency, the phase noise rolls down to the system noise level and it will be shown that this coherence would not impact the RMS jitter significantly. Based on this data, it can be asserted that the excess phase noise now measured would be caused by the transmission medium and not the receiver system.

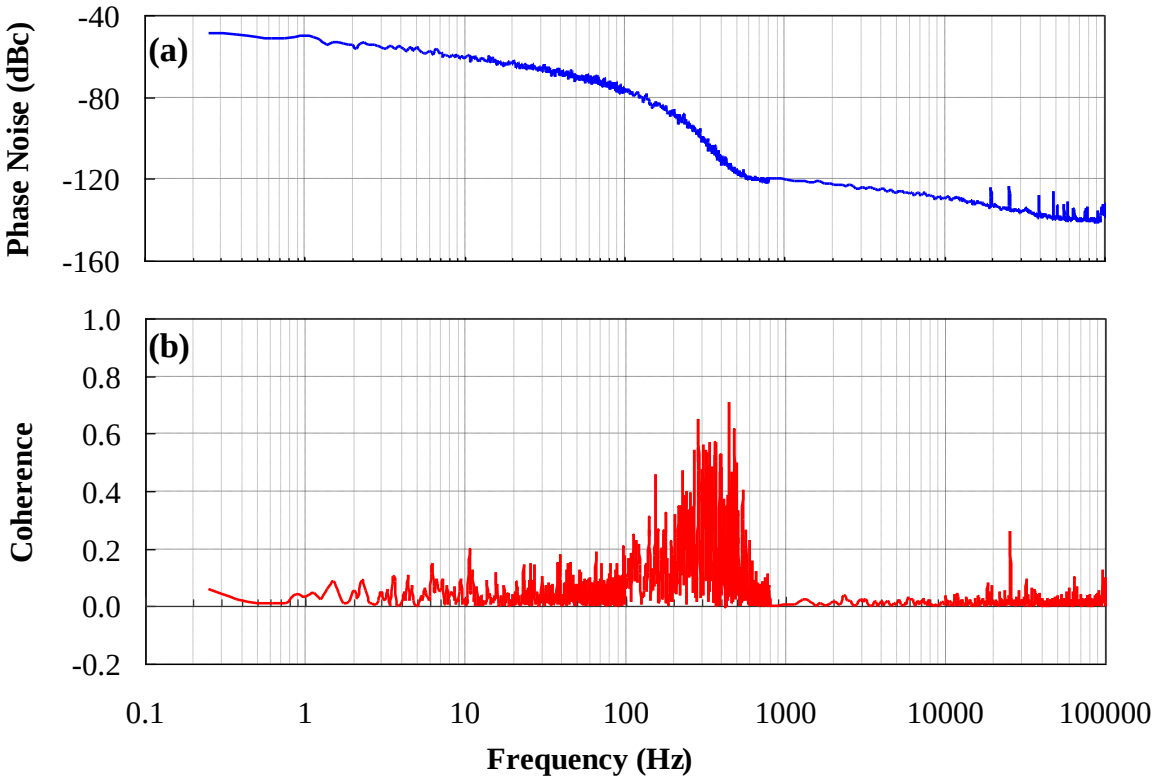

Figure 8.8 (a) The excess phase noise measured simultaneously corresponding to the coherence shown in (b). (b) Coherence between the power and the phase of the transmitted signal obtained with the modified receiving system.

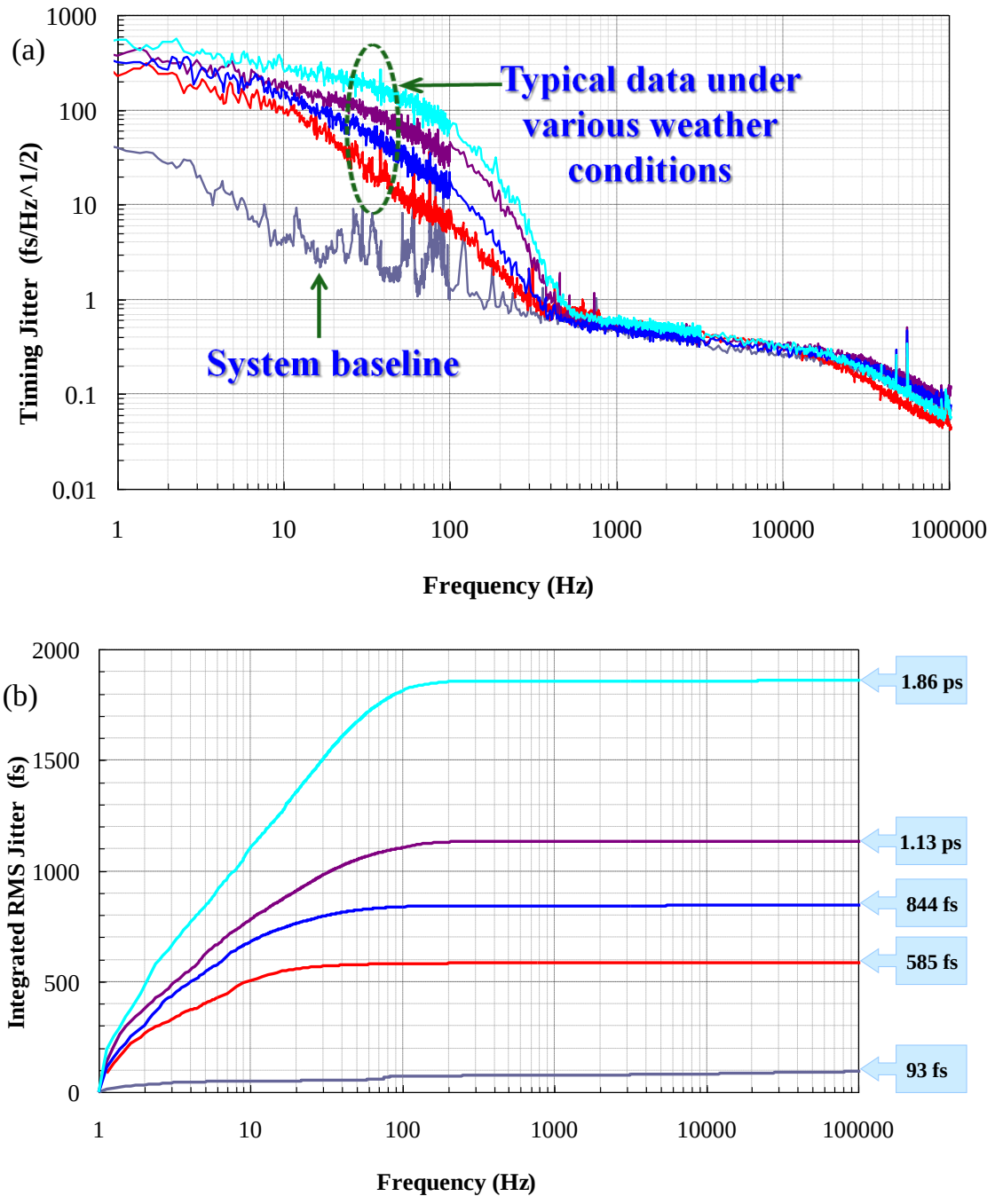

Figure 8.9 Excess phase noise obtained with the modified focusing lens-homemade detector combination. The value of the timing jitter value at 1 Hz has improved from a scale above 10,000 $\frac{\mathbf{fs}}{\sqrt{\mathbf{Hz}}}$ to less than 1,000 $\frac{\mathbf{fs}}{\sqrt{\mathbf{Hz}}}$. Also shown is the system baseline and different phase noise spectra under various weather conditions. (b) Integrated RMS jitter improved from a scale larger than 12 ps to smaller than 2 ps in the largest case. Curves of different curves here correspond to the same cases of weather conditions shown in (a).

8.4 Allan Deviation Measurements

The long term stability characterization of the microwave clock transfer via the atmosphere over a 60 m round-trip propagation was done by measuring the Allan deviation from 1 s to 500 s sampling time. The fractional stability at 1 s sampling time was measured to be ~ 3 x 10^{-12}, and the measurements are shown in Figure 8.10. The data curve follows a τ^{-1} behavior which signifies the influence of white phase noise, as shown in Table 3.1, and this behavior is different compared to the microwave clock transfer over a fiber-optic network where it has $\tau^{-1/2}$ behavior (Foreman, 2007).

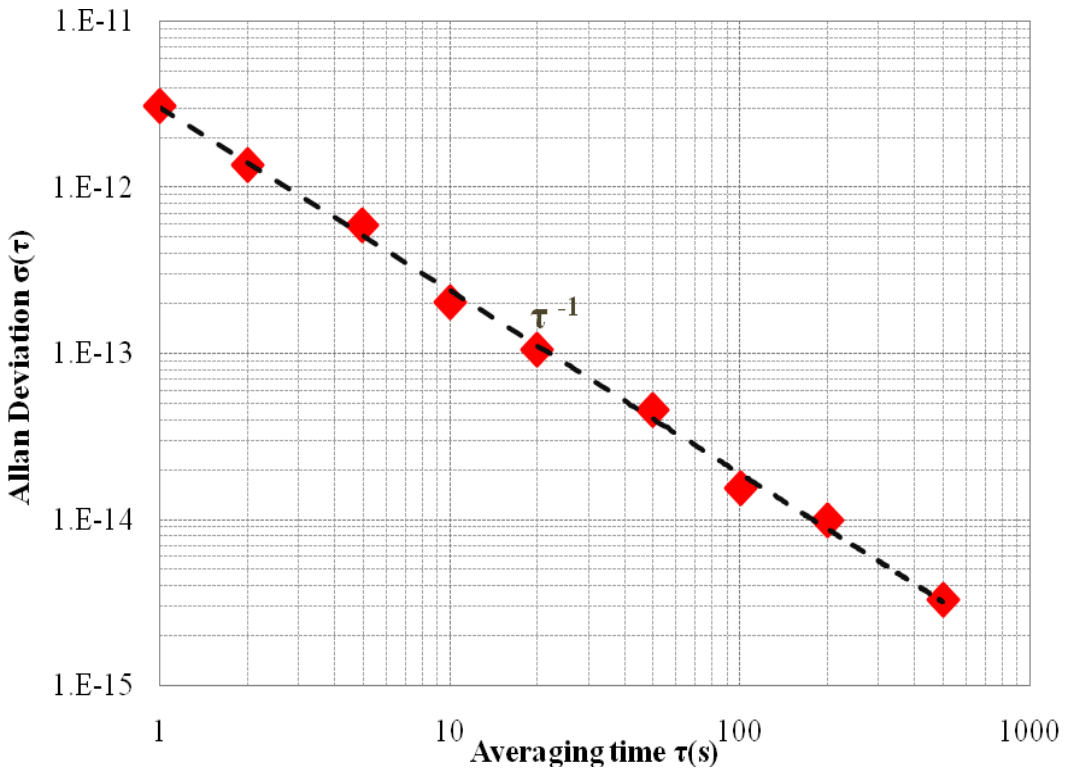

Figure 8.10 Allan deviation *vs* averaging time giving the long-term stability of the microwave clock transfer. The fractional stability is 3 x 10^{-12} at 1 s averaging time with a τ^{-1} behavior (Gollapalli, 2010).

8.5 Comparison of RMS Jitter Values with Values from Theoretical Models

The propagation of an optical pulse train through an atmospheric communication channel is susceptible to the refractive-index fluctuation caused by clear-air turbulence. Such influence has been observed and the wind speed is found to be the prominent factor affecting the amount of excess phase noise. A quick comparison can be made from the calculations based on the group index of the transmission medium, the air. From the RMS timing jitter, we can derive the RMS fluctuation of the group index n_g, using the relation

$$\Delta n_g = \left(\frac{c}{L}\right)\Delta T, \tag{8.2}$$

where c is the speed of light in a vacuum, L is the total propagation distance, and ΔT represents the RMS timing jitter of the FFC.

Using $\Delta T = 2\ ps$ and $L = 60\ m$, the value of Δn_g is calculated to be 1 x 10^{-5}. Meanwhile, it has been shown that

$$\Delta n_g \approx a \cdot \Delta n, \tag{8.3}$$

where Δn is the fluctuation of the phase index and the proportional constant a is approximately equal to 3 in the visible and near infrared wavelength range. This leads to an estimated RMS phase index fluctuation of several parts per million, which agrees with the well-known scale of such fluctuation due to clear-air turbulence.

Based on the discussion from 5.3, the pulse-arrival jitter can be calculated based on theoretical models. The elevation at which this research work on the frequency reference transfer was performed is considered ground-level transmission and also the propagation of the optical pulse-train is in horizontal direction, for which the typical

values of C_n^2 range between 6 x 10^{-13} $m^{-2/3}$ and 1 x 10^{-13} $m^{-2/3}$. With the outer scale of turbulence, $L_0 = 100\ m$, propagating a pulse-train consisting with pulses of 70 ps pulse-width over 60 m in the atmosphere, using equation (5.5), the root variance in the pulse-arrival jitter is calculated to vary from 0.337 ps to 0.822 ps. As shown in Figure 8.9(b), the integrated RMS timing jitter varies from 0.585 ps to 1.821 ps. This integrated jitter is actually twice the statistical variance given by equation (5.5) and so in comparison it varies from 0.292 ps to 0.9 ps, which is the range of the RMS timing jitter values shown in Figure 8.9(b). It is clearly seen that the integrated RMS timing jitter values calculated from the measured excess phase noise acquired by a microwave clock agree with the numerical values suggested by the theoretical models of pulse propagation through turbulent atmosphere.

8.6 Summary and Discussion on Microwave Clock Delivery

The microwave clock transfer via the atmosphere is influenced by weather elements, prominently, wind, temperature and humidity. Based on the complexity of the uncontrolled weather elements, a numerical relation between the excess phase noise and the wind, temperature or humidity, however, a qualitative conclusion can be made. The clock transfer is primarily influenced by the wind and higher the wind speed, the excess the phase noise measured. This can be understood from the scenario in which the wind packets would change the effective transmission link, working as phase modulator causing jitter in the pulse arrival time causing larger excess phase noise during gusty wind conditions. The optical receiving system has a major role, drastically influencing the scale of the excess phase noise measured, as optical beam wandering spatially can channel into phase noise through power-to-phase coupling. This receiving system

induced phase noise can be effectively reduced by increasing the receiving aperture. By minimizing the power-to-phase modulation due to the optical receiving system, the timing jitter was reduced from a scale larger than 10,000 $\frac{fs}{\sqrt{Hz}}$ to a scale below 1,000 $\frac{fs}{\sqrt{Hz}}$ under various weather conditions. Correspondingly the integrated RMS timing jitter, integrated from 1 Hz to 100 kHz, varies from 0.6 – 2 ps under various weather conditions over 60 m round-trip distance. The fractional instability is 3 x 10^{-12} at 1s averaging time. The Allan deviation has τ^{-1} dependence from 1 s to 500 s (*vs.* $\tau^{-1/2}$ in fiber) indicating white phase noise influence. Under the lab conditions, over 10 m effective transmission distance, the integrated RMS timing jitter was 95 fs and the root Allan variance over 1 s was 4 x 10^{-13}. Under the same lab conditions, the projected values for RMS timing jitter for 60 m transmission distance was ~600 fs. This value compared to an effective 60 m round-trip propagation distance via the atmosphere indicates many random processes in the atmosphere are dominated by the refractive index fluctuations, temperature, wind speed, humidity, etc. With all this said, the important question is, "why and how is this important?" Based on currently published reports; over a fiber-optic network, a microwave clock was transferred over 7 km distance with a stability ~3 x 10^{-14} at 1 s averaging time. Using CW laser modulation technique, a microwave clock was transferred via atmosphere over 100 m with a stability ~1.31 x 10^{-10} at 1 s averaging time. By transferring a microwave clock using an optical frequency comb over 60 m transmission distance via atmosphere, the fractional stability accomplished with our system is 3 x 10^{-12} at 1 s averaging time (Sprenger, 2009). The obtained stability is nearly two orders of magnitude better than the CW modulated microwave clock transfer;

however, in this work, the propagation distance is a little longer than half the propagation distance of the mentioned work (Sprenger, 2009). Moreover, the Allan deviation has a τ^{-1} dependence, indicating that with longer averaging time, we can reduce the fractional instability faster than possible with clock transfer over a fiber-optic network where there is a $\tau^{-1/2}$ dependence. With this result, with confidence we can claim that transfer of a microwave clock via the atmosphere over short distances lesser than a kilometer range, is feasible and meets the expected and accepted stability levels.

Chapter IX

ATMOSPHERIC DELIVERY OF OPTICAL FREQUENCY REFERENCES

Atomic optical clocks have stability in the order of 10^{15} at 1 s averaging time; the ability to transmit and distribute this clock information would enable many applications in various fields. A femtosecond frequency comb can be used to transmit optical frequencies, enabling locking of lasers to the highest precision. The field of high precision spectroscopy, synchronizing system components and comparison of atomic clocks all would benefit from the availability of high precision frequency references. Such precise frequency references may be distributed by remote delivery of a femtosecond frequency comb via the atmosphere. This chapter addresses the question of the type and amount of frequency stability that may be achieved when an optical frequency reference is remotely delivered via the atmosphere over short distances.

9.1 Optical Heterodyning Technique

Study of frequency stability with transmission of frequency references involves measuring the optical phase fluctuations the optical pulse undergoes as it travels through a transmission medium. Photodetectors are usually sensitive to the intensity, but insensitive to the optical phase. The mixing of an optical field with a coherent reference optical field of stable phase and detecting the beating signal of these two interfering optical fields provides the information related to the amplitude and phase of the signal

field. This technique is called *"optical heterodyning," optical mixing," "photo-mixing," "light beating"* or *"coherent optical detection."* A schematic of such a technique is shown in Figure 9.1.

Let the optical field of the signal be defined by the equation:

$$\tilde{E}_s = Re\{A_s \exp(j2\pi\nu_s t)\}, \tag{9.1}$$

where $A_s = |A_s|\exp(j\varphi_s)$. is the complex amplitude and ν_s is the frequency of the field.

In this technique, the magnitude $|A_s|$ or the phase φ_s is modulated with the information signal at a rate much lower than ν_s. Similarly let the reference optical field, usually termed as the local oscillator field, be defined as

$$\tilde{E}_L = Re\{A_L \exp(j2\pi\nu_L t)\}, \tag{9.2}$$

$$A_L = |A_L|\exp(j\varphi_L). \tag{9.3}$$

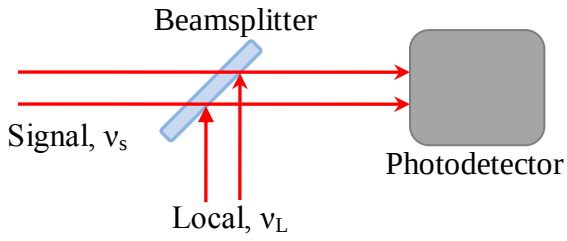

Figure 9.1 Schematic of Optical Heterodyning

These two optical fields are mixed using a beam-splitter or a coupler as shown in the schematic. If the incident fields are perfectly parallel plane waves and have precisely the same polarization, the total field is the sum of the two constituent fields, $\tilde{E} = \tilde{E}_s + \tilde{E}_L$.

The absolute square of the sum of the complex amplitudes would give

$$: = |E^{-}_{\downarrow}s + E^{-}_{\downarrow}L\ |^{\uparrow}2 \tag{9.4}$$

$$(j2\pi\nu_s t) + \{A_L \exp(j2\pi\nu_L t)\}\Big|^2 \tag{9.5}$$

$$= |A_s|^2 + |A_L|^2 + 2\,|A_s||A_L|\cos[2\pi(\nu_s - \nu_L)t + (\varphi_s - \varphi_L)]. \tag{9.6}$$

As seen from the equation (9.6), the current produced in a photodetector is proportional to the phase of the resulting beat optical field.

9.2 Experimental Setup for Optical Frequency Reference Transfer

The setup used for the optical frequency transfer characterization is similar to the setup used for the microwave clock frequency transfer characterization, with modifications in the optics to achieve optical heterodyning, and is shown in Figure 9.2.

As explained earlier, to achieve optical heterodyning, the signal and the local need to be at two slightly different frequencies. An acousto-optic modulator (AOM) is used to frequency-shift the reference optical signal by the amount of the AOM driving frequency. The AOM used in this experiment is driven at 80 MHz and the first order deflection of the reference signal is selected. The major requirement here is to have a provision to spatially overlap the reference and transmitted optical signals to obtain the optical heterodyne beat signal. The femtosecond pulse laser produces pulses at a 90 MHz repetition rate which gives a spatial separation of ~ 3.33 m between consecutive pulses in the air (in an optical fiber the spatial spacing between each pulse would be $\sim \frac{3.33\ m}{1.5\ (refractieve\ index\ of\ light\ in\ a\ regular\ SMF)} = 2.22$ m). The first order

deflected reference signal then passes through a tunable delay line, which provides a means to find the position where the transmitted and the reference optical pulses would overlap. The delay line is built using a combination of two translation stages each with a 10-cm travelling distance, providing 20 cm total travelling distance. The reference optical signal is reflected off by a beam-splitter, while the transmitted signal passes through the same beam-splitter, where they are collinearly combined producing a beat signal at 80 MHz. This beat-note signal is collected by a focusing lens and focused at the photodiode as shown in Figure 9.3.

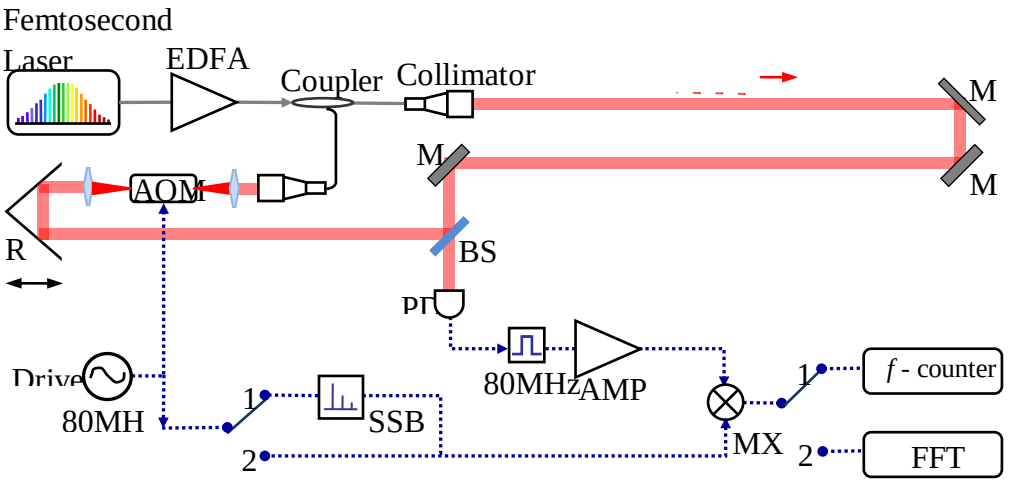

Figure 9.2 Schematic of the outdoor optical frequency transmission test system. AMP: microwave amplifiers, AOM: acousto-optic modulator, BS: beam splitter, EDFA: erbium-doped fiber amplifier, M: silver mirrors, MXR: mixer, PD: photodetector, PS: phase shifter, R: retro-reflector, and SSBM: single-side band modulator

The beat-note signal detected by the photodiode is phase compared to a copy of the original 80-MHz that drives the AOM. This beat-note signal contains the excess phase noise the transmitted optical frequency reference signal has accumulated as it propagated in the atmosphere. For the purposes of the Allan deviation measurement, the

beat signal is frequency down-shifted to 500 kHz by a single-sideband modulator (SSBM) and measured by a frequency counter.

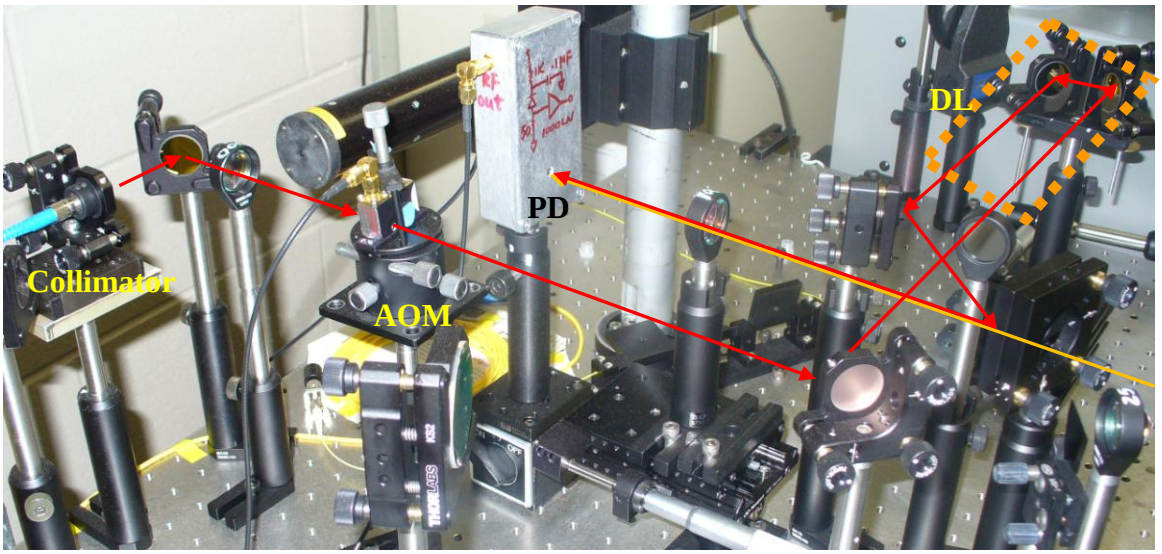

Figure 9.3 Optical set-up to achieve optical heterodyning. Red line shows the path followed by the reference signal going through the AOM and the delay line to facilitate the overlap of the reference and transmitted optical pulses to achieve the optical heterodyning. AOM: acousto-optic modulator, DL: Delay Line, represented with a dotted parallelogram, PD: photodiode.

9.3 Evaluation of Impact of Air Dispersion on Heterodyning Measurement Setup

The dispersion of the transmission medium, which is air (atmosphere) in these experiments, impacts the spectral bandwidth of the heterodyne measurement setup, which is explained in 5.5. To perform the optical heterodyning measurement, the reference optical signal is frequency shifted by an AOM. The spectral bandwidth of the reference optical signal after passing through the AOM is impacted by the air dispersion which limits the bandwidth of the heterodyne measurement system. The measured bandwidth of the reference optical signal after AOM spans from 1555 nm to 1570 nm. To achieve

effective heterodyning, the phase difference between these two spectral lines should be less than π.

Equations mentioned in 5.5 are used to calculate the refractive index of air at both 1555 nm and 1570 nm wavelengths. The difference in the air refractive index between these two spectral lines is calculated to be 1.1×10^{-8}. For a transmission distance over 60 m this difference in air refractive index corresponds to phase difference of $0.852\ \pi$. As this value is less than π, we can be assured that the spectral bandwidth of the optical heterodyne system ensures effective heterodyne beat signal measurement.

9.4 Allan Deviation Measurements

Allan deviation measurements were performed to characterize the long-term frequency stability of optical frequency references transferred via the atmosphere. These measurements were done under hot and cool weather conditions and both during day and night times. Even though the measurements were done during windy weather conditions, the data obtained is not reliable. This is due to the fact that under unstable weather, the atmosphere acts as a refractive index modulator, causing large phase change and thereby causing jitter between the optical pulses. This causes a considerable change in the position where the reference and the transmitted pulses would overlap, which results in a loss of the heterodyning beat signal at the detector. The reading obtained at such a time would carry no information about the phase noise accumulated by the optical frequency reference.

Figure 9.4 shows typical data of the Allan deviation measurement. The fractional stability achievable with atmospheric transfer of an optical frequency reference over a 60 m distance is measured to be $10^{-14} - 10^{-13}$ at 1 s sampling/gate time. Curve (b) in

Figure 9.4 shows the Allan deviation measured during a very hot day with unsteady weather, which shows that the fractional stability at 1 s sampling time, is at least two magnitudes larger compared to the value obtained during calm weather conditions as shown in Figure 9.4(a). This shows that the frequency stability is indeed affected by the weather factors such as temperature and unsteady wind. This can be understood that the higher temperature may be affecting the overall pulse characteristics and the unsteady wind acts a phase modulator which will lead to larger Allan deviation values. At higher sampling times, in Figure 9.4(b), we see that the Allan deviation seems to remain more or less around the value obtained at a lower sampling time 1 s. This is in contrast to the behavior noticed under steady, calm and slightly windy weather conditions, as in Figure 9.4 (a), where at higher sampling gate times, the Allan deviation seems to roll off with τ^{-1} dependence. The reason might be again due to the influence of the weather and also the drift of the pulse overlap position from the optimum position at higher sampling gate times.

It is important to note that the data taken at higher windy and unsteady conditions tend to have a high occurrence of beat signal loss at the detector due to the change in the effective transmission link and drift of the pulse overlap position. Also shown in Figure 9.5 is the Allan deviation data taken both during day and evening times, under slightly windy weather conditions, where the wind speed is about 2 m/s. This figure provides a rough estimate of the upper and the lower limits of the Allan deviation values under the above explained situations, and the line represents the average of the values shown in the figure.

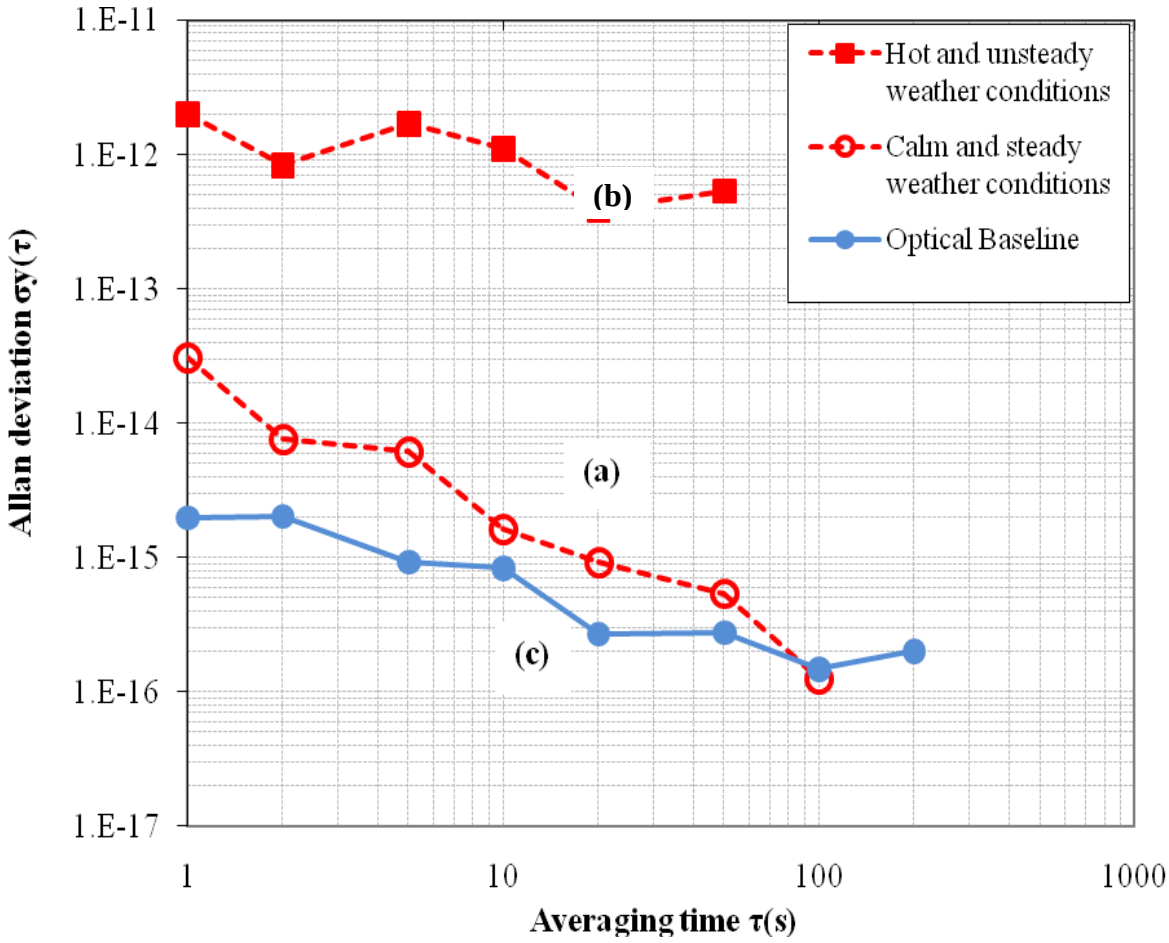

Figure 9.4 Typical profiles of Allan deviation of optical frequency reference transfer via atmosphere. (a) Shows profile of Allan deviation obtained under calm and steady weather in the evening time. (b) Typical profile under hot and unsteady weather during daytime. (c) This is the baseline of the optical transfer system.

It should be noted that the data in all these cases, the data was obtained only after optimizing the pulse overlap and a higher beat signal is detected at the photodiode. The RF circuit used for the Allan deviation measurements is shown in Figure B.2. Because of the limitation of the frequency counter used for Allan variance measurement, data only at the averaging time shown in the graph were obtained and not the intermediate values.

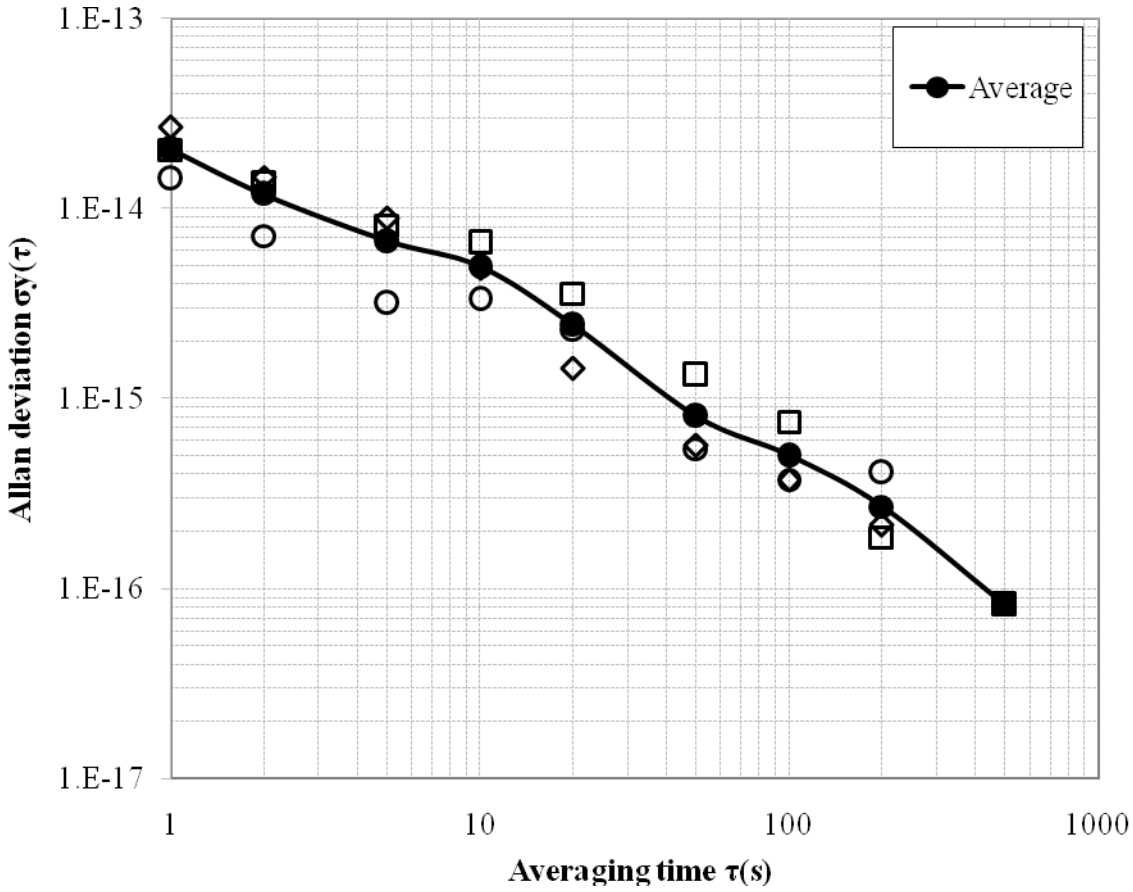

Figure 9.5 This graph shows the different values of Allan deviation obtained under different conditions such as day and night, calm and slightly windy weather conditions. The line gives the average values of these values. This graph does not include data obtained during the very hot and unsteady weather conditions (Gollapalli, 2010).

9.5 Beat-Note Frequency Fluctuation Measurements

The considerable drift of the pulse overlap and the subsequent loss of the beat signal prompted studying the characteristics of the fluctuations of the beat signal. At the frequency counter instead of measuring the root Allan variance, the frequency fluctuations of the frequency down-shifted 543 kHz beat signal are measured. The

frequency is measured with different sampling/gate times such as 0.01 s, 0.05 s, 1 s, 5 s and 10 s, and for different durations, with no averaging; measured consecutively over longer times.

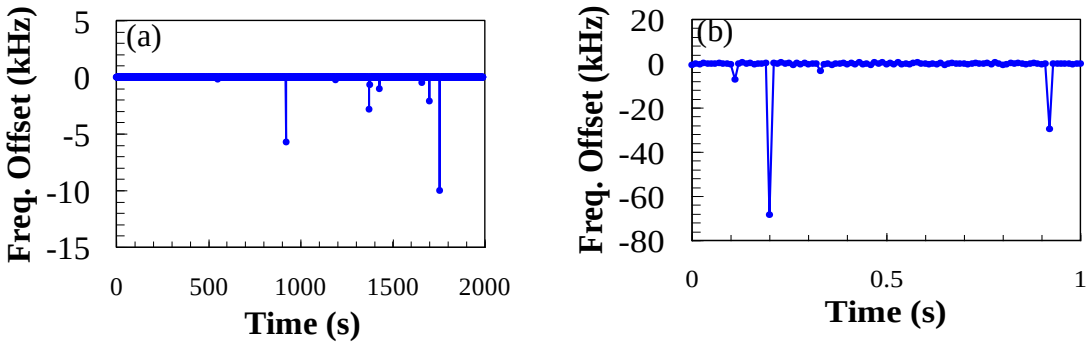

Figure 9.6 (a) Consecutive frequency readings of the 543 kHz beat note (offset by the nominal frequency and with a 1 s gate time) show spurious noise characterized by dramatic frequency dips. (b) A fast capture of such frequency dips using a 0.01 s gate time reveals that these events are very brief (Gollapalli, 2010).

In all the frequency fluctuation readings, the interesting feature is the dips of the frequency values which exceed the scale of the frequency fluctuation during the majority of the time. Though the occurrence of these dips seems to be random in nature, they tend to be more frequent and prominent at the end of long measurements that last for more than 15 minutes. The occurrence of these dips seem to coincide with a change in the transmission path, for example, a gusty wind which would change the effective transmission path seen by the transmitted signal, causing a loss in the beat signal seen by the photodiode. Along the same lines of argument, the dips at the end of a measurement can be attributed to the drift of the pulse overlap position long after optimization at the beginning of the measurement. This loss of the pulse overlapping is a critical element in deciding how long a measurement can be made, which is in turn dependent on the

weather conditions. The frequency fluctuation data taken with the shortest possible gate time with our frequency counter, which is 0.01 s, suggests that the dips occur in less than 10 ms (plus a few milliseconds instrument dead time). Typical frequency fluctuations are shown in Figure 9.6, and it should be noted that the frequency readings have been offset to the nominal value of 543 kHz. All frequencies reported in this figure are measured consequently over a period of time during the same evening.

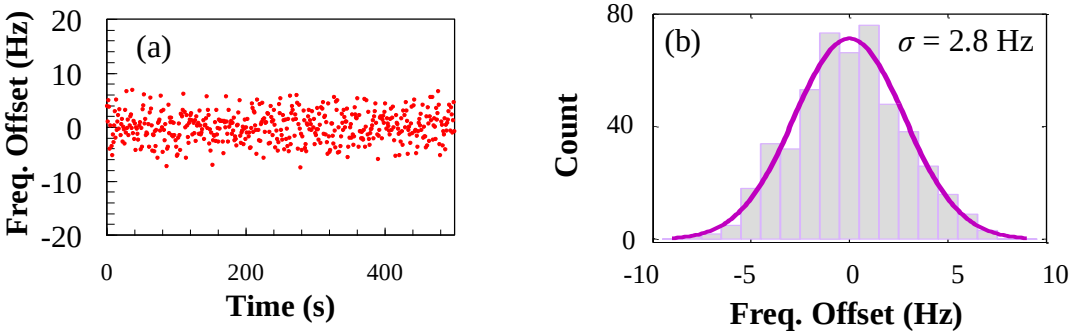

Figure 9.7 A close-up look at an uninterrupted portion of the frequency measurements with a 1 s gate time (a) shows random frequency distribution around the nominal frequency. (b) The histogram of (a) and a fitting to the normal distribution lead to a standard deviation of 2.8 Hz (Gollapalli, 2010).

A study was performed to understand the distribution nature of the beat note frequency around the nominal frequency. In Figure 9.7 we consider the case of frequency measured with 1 s sampling/gate time and also frequency data from the region where we do not have the occasional dips, and a histogram analysis of this data in Figure 9.7(a) reveals a normal distribution as shown in Figure 9.7(b). A Gaussian fit to this distribution results in a frequency deviation of 2.8 Hz which agrees with the scale of the Allan deviation result (Gollapalli, 2010).

9.6 Spectral Broadening Measurements

The spectral analysis of the nature of noise experienced by the optical reference is done by studying the broadening of the 543 kHz beat note spectrum. The phase modulation experienced by the optical frequency references propagating through atmosphere is generally much greater than 2π. This is clearly seen from the significantly broadened 543 kHz beat note spectrum, as shown in Figure 9.8. This trace is averaged over 1 s and centered at the nominal frequency. A typical spectrum like this features a central peak with near-flat top and steep sides. The 3-dB full width of the peak ranges from a few hundred Hz to 1 kHz. A close look at the peak can be gained through the phase noise spectrum of the beat note, which is assembled from spectral measurements over two frequency spans and is shown in Figure 9.8. A white noise is seen below 200 Hz and is followed by a quick roll-off from 500 Hz to 1 kHz. Such characteristics signify a slow phase modulation with a very large depth of modulation. This is confirmed, as shown in Figure 9.8 inset, by time-domain measurement of the beat note when it is downshifted to zero frequency. Figure B.1 shows the circuit used for the line-width measurements for spectral analysis of the optical frequency transfer via the atmosphere. The phase modulation is a consequence of refractive index fluctuation over the transmission path due to wind and turbulence, which effectively work as a noisy phase modulator. Because of the short wavelengths of the optical frequency references (in comparison with microwave clocks), the variation of optical path length can be many times the wavelengths, leading to phase modulation depths much greater than 2π.

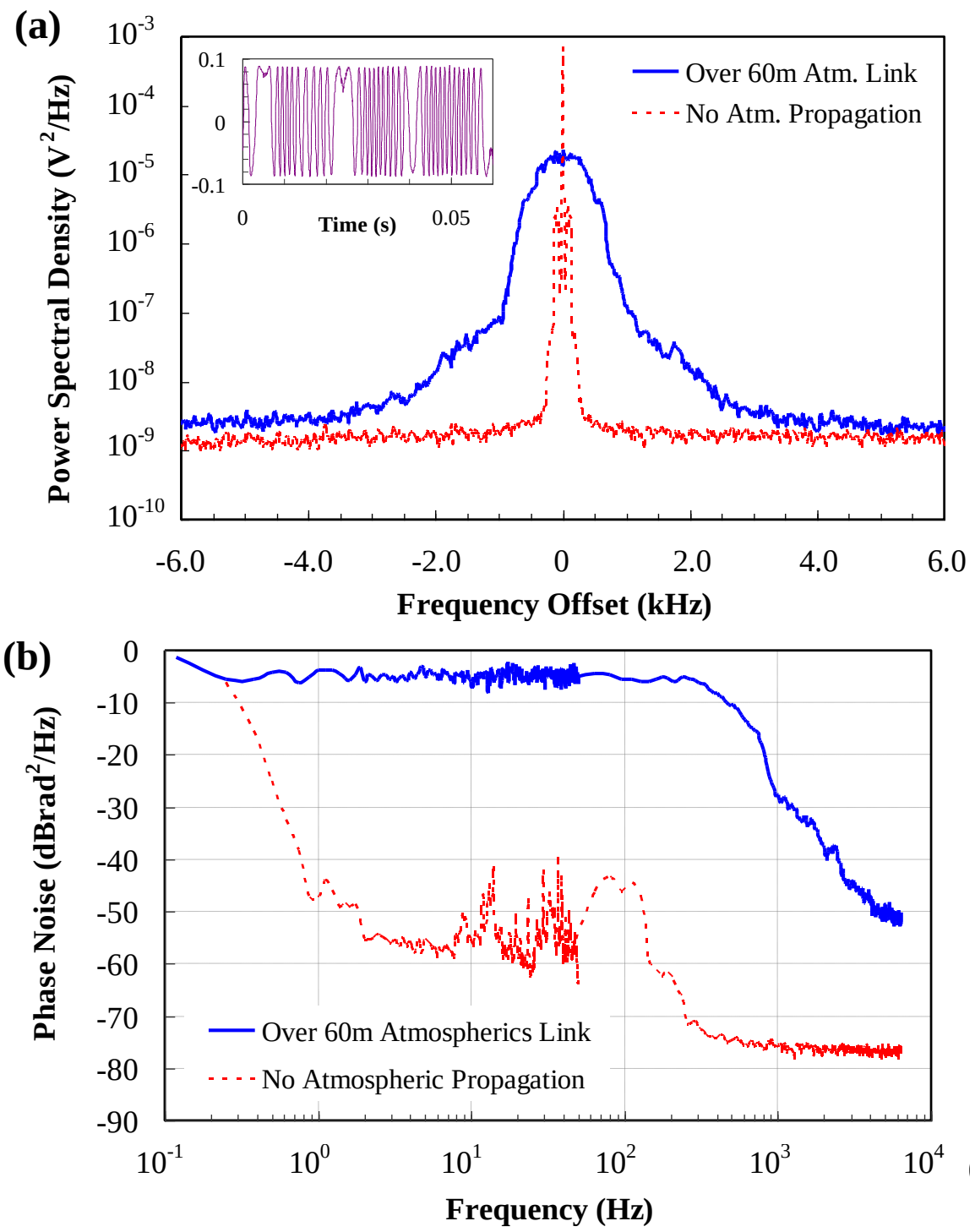

Figure 9.8 (a) Fourier spectrum of the 543 kHz heterodyne beat note shows a kHz-scale line-width due to spectral broadening caused by the atmospheric propagation. (b) The phase noise spectrum of the beat note has a flat top and a quick roll-off, indicating large phase modulation depths, which are confirmed by the time-domain trace (inset) of the beat note when its nominal frequency is downshifted to zero.

As explained in 9.2, the heterodyne signal was obtained by beating the pulses from the reference signal and the transmitted signal propagating in the atmosphere. For a faithful and complete study of the influence of the transmission medium on propagating pulse-train, the heterodyne signal should be obtained by beating the sister-copy of the same pulse in the reference and transmitted arm at the detector; however, this was not accomplished in these measurements. The main drawback with this type of heterodyne signal is that it also includes the jitter of the pulse-train originating from the laser source. The spectral measurements shown in Figure 9.8, consist of the pulse-jitter of the fiber laser source used for generating the pulse-train. But to the advantage, these spectral broadening measurements can be used as an upper-limit towards the study of the spectral studies of optical pulse propagation in the atmosphere.

In the next step of spectral measurements, the reference signal was passed through a fiber-optic cable over 40 m, which is the equivalent distance of 60 m propagation distance in the air. Heterodyne signal was obtained by beating this reference signal through the 40 m fiber-optic cable, with the atmosphere transmitted signal. The spectral characteristics of this beat signal are shown in Figure 9.9. From these measurements it is clear that the spectral broadening is indeed caused by the propagation medium which is the atmosphere.

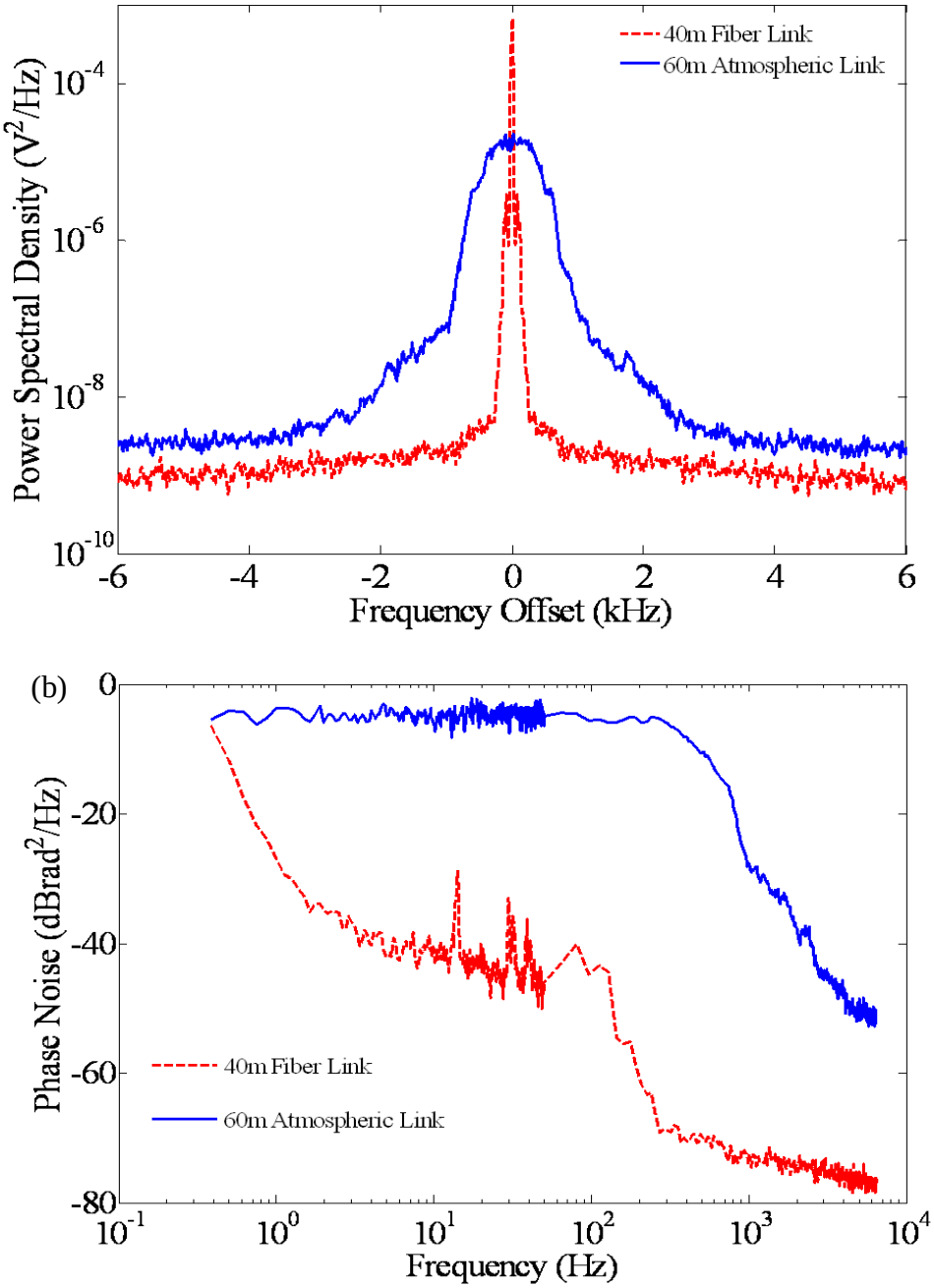

Figure 9.9 (a) Blue trace is the fourier spectrum of the 543 kHz heterodyne beat note obtained by beating the reference signal passed through fiber and transmitted signal through atmosphere. Spectral broadening caused by the atmospheric propagation is obvious here. The width of the spectrum obtained with no atmospheric propagation is comparable to the trace in Figure 9.8. The phase noise comparison is shown in (b).

9.7 Comparison with CW Laser Optical Frequency Reference Transfer

Two studies have been reported on the remote delivery of frequency references in optical regime (Sprenger, 2009), (Djerroud, 2010). *Sprenger et al.* used a CW laser modulation to transfer the frequency reference over 100 m via the atmosphere at ground-level and achieved fractional stability 2×10^{-13} at 1 s averaging time. In comparison with this present work, the fractional stability is one order of magnitude better than using a CW laser modulation. *Djerroud et al.* also used CW laser to transfer optical frequency reference over 5 km via the atmosphere and fractional stability at 1 s averaging time achieved was 2×10^{-14}. However, this frequency transfer was done at an elevation of 1323 m and not at ground level. At such elevations, the atmospheric turbulence is relatively small compared to turbulence at ground level, the longer distance and the better stability may be attributed to these differences compared to this present work. Also, the use of large-scale optics reported in the work of *Djerroud et al.* may have contributed to the better values of fractional stability. In this dissertation a pulsed-laser is used to transmit the frequency references and for the heterodyne measurement system, where achieving the pulse-overlap of the reference and transmitted pulses is the key element. This places a strict requirement to achieve the optimum pulse-overlap; however, no such requirement exists when a CW laser modulation is used to transmit frequency references.

9.8 Summary and Discussion on Optical Frequency Reference Delivery

Atmospheric transfer of optical frequency references is largely affected to a higher degree by the atmospheric elements causing phase modulation larger than 2π. The broadening of the beat note spectrum indicates a large depth of phase modulation caused by the atmosphere. The detection of the beat note signal is primarily influenced by the

optimization of the overlap of both the reference and transmitted optical pulses. The gusty winds and hot temperature seem to have a huge affect on the pulse overlap position, which also dictates the length of time a frequency transfer measurement can be made, especially to characterize the long-term stability. A fractional stability ~3 x 10^{-14} at 1 s averaging time was achieved for the transfer of an optical frequency reference over 60 m via the atmosphere. A definite statement on the dependence of the Allan deviation with τ , the averaging time, cannot be made from the data. This indicates the influence of different types of noises on the delivery of optical frequency reference via the atmosphere.

Chapter X

SUMMARY

The primary goal of this research was to study the feasibility and characterize remote delivery of frequency references via the atmosphere. This was accomplished in two stages; in the first stage, a phase coherent supercontinuum was generated for the study of frequency reference transfer and in the second stage, remote delivery of frequency references via the atmosphere was experimentally demonstrated.

To develop an EDFA for femtosecond-pulse amplification, numerical simulations were carried out to gain more insight into the femtosecond pulse evolution in a gain medium. In particular, I studied the evolution of the temporal phase and how it is related to pulse breaking. Through this work, I found that the amplified pulse starts to break up into sub pulses when the temporal phase has a sharp characteristic positive slope. This finding offers a new insight into the mechanism of pulse breaking in gain fibers for femtosecond pulses.

On the experimental side, phase noise measurements were done during the transfer of microwave reference transfer via the atmosphere. From these measurements the root-mean-square timing jitter was calculated, from which the phase fluctuation of the atmosphere was estimated. The estimated values also agree well with the theoretical models. This work provides insight into the fluctuations the propagating pulses would undergo and may be used to characterize the atmosphere.

For the first time a demonstration of femtosecond laser-based clock transfer through the open atmosphere was made. Other recent work has shown the feasibility to transfer frequency references through optical fibers or in a controlled free-space laboratory environment. In this work, frequency references both in the microwave and optical frequency regimes were successfully transmitted and characterized through an uncontrolled atmospheric link. The accuracy achieved by this transmission method demonstrates the feasibility of using the atmosphere to transfer clock signals and provides the missing link of a "wireless" version in the field of frequency reference distribution methods. This is the primary contribution of this research work. This demonstration opens up an avenue to a wide range of applications and situations.

To show the significance of this work, a few possible applications are described. GPS is the technology used to transmit clock signals over hundreds of kilometers via the atmosphere; however, it has a drawback in that it only provides high stability when averaged over a 24-hour period. The stability achieved in this research work indicates that we can transmit a frequency reference to a nearby user, with averaging less than 10 min. For example, consider the case of a user who needs access to a highly stable clock signal. If this user is within a short distance, less than a kilometer range from an atomic clock, the clock signal from this atomic clock can be transmitted to the user without the need for laying an expensive fiber-optic network. Also in the case of users in different buildings within a campus, which are only short distance away from a highly stable clock signal source, a highly stable clock signal can be distributed to all the users in all these buildings via the atmosphere.

Time-resolved pump-probe experiments require synchronization of laser pulses within sub-100 fs time scales. For these experiments if the pump-signal source and probe-signal source are within short distance from a master oscillator, the clock signal from the master oscillator can be distributed to the pump and probe-signal sources. By locking these two laser-sources, the timing jitter between them can be reduced thereby increasing the utility and flexibility of time-resolved spectroscopy systems.

This work demonstrates the feasibility of distributing a highly stable frequency reference to a user who is very near, less than a kilometer distance away. However, the numerical data presented in this research need not be taken as a limit in terms of the stability achievable with the transfer of frequency references via the atmosphere. Noise-cancellation techniques have been proven to reduce the noise and increase the stability of frequency references transferred via optical fibers. Such adaptive noise-cancellation techniques may be implemented to achieve better results. Also the use of better optics may help achieve better results with distances longer than those reported in this work.

APPENDICES

APPENDIX A

THEORY OF AUTOCORRELATION

Mathematically the cross-correlation of two complex square-integrable functions, $f(x)$ and $g(x)$ is defined as

$$(f * g)(x) \equiv \int_{-\infty}^{\infty} f^*(t)g(x+t)dt\ , \tag{A.1}$$

where f^* is the complex conjugate of f . It is a measure of how similar two functions are for different values of x. When $f(x) = g(x)$, the above equation gives a cross-correlation of f with itself, which is called the auto-correlation of $f, A_f(x)$. The autocorrelation of a function describes how similar a function is to a time-delayed copy of itself.

$$A_f(x) = \int_{-\infty}^{\infty} f^*(t)f(x+t)dt \tag{A.2}$$

$$= \int_{-\infty}^{\infty} f^*(t-x)f(t)dt \tag{A.3}$$

An optical field maybe written as

$$E(t) = \varepsilon(t)e^{i(\omega_0 + \Phi(t))} + c.c.\ , \tag{A.4}$$

where $c.c.$ denotes the complex conjugate, ω_0 is the carrier frequency of the optical field, $\varepsilon(t)$ is the electric field amplitude of the optical signal and $\Phi(t)$ is the time dependent phase. The first order autocorrelation of an optical field $E(t)$ with a delay τ , maybe written as

$$A^{(1)}(\tau) = \int_{-\infty}^{\infty} E(t)E^{*}(t-\tau)dt \ . \tag{A.5}$$

As this correlation is over the electric field, this first order correlation is also called the field autocorrelation. The Fourier transform of the correlation of two functions is the product of the Fourier transforms of the individual functions, which yields the following for two optical fields $E_1(t)$ and $E_2(t)$ as

$$A^{(1)}(\Omega) = E_1(\Omega)E_2^{*}(\Omega). \tag{A.6}$$

The above equation tells that the Fourier transform of the autocorrelation of a signal is proportional to the spectral intensity of the pulse. The second order autocorrelation, also called the Intensity autocorrelation, can be defined as

$$A^{(2)}(\tau) = \int_{-\infty}^{\infty} \langle |[E_1(t-\tau) + E_2(t)]^2|^2 \rangle dt \ , \tag{A.7}$$

where $\langle \square \rangle$ is averaging over the fast oscillations of the electrical field and the integral stands for integration over the pulse envelope. Substituting the fields by the usual envelope and phase functions, and on averaging results with the following equation

$$A^{(2)}(\tau) = A_0(\tau) + Re\left[A_1(\tau)e^{-i\omega_l\tau}\right] + Re\left[A_2(\tau)e^{-2i\omega_l\tau}\right] \tag{A.8}$$

$$where, A_0(\tau) = \int_{-\infty}^{\infty} \left[\mathcal{E}_1^4(t-\tau) + \mathcal{E}_2^4(t) + 4\mathcal{E}_1^2(t-\tau)\mathcal{E}_2^2(t)\right]dt \ .$$

For autocorrelation, when $E_1 = E_2 = E$ at $\tau = 0$, the peak value of the function $A^{(2)}(\tau = 0) = 16\int \mathcal{E}^4(t)dt.$ For large delays, compared to the pulse duration, cross products containing terms with $\mathcal{E}(t-\tau)\mathcal{E}(t)$ vanish, leaving a background of $A^{(2)}(\tau = \infty) = 2\int \mathcal{E}^4(t)dt.$ The peak to background ratio for the interferometric autocorrelation is thus 8 to 1. The interferometric autocorrelation is a symmetric function,

and unlike intensity autocorrelation, it carries the phase information. From an interferometric autocorrelation, the type of phase modulation, linear chirp and the pulse shape and phase using fitting methods. A typical interferometric autocorrelation of a Gaussian pulse is shown in Figure A.1 in which the peak-to-background ratio 8:1 is clearly seen as suggested by the above equations.

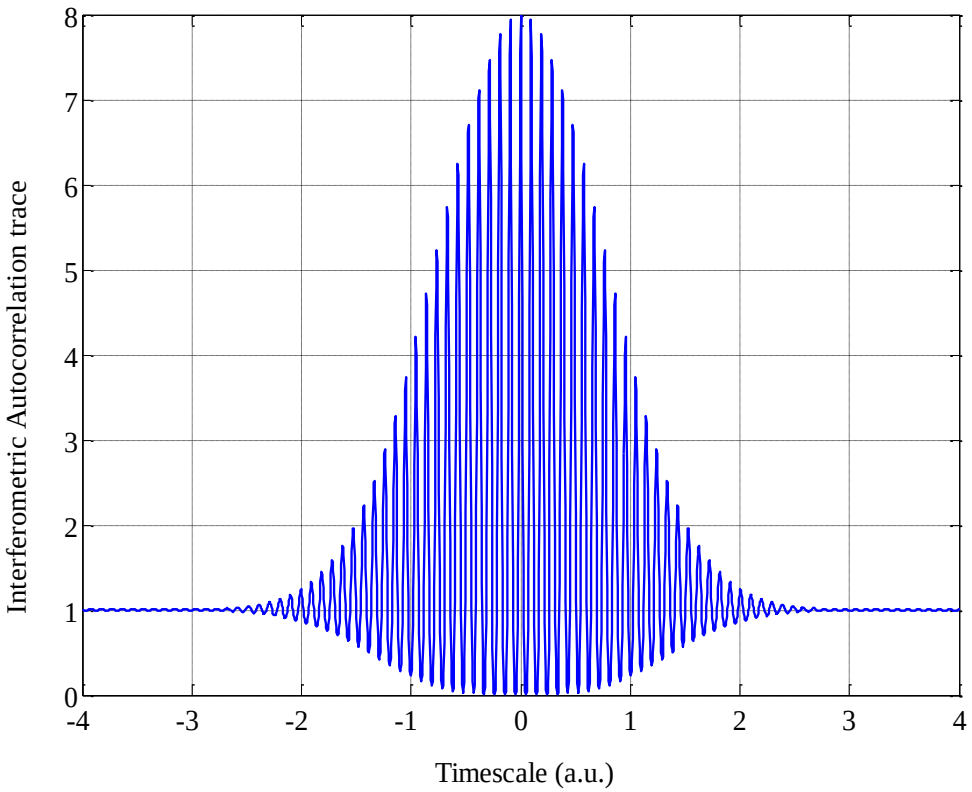

Figure A.1: A typical interferometric autocorrelation of a Gaussian pulse. The 8:1 peak-to-background ratio is clearly seen in the picture.

APPENDIX B

RF CIRCUITS

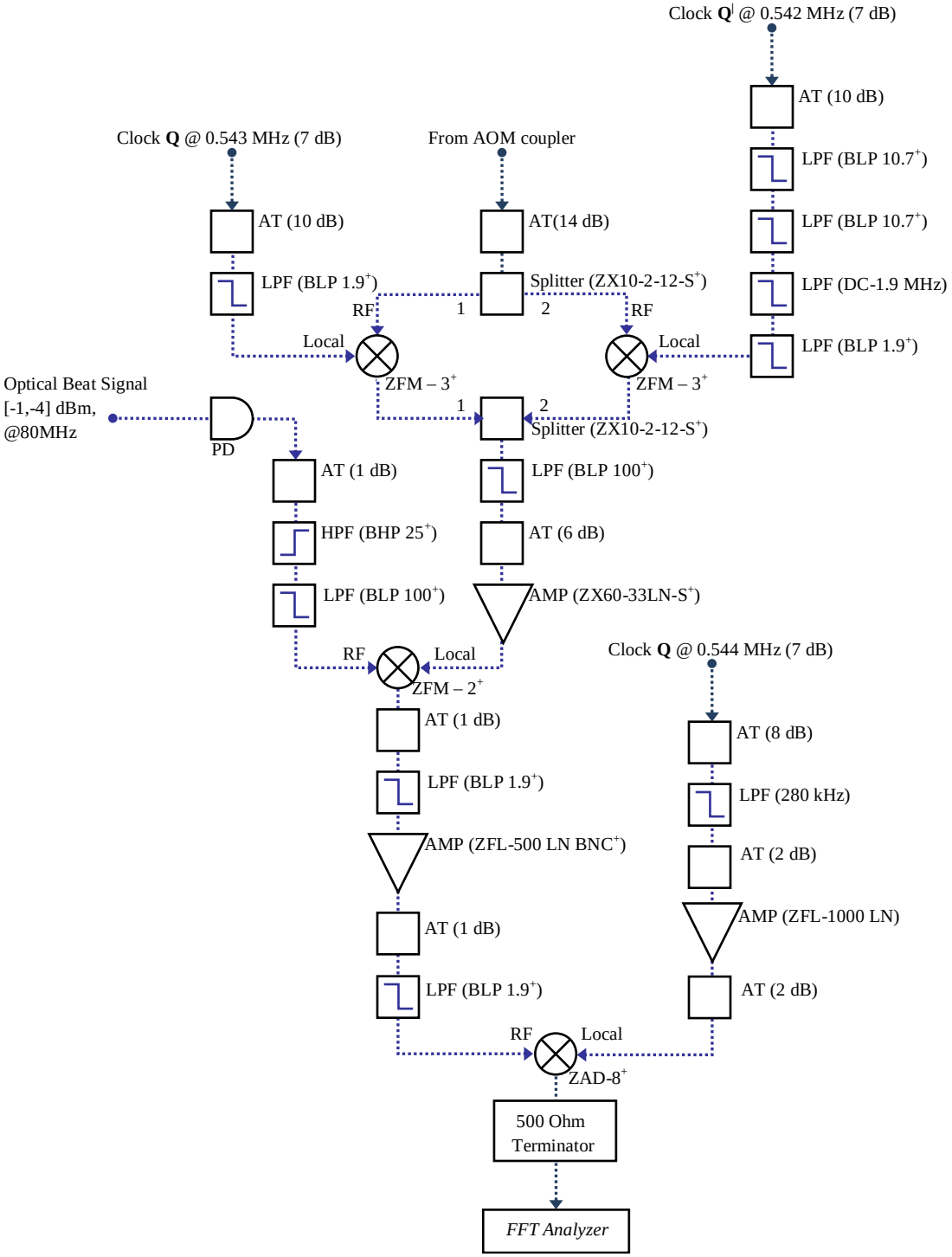

Figure B.1: Circuit for the spectral analysis of optical frequency reference transfer via atmosphere. AMP: RF amplifier, AT: attenuator, LPF: low-pass filter, HPF: high-pass filter. The identification codes of the RF circuit element are given in the brackets.

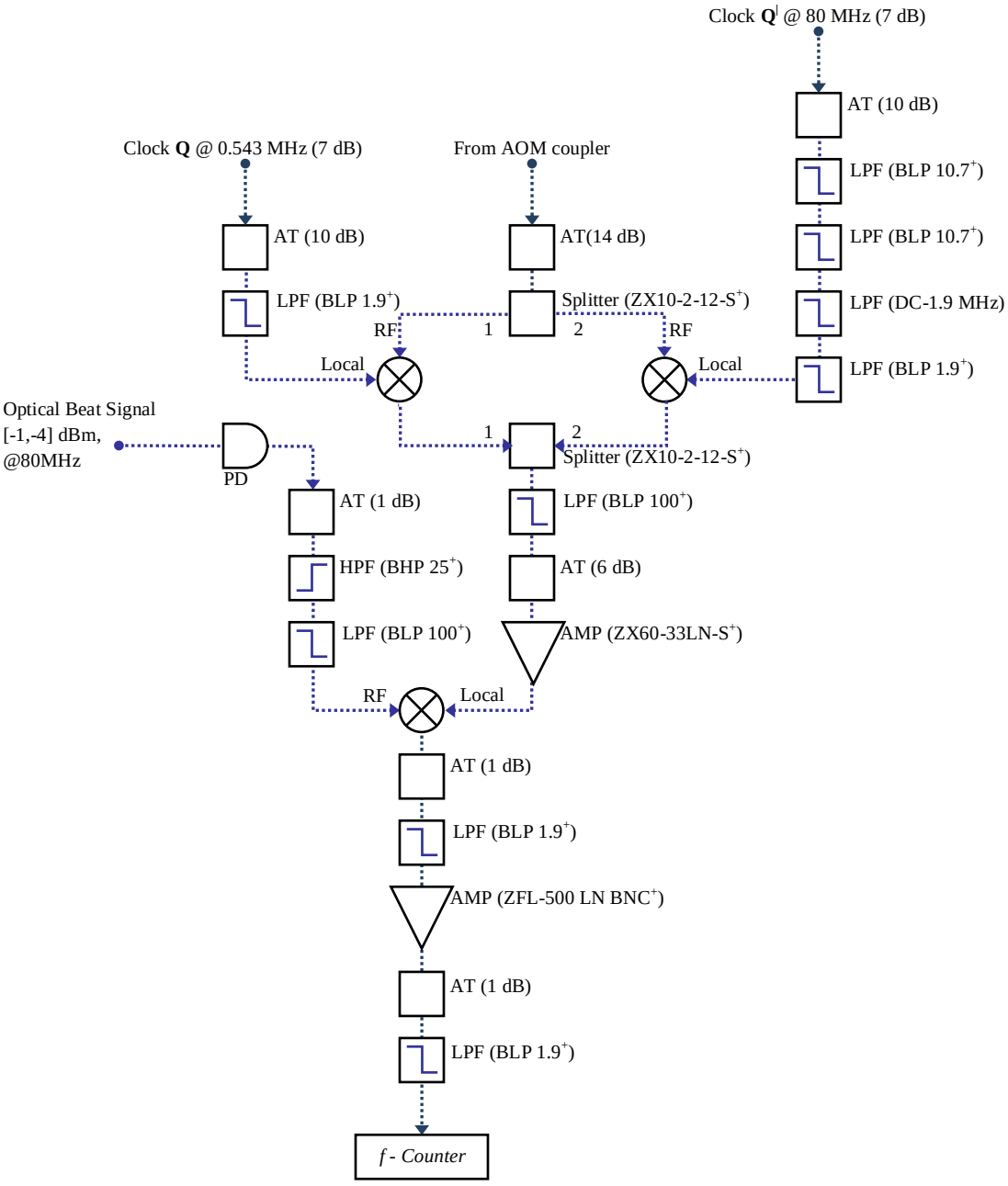

Figure B.2: Circuit for Allan Deviation Measurement. AMP: RF amplifier, AT: attenuator, LPF: low-pass filter, HPF: high-pass filter. The identification codes of the RF circuit element are given in the brackets.

APPENDIX C

SIMULATIONS PROGRAM CODE

MATLab® software was used to simulate the femtosecond pulse propagation in a gain medium. The autocorrelator output of the femtosecond pulse and its spectrum are given as input to the PICASO program which provides the temporal and phase characteristics of the pulse. The following program code uses this information as the input pulse and simulates the pulse evolution in a gain medium with a +3dB gain.

Start of Program code

****----------****

```
% Split-Step Fourier Method for Pulse Propagation calculations
% This is Simulation of the Input of the Pulse taken from the Intensity
% output of the Picaso software. I am also extending the time window of
% the input, by adding extra zeros to the time data, gradually

clear all; clc;
cputime = 0; tic;

% Constants & Parameters
i = sqrt(-1);                % Imaginary number 'i'
c0 = 3e8;                    % Velocity of light in vaccum
beta2 = -20e-27;             % units s^2/m
beta3 = 0.1e-39;             % units s^3/m
gamma = 2e-3;                % Nonlinearity Parameter, units 1/(W-m)

Pavg = 3.9e-3;               % Average Power of the Laser Pulse, units W
```

```
Reprate = 90e6;              % Laser Pulse repetition rate, Hz
Tfwhm = 120e-15;             % Input pulse FWHM in femtosecond
lambda0 = 1558e-9;           % Wavelength of the Input Pulse, units nm
v0 = c0/lambda0;             % Central Frequency in Hz
w0 = 2*pi*v0;                % central frequency in radians
T0 = Tfwhm/1.76;             % "1.76" is the factor for Sech Pulse

% Input Sech Pulse
Time_Inp = xlsread('PicasoInput.xls',2,'A3:A2050');
Inte_Inp = xlsread('PicasoInput.xls',2,'B3:B2050');
Phas_Inp = xlsread('PicasoInput.xls',2,'C3:C2050');
Time_Inp = Time_Inp'*1e-15; Inte_Inp = Inte_Inp'; Phase_Inp =
Phas_Inp';
data_points_Inp = max(size(Time_Inp));
dt_Inp = (max(Time_Inp) - min(Time_Inp))/data_points_Inp;

% Finding the area under the curve of the Intensity & Time obtained
from the Picaso Output. This uses "Trapezium rule" of Numerical
Integration %
CurveArea = ( dt_Inp/2 )*( 2*sum(Inte_Inp)-
(3/2)*(Inte_Inp(1)+Inte_Inp(data_points_Inp)) );


Pulse_energy = Pavg/Reprate;
PeakPower = Pulse_energy/CurveArea;
disp('Pulse Peak Power is:'); disp(PeakPower);

Pulse_Inp = sqrt(Inte_Inp);
disp('Max of the Input Pulse:'); disp(max(Pulse_Inp));
```

```
plot(Time_Inp,Inte_Inp,'LineWidth',2,'Color','b'); grid on; hold on;
plot(Time_Inp,Pulse_Inp,'LineWidth',2,'Color','r');
legend('Intensity','Picaso Input Pulse'); hold off
xlabel('Input Time, units: s'); ylabel('a.u.');

time_extend1 = [-dt_Inp*(8192+1):dt_Inp:min(Time_Inp)-dt_Inp];
time_extend2 = [max(Time_Inp)+dt_Inp:dt_Inp:dt_Inp*8192];
Time_Extend = [time_extend1 Time_Inp time_extend2];
Pulse_extend1 = zeros(1,max(size(time_extend1)));
Pulse_extend2 = zeros(1,max(size(time_extend2)));
Pulse_Extend = [Pulse_extend1 Pulse_Inp Pulse_extend2];
Pulse_Extend(7140:7169) = linspace(0,Pulse_Extend(7169),30);
Pulse_Extend(9217:9246) = linspace(Pulse_Extend(9217),0,30);
Phas_extend1 = Phase_Inp(1)*ones(1,max(size(time_extend1)));
Phas_extend2 =
Phase_Inp(data_points_Inp)*ones(1,max(size(time_extend2)));
Phase_Extend = [Phas_extend1 Phase_Inp Phas_extend2];
disp('Input Phase matrix size:'); disp(size(Phase_Inp));
figure('Color',[1 1 1]);
subplot(2,1,1); plot(Time_Extend,Pulse_Extend,'LineWidth',2);
xlabel('Extended Time'); ylabel('Expanded Pulse'); grid on;
subplot(2,1,2); plot(Time_Extend,Phase_Extend,'LineWidth',2);
xlabel('Extended Time'); ylabel('Expanded Phase'); grid on;

% Normalizing of the Input 'TIME' and 'dt'
u = Pulse_Extend;
time = Time_Extend/T0;
data_points = length(time);
dt = ( max(time)-min(time) )/data_points;
```

```
% Frequency calculations for FFT
fmax1 = -1/(2*dt);          % The -Fmax in the Fourier domain
fmax2 = 1/(2*dt);           % The +Fmax in the Fourier domain
fspan = fmax2-fmax1;        % Total Freq BW
dfreq = fspan/data_points;  % The Freq increment, or Delta 'f'
freq1 = fmax1:dfreq:fmax2;   % Total Freq span in increments of Delta
'f'
freq = [freq1(1:data_points)];  % Taking only the required
freq2 = freq1(2:data_points+1);

w = freq*2*pi;
fftu = fftshift(fft(u));

P0 = PeakPower;             % Peak power of the Input Pulse, units W
Ld = T0^2/abs(beta2);       % Dispersion Length
z0 = (pi/2)*Ld;             % Soliton Period
N = sqrt(gamma*P0*Ld);      % Input Soliton Order
s = -1;                     % Second Order Dispersion
tod = beta3/(6*abs(beta2)*T0);% Third Order Dispersion
gain = log(3);             % gain due to dopants
TR = 3e-15;                 % Raman Resonant Time Constant
raman = TR/T0;              % Raman term;
T2 = 80e-15;                % Dipole Relaxation Time, units 's'
d = gain*Ld*(T2/T0)^2;      % gain dispersion
ss = 1/(w0*T0);             % Self-Steepening factor

%%%%%%%%%%%%%%%%%%%%%%%%%%%%%%
Nsqr = N^2;
zi = 15;
```

```
dzi = 2.5e-4;
stor_count = 1;
storcount = 0;

evolvpulse(stor_count,:) = u;
pulse(stor_count,:) = abs(u).^2;
spectrum(stor_count,:) = abs(fftu).^2;

du_fftu = ( ((i/2)*(s+i*d)*(w.^2)) + (-i*tod.*w.^3) + (gain/2) )*dzi/2;

fprintf(1,'\nStage # 1: ');
fprintf(1,'\nSimulation from zero to'); disp(zi);
fprintf(1, 'In Stage # 1, Simulation done till...      ');

for travdist = dzi:dzi:zi
    storcount = storcount+1;

    fftu = fftu.*exp(du_fftu);
    fftu = [fftu(1,data_points/2+1:data_points)
fftu(1,1:data_points/2)];

    u = (ifft(fftu));
    Umod_sqr = abs(u).^2;
    umodi = [u(2) u u(data_points) ];
    U1 = [Umod_sqr(2) Umod_sqr Umod_sqr(data_points)];
    for k = 2:(data_points+1)
        diff1(k-1) = (1/2)*( umodi(k+1)-umodi(k-1) )/dt;
        diff2(k-1) = (1/2)*( U1(k+1)-U1(k-1) )/dt;
    end
```

```
    du_u = (i*Nsqr*(Umod_sqr + i*ss*( conj(u).*diff1 + diff2 ) -
raman*diff2 ) )*dzi;
    u = u.*exp(du_u);

    fftu = fftshift(fft(u)).*exp(du_fftu);

    if (storcount == 250 )
        stor_count = stor_count+1;
        zivalue(stor_count,:) = travdist;
        spectrum(stor_count,:) = (abs(fftu).^2);
        signal = ifft([fftu(1,data_points/2+1:data_points)
fftu(1,1:data_points/2)]);
        evolvpulse(stor_count,:) = signal;
        pulse(stor_count,:) = abs(ifft(fftu)).^2;
        storcount = 0;
    end
    fprintf(1,'\b\b\b\b\b\b%5.2f%%',travdist*100.0/zi );
end
toc; cputime = toc;

disp('Time Resolution:'); disp(dt);
disp('Total Time Data Points:'); disp(data_points);

% % Plot the Pulse Evolution
figure('Color',[1 1 1]);
dist = (0:dzi*25:zi);
mesh(time(7300:2:data_points-7300),dist,pulse(:,7300:2:data_points-
7300))
axis([-10 10 0 zi 0 max(max(pulse))])
```

```
view(-90,0)
title('Pulse- N:0.3332,raman:0.044,s:-
1,d:0.7368,gain:10dB,tod:0.0122,ss:0.0121;25pulses;dzi:25e-
5;dt:0.75fs;TWin:12.2ps Set-1');
xlabel('Time'); ylabel('Distance (z/Ld)'); zlabel('Intensity');
              ****----------------------------------------------------****
```

End of Program code

REFERENCES

Agrawal, G.P. Nonlinear Fiber Optics [Book]. - San Diego: Academic Press, 2001. - 3rd.

Alatawi, A., Gollapalli, R.P., and Duan, L. Radio-frequency clock delivery via free-space frequency comb transmission [Journal] // Optics Letters. - November 2009. - 21: Vol. 34. - pp. 3346 - 3348.

Alfano, R.R. The Supercontinuum Laser Source, Fundamentals with Updated References [Book]. - New York: Springer Science, 2006. - 2nd.

Bellini, M. and Hansch, T.W. Phase-locked white-light continuum pulses: Toward a universal optical frequency-comb synthesizer [Journal] // Optics Letters. - July 15, 2000. - 14: Vol. 25. - pp. 1049-1051.

Box, G. E. P. and Jenkins, G. M. Time Series Analysis: Forecasting and Control [Book]. - San Francisco: Holden-Day, 1970.

Chen, Y.F., Jiang, J., and Jones, D.J. Remote distribution of a mode-locked pulse train with sub 40-as jitter [Journal] // Optics Express. - [s.l.]: Optical Society of America, 2006. - 25: Vol. 14. - pp. 12134 - 12144.

Ciddor, P.E. Refractive index of air: New equations for the visible and near infrared [Journal] // Applied Optics. - March 20, 1996. - 9: Vol. 35. - pp. 1566-1573.

Cruz, F.C. High precision measurements and generation of optical and microwave frequencies using narrow-band and short-pulse lasers [Conference] // SBMO/IEEE MTT-S IMOC . - [s.l.]: IEEE, 2003. - pp. 279-281.

Cundiff, S.T. Phase stabilization of ultrashort optical pulses [Journal] // Journal of Physics D: Applied Physics. - 2002. - Vol. 35. - pp. R43-R59.

Diels, J.C. and Rudolph, W. Ultrashort Laser Pulse Phenomena: Fundamentals, Techniques, and Applications on a Femtosecond Time Scale [Book]. - [s.l.]: Academic Press (Elsevier Inc), 2006.

Djerroud, K., Acef, O., Clairon, A., Lemonde, P., Man, C. N. Samain, E., and Wolf, P. Coherent optical link throught the turbulent atmosphere [Journal] // Optics Letters. - May 1, 2010. - 9: Vol. 35. - pp. 1479 - 1481.

Eckstein, J.N., Ferguson, A.I., and Hansch, T.W. High-resolution two-photon spectroscopy with picosecond light pulses [Journal] // Physical Review Letters. - 1978. - 13: Vol. 40. - pp. 847-850.

Evenson, K.M., Wells, J.S., Petersen, F.R., Danielson, B.L., and Day, G.W. Accurate frequencies of molecular transitions used in laser stabilization: The 3.39-micron transition in CH4 and 9.33- and 10.18-micron transitions in CO2 [Journal] // Applied Physics Letters. - 1973. - Vol. 22. - pp. 192-195.

Fante, R. L. Two-position, two-frequency mutual-coherence function in turbulence [Journal] // Journal of Optical Society of America. - 1981. - Vol. 71. - pp. 1446 - 1461.

Fante, Ronald L. Electromagnetic beam propagation in turbulent media [Journal] // Proceedings of the IEEE. - December 1975. - 12: Vol. 63. - pp. 1669-1692.

Foreman, S. M., Holman, K.W., Hudson, D. D., Jones D. J., and Ye, J. Remote transfer of ultrastable frequency references via fiber networks [Journal] // Rev. Sci. Instrum. - 2007. - Vol. 78. - pp. 021101-021125.

Gollapalli, R. P. and Duan, L. Atmospheric transfer of microwave clock using an Optical Frequency Comb [Journal] // CLEO / QELS 2010. - 2010. - p. Session: CTuDD2.

Gollapalli, R. P. and Duan, L. Delivery of optical frequency references via atmosphere using a frequency comb [Journal] // FiO 2010 / LS XXVI. - Rochester, NY: Optical Society of America, 2010. - p. Session: FTuL5.

Hill, R. J. and Clifford, S. F. Modified spectrum of atmospheric temperature fluctuations and its application to optical propagation [Journal] // Journal of Optical Society of America. - 1978. - Vol. 68. - pp. 892 - 899.

Hill, R. J. and Ochs, G. R. Inner-scale dependence of scintillation variances measured in weak scintillation [Journal] // Journal of Optical Society of America A. - 1992. - Vol. 9. - pp. 1406 - 1411.

Karshenboim, S.G. Some possibilities for laboratory searches for variations of fundamental constants [Journal] // Can.J.Phys/Rev.Can.Phys. - 2000. - 7: Vol. 78. - pp. 639-678.

Kourogi, M., Nakagawa, K., and Ohtsu, M. Wide-span optical frequency comb generator for accurate optical frequency difference measurement [Journal] // IEEE Journal of Quantum Electronics. - [s.l.] : IEEE, October 1993. - 10: Vol. 29. - pp. 2693-2701.

Leemans, W.P. and Schoenlin, R.W. X-ray based subpicosecond electron bunch characterization using 90° Thomson scattering [Journal] // Physics Review Letters. - 1996. - Vol. 77. - pp. 4182-4185.

Levine, J. Introduction to time and frequency metrology [Journal] // Review of Scientific Instruments. - 1999. - Vol. 70. - p. 2567.

Milonni, P. W. and Eberly, J. H. Lasers [Book]. - New York: John Wiley & Son, Inc, 1988.

Owens,J. C. Optical refractive index of air: Dependence on pressure, temperature and compositions [Journal] // Applied Optics. - 1967. - Vol. 6. - pp. 51-59.

Ranka, J.K., Windeler, R.S., and Stentz, A.J. Visible continuum generation in air-silica microstructure optical fibers with anomalous dispersion at 800 nm [Journal] // Optics Letters. - 2000. - 1: Vol. 25. - pp. 25-27.

Reichert, J., Holzwarth, R., Udem, Th., and Hänsch, T. W. Measuring the frequency of light with mode-locked lasers [Journal] // Optics Communications. - December 15, 1999. - Vol. 172. - pp. 59-68.

Riley, W. J. Handbook of Frequency Stability Analysis [Report]. - [s.l.] : National Institute of Standards and Technology, 2008. - CODEN: NSPUE2. - NIST Special Publication 1065.

Rutman, J. Characterization of phase and frequency instabilities in precision frequency sources: Fifteen years of progress [Journal] // IEEE Proceedings. - 1978. - pp. 1048 - 1075.

Schibli, T. R., Minoshima, K., Bitou, Y., Hong, F.L., Inaba, H., Onae, A., and Matsumoto, H. Displacement metrology with sub-pm resolution in air based on a fs-comb wavelength synthesizer [Journal] // Optics Express. - 2006. - 13: Vol. 14. - pp. 5984-5993.

Schliesser, A., Gohle, C., Udem, T., and Hansch, T.W. Complete characterization of a broadband high-finesse cavity using an optical frequency comb [Journal] // Optics Express. - 2006. - Vol. 14. - pp. 5975-5983.

Schoenlein, R.W., Leemans, W.P., Chin, A.H., Volfbeyn, P., Glover, T.E.,... Propagation and guiding intense light pulses in plasmas [Journal] // Science. - 1996. - Vol. 274. - p. 236.

Shillue, B., AlBanna, S., and D'Addario, L. [Conference] // IEEE International Topical Meeting on Microwave Photonics Technical Digest. - Piscataway, NJ: IEEE, 2004. - pp. 201-204.

Spence, D.E., Kean, P.N., and Sibbett, W. 60-fsec pulse generation from a self-mode-locked Ti:sapphire laser [Journal] // Optics Letters. - 1991. - 1: Vol. 16. - pp. 42-44.

Sprenger, B., Zhang, Z., Lu, Z.H., and Wang, L.J. Atmospheric transfer of optical and radio frequency clock signals [Journal] // Optics Letter. - 2009. - Vol. 34. - pp. 965-967.

Sreenivasiah, I., Ishimaru, A., and Hong, S. T. Two-frequency mutual coherence function and pulse propagation in a random medium: An analytic solution to the plane wave case [Journal] // Radio Science. - 1976. - Vol. 11. - pp. 775 - 778.

Stanford University SLAC Linac Coherent Light Source [Online]. - http://www-ssrl.slac.stanford.edu/lcls.

Stein, S. R. Frequency and Time: Their Measurement and Characterization [Book]. - New York: Academic Press, 1985. - 2. - 0-12-280602-6.

Tatarskii, V. I. The Effects of the Turbulent Atmosphere on Wave Propagation [Book]. - [s.l.]: NOAA (by Israel Program for Scientific Translations, Jerusalem), 1971.

Telle, H.R., Meschede, D., and Hansch, T. Realization of a new concept for visible frequency division: Phase locking of harmonic and sum frequencies [Journal] // Optics Letters. - [s.l.] : Optical Society of America, May 15, 1990. - 10: Vol. 15. - pp. 532-534.

Thorpe, M.J., Moll, K. D., Jones, R.J., Safdi, B., and Ye., J. Broadband cavity ringdown spectroscopy for sensitive and rapid molecular detection [Journal] // Science. - March 17, 2006.

Udem, Th., Holzwarth, R., and Hansch, T.W. Optical freqency metrology [Journal] // Nature. - March 2002. - Vol. 416. - p. 23.

Udem, Th., Reichert, J., Holzwarth, R., and Hänsch, T. W. Accurate measurement of large optical frequency differences with a mode-locked laser [Journal] // Optics Letters. - 1999. - Vol. 24. - pp. 881-883.

Ye, J. and Cundiff, S.T. Femtosecond Optical Frequency Comb Technology [Book]. - New York: Springer Science, 2005.

Young, C. Y., Andrews, L. C., and Ishimaru, A. Time-of-arrival fluctuations of a space-time Gaussian pulse in weak optical turbulence: An analytic solution [Journal] // Applied Optics. - November 1998. - 33: Vol. 37. - pp. 7655 - 7660.

Young, C. Y., Ishimaru, A., and Andrews, L. C. Two-freuqency mutual coherence function of a Gaussian beam pulse in weak optical turbulence: An analytic solution [Journal] // Applied Optics. - 1996. - Vol. 35. - pp. 6522 - 6526.